ARCHIVES OF MECHANICS **Appears since 1949**

Aims and Scope

ARCHIVES OF MECHANICS provides a forum for original research on mechanics of solids, fluids and discrete systems, including the development of mathematical methods for solving mechanical problems. The journal encompasses all aspects of the field, with the emphasis placed on:

- mechanics of materials: elasticity, plasticity, time-dependent phenomena, phase transformation, damage, fracture; physical and experimental foundations, micromechanics, thermodynamics, instabilities
- methods and problems in continuum mechanics: general theory and novel applications, thermomechanics, structural analysis, porous media, contact problems
- dynamics of material systems
- fluid flows and interactions with solids

Address of the Editorial Office:
Institute of Fundamental Technological Research
Świętokrzyska 21
PL 00-049 Warsaw, Poland

Tel.(48-22) 826 60 22, Fax (48-22) 826 98 15, E-mail: publikac@ippt.gov.pl

Abstracted/indexed in:

Applied Mechanics Reviews, Current Mathematical Publications, Mathematical Reviews, MathSci, Zentralblatt für Mathematik, UnCover, Inspec.

http://am.ippt.gov.pl/

Polish Academy of Sciences
Institute of Fundamental Technological Research

Archives of Mechanics

Archiwum Mechaniki Stosowanej

volume 54 issue 2

DRUKARNIA BRACI GRODZICKICH

SUBSCRIPTIONS

Address of the Editorial Office: Archives of Mechanics
Institute of Fundamental Technological Research, Świętokrzyska 21
PL 00-049 Warsaw, Poland
Tel. 48 (*prefix*) 22 826 60 22, Fax 48 (*prefix*) 22 826 98 15,
e-mail:publikac@ippt.gov.pl

Subscription orders for all journals edited by IFTR may be sent directly to the Editorial Office of the Institute of Fundamental Technological Research

Subscription rates

Annual subscription rate (2002) including postage is US $ 240.
Please transfer the subscription fee to our bank account: Payee: IPPT PAN,
Bank: PKO SA. IV O/Warszawa,
Account number 12401053-40054492-3000-401112-001.

All journals edited by IFTR are available also through:

- Foreign Trade Enterprise ARS POLONA Krakowskie Przedmieście 7,
  00-068 Warszawa, Poland fax 48 (*prefix*) 22 826 86 73

- RUCH S.A. ul. Towarowa 28,
  00-958 Warszawa, Poland fax 48 (*prefix*) 22 620 17 62

- International Publishing Service Sp. z o.o. ul. Noakowskiego 10 lok. 38
  00-664 Warszawa, Poland tel./fax 48 (*prefix*) 22 625 16 53, 625 49 55

Warunki prenumeraty

Redakcja przyjmuje prenumeratę na wszystkie czasopisma wydawane przez IPPT PAN. Bieżące numery można nabyć, a także zaprenumerować roczne wydanie Archiwum Mechaniki Stosowanej bezpośrednio w Dziale Wydawnictw IPPT PAN, Świętokrzyska 21, 00-049 Warszawa, Tel. 48 (*prefix*) 22 826 60 22; Fax 48 (*prefix*) 22 826 98 15.
Cena rocznej prenumeraty z bonifikatą (na rok 2002) dla krajowego odbiorcy wynosi 300 PLN

Również można je nabyć, a także zamówić (przesyłka za zaliczeniem pocztowym) we Wzorcowni Ośrodka Rozpowszechniania Wydawnictw Naukowych PAN,
00-818 Warszawa, ul. Twarda 51/55, tel. 48 (*prefix*) 22 697 88 35.
Wpłaty na prenumeratę przyjmują także jednostki kolportażowe RUCH S.A. Oddział Krajowej Dystrybucji Prasy, 00-958 Warszawa, ul. Towarowa 28. Konto: PBK. S.A. XIII Oddział Warszawa nr 11101053-16551-2700-1-67. Dostawa odbywa się pocztą lotniczą, której koszt w pełni pokrywa zleceniodawca. Tel. 48 (*prefix*) 22 620 10 39, Fax 48 (*prefix*) 22 620 17 62

Arkuszy wydawniczych 9. Arkuszy drukarskich 6.8
Papier offset. kl III 70g. B1.
Oddano do składania w marcu 2002 r. Druk ukończono w kwietniu 2002 r.
Skład w systemie TEX: E. Jaczyńska.
Druk i oprawa: Drukarnia Braci Grodzickich, Piaseczno ul. Geodetów 47A.

Arch. Mech., 54, 2, pp. 103–126, Warszawa 2002

A uniform strain, discrete-grain model for evolving anisotropy of polycrystalline ice

R. STAROSZCZYK[1)]

School of Mathematics, University of East Anglia
Norwich NR4 7TJ, United Kingdom
e-mail : r.staroszczyk@uea.ac.uk

A DISCRETE-GRAIN MODEL accounting for the induced anisotropy of polycrystalline ice is formulated. An individual ice crystal is supposed to be a transversely isotropic medium whose behaviour is linearly viscous. For such a crystal a frame-indifferent constitutive law involving three microscopic rheological parameters is derived. Assuming that each crystal undergoes a homogeneous deformation of the polycrystalline aggregate (the Taylor approximation), the macroscopic viscous behaviour of the material is determined. The considerations are illustrated by the results of numerical simulations of simple flows, showing the evolution of the oriented structure of the material and the variation of macroscopic viscosities with increasing strains. In addition, the influence of the parameters describing the single crystal anisotropy on the overall behaviour of the aggregate is investigated.

Key words: polycrystalline ice, induced anisotropy, constitutive law.

Notations

A, B	ice crystal dimensionless rheological parameters
$\mathbf{c}$	crystal c-axis unit vector
$\mathbf{D}$	strain-rate tensor
$\mathbf{I}$	unit tensor
$\mathbf{L}$	velocity gradient tensor
$\mathbf{M}$	structural tensor
$\mathbf{Q}$	rotation matrix
$\mathbf{S}$	deviatoric Cauchy stress tensor
$\mathbf{W}$	spin tensor
$x_i \ (i = 1, 2, 3)$	global spatial Cartesian co-ordinates
$x_i^g \ (i = 1, 2, 3)$	local spatial Cartesian co-ordinates
ϑ	angle defining the crystal c-axis orientation
κ	shear strain
μ	viscosity for shear on a crystal basal plane
μ_0	isotropic polycrystalline ice viscosity
$\mu_{ij} \ (i, j = 1, 2, 3)$	instantaneous viscosities
$\boldsymbol{\sigma}$	Cauchy stress tensor
φ	angle defining the crystal c-axis orientation

[1)] On leave from the Institute of Hydroengineering, Polish Academy of Sciences, ul. Waryńskiego 17, 71-310 Szczecin, Poland

1. Introduction

ICE CORES RETRIEVED from polar ice caps in Antarctica and Greenland reveal strong fabrics (THORSTEINSSON *et al.* [31]), with individual ice grain c-axes (the axes of the crystal hexagonal symmetry) aligned along some preferential directions, with the degree of the alignment usually increasing with the depth of ice, in response to changing loading conditions. Such a phenomenon, in which the internal structure of the material, and hence its macroscopic properties, evolve due to current stress and strain configurations, is known as induced anisotropy.

The main mechanisms taking place on the microscopic level of a single ice grain that are involved in the formation and subsequent evolution of the oriented structure of the medium include, according to ALLEY [1], (1) crystal lattice rotation, a process, in which the crystal c-axes rotate towards the principal axes of compression and away from the principal axes of extension, (2) polygonisation (also referred to as rotation recrystallisation), a mechanism in which the existing crystals are split and new grains are formed, and (3) dynamic (or migration) recrystallisation, a process phenomenon in which, due to high shear stresses and high temperatures, new grains are created at the expense of old grains that subsequently disappear. The role of these three micro-processes changes considerably with the depth in an ice sheet. In the present work, we are concerned with only the first of these processes, namely the crystal lattice rotation, a mechanism which, unlike the other two, occurs throughout the whole depth of a polar ice cap, and dominates the evolution of ice fabric in the upper half of a polar ice sheet.

A single crystal of ice is highly anisotropic, much more anisotropic than most metallic crystals. As indicated by DUVAL *et al.* [9], a stress needed to shear the crystal on its basal plane at a given strain-rate is about two orders of magnitude smaller than those required for other, non-basal, slips. The hexagonal symmetry of the ice monocrystal is practically insignificant in terms of its mechanical behaviour, therefore the single grain can be regarded as a transversely isotropic body (KAMB [16]). At temperatures and stresses typical of polar ice masses, ice deforms mainly by viscous creep. Plastic (rate-independent) behaviour is observed only at the stress magnitudes of 100 MPa (DUVAL *et al.* [9]), by far exceeding those occurring in natural conditions. The strong anisotropy of the single crystal has significant consequences for the overall flow of polar ice sheets as the oriented structure of the polycrystalline material develops. This has been confirmed by the results of numerical simulations of polar ice sheets (MANGENEY *et al.* [19, 20], STAROSZCZYK and MORLAND [29]), showing that the rates at which the whole sheet flows are about twice as high for an anisotropic ice with oriented fabric than those calculated on the assumption of isotropic ice with a random distribution of crystal c-axes. This clearly indicates that the mechanism

of induced anisotropy must be taken into account in the analysis of polar ice behaviour if realistic results are to be obtained.

When modelling the behaviour of polycrystalline ice, a material with evolving micro-structure, two distinct approaches can be pursued. In the first approach, based on the methods of classical continuum mechanics, ice is treated as a continuum in which each material point contains crystals of all possible orientations. The distribution of these orientations in space can be described by a so-called orientation distribution function, whose evolution determines the directional changes in the internal structure of the aggregate (SVENDSEN and HUTTTER [30], MEYSSONNIER and PHILIP [21], GÖDERT and HUTTER [14], GAGLIARDINI and MEYSSONNIER [21], GAGLIARDINI *et al.* [11]). Another continuum approach, in which the micro-structure of ice is ignored by assuming that the macroscopic behaviour of the material depends entirely on the macroscopic variables, such as stress, strain-rate and strain, has been followed by MORLAND and STAROSZCZYK [24], STAROSZCZYK and MORLAND [28] and STAROSZCZYK [26].

A fundamentally different approach is to treat each point of the polycrystal as a collection of a finite number of discrete grains. In such a method the behaviour of each crystal is followed separately, and the macroscopic response of ice is derived from the responses of all individual grains by applying a homogenisation technique. Employing this method, AZUMA [2] has developed a model, in which an individual crystal is assumed to deform only by basal slip, and the microscopic stress applied to each crystal is related to the bulk macroscopic stress in a way determined on the basis of experimental results. VAN DER VEEN and WHILLANS [32] have adopted a similar approach, by supposing that the only slip system active during the viscous deformation of a grain is that associated with basal gliding, but, following LLIBOUTRY [17], have made an assumption of a uniform stress, requiring that the stress in each grain is the same as the macroscopic stress applied to the polycrystal. Yet another approach is the self-consistent model based on the theory developed by HUTCHINSON [15] and extended by MOLINARI *et al.* [23], in which no assumptions on the relations between the microscopic and macroscopic strains and stresses are needed. In that formulation each crystal is treated as an idealised geometric inclusion in an infinite homogeneous medium with properties supposed to represent the macroscopic behaviour of the polycrystal, and on this basis interaction forces between the grain and the aggregate are determined. Following this method, CASTELNAU *et al.* [7] have constructed a model for polycrystalline ice in which the crystal slips on basal, prismatic and pyramidal planes are incorporated.

In this work we formulate a discrete-grain model, in which the crystal slips can occur on basal and prismatic planes (the latter are the planes parallel to the crystal c-axis), which in terms of its generality and complexity places this model between the simpler AZUMA [2] and VAN DER VEEN and WHILLANS [32] models

on one side, and the much more complex and elaborate CASTELNAU *et al.* [7] model on the other. A single crystal is supposed to be a transversely isotropic and linearly viscous medium. The anisotropic properties of the crystal are described by means of two rheological parameters. For such a material, a constitutive law that relates microscopic stresses to strain-rates is formulated. Adopting then the Taylor assumption of the homogeneity of strain throughout the polycrystalline aggregate, a uniform deformation model is constructed. Correlating the model predictions with experimental data describing the limit macroscopic viscosities of ice in compression and simple shear, the two microscopic rheological parameters are determined. For illustration purposes, the model is used to simulate the viscous behaviour of polycrystalline ice in uniaxial compression and simple shear flows. The results obtained demonstrate how the initially isotropic fabric with a random distribution of crystal c-axes evolves as the deformation proceeds, and the variation of the macroscopic viscosities with increasing deformation is illustrated. In addition, the influence of the two rheological parameters describing the anisotropy of the single grain on the macroscopic behaviour of a polycrystalline ice aggregate is investigated.

2. Single crystal kinematics

We adopt material rectangular Cartesian co-ordinates OX_i $(i = 1, 2, 3)$ with base vectors $\mathbf{e}_i$ $(i = 1, 2, 3)$, and fixed spatial rectangular co-ordinates Ox_i $(i = 1, 2, 3)$ with the same origin O and the base vectors $\mathbf{e}_i$. In order to describe a changing position of a single crystal, we use a local spatial reference frame associated with the ice grain, with the axes Ox_i^g $(i = 1, 2, 3)$ and the base vectors $\mathbf{e}_i^g$.

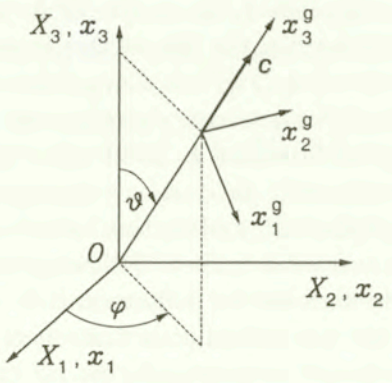

FIG. 1. Global and local co-ordinate systems, with the angles θ and φ defining the crystal c-axis orientation.

Due to the transverse isotropy of the single crystal of ice, with the direction of the axis of its transverse symmetry coinciding with the crystal c-axis and defined by the unit vector $\mathbf{c}$, it suffices to follow the orientation of the vector $\mathbf{c}$ in space to uniquely describe the position of an individual crystal. Accordingly, we assume that $\mathbf{c} = \mathbf{e}_3^g$, and to complete the definition of the local reference frame, we further assume that the x_1^g axis lies in the meridian plane $Ox_3x_3^g$, and the x_2^g axis is chosen in such a way that the right-handedness of the local co-ordinate system is preserved (see Fig. 1).

In order to position the local frame Ox_i^g relative to the global frame Ox_i, we introduce two angles: the co-latitude, or the zenith angle, ϑ, and the longitude φ. In terms of these two angles, the rotation matrix $\mathbf{Q}$, with the components given by $Q_{ij} = \mathbf{e}_i \cdot \mathbf{e}_j^g$, which transforms the components of non-scalar quantities from the local to the global reference frame, is given by

$$\mathbf{Q} = \begin{pmatrix} \cos\vartheta\cos\varphi & -\sin\varphi & \sin\vartheta\cos\varphi \\ \cos\vartheta\sin\varphi & \cos\varphi & \sin\vartheta\sin\varphi \\ -\sin\vartheta & 0 & \cos\vartheta \end{pmatrix}. \tag{2.1}$$

In what follows, we will be concerned with both microscopic quantities, referring to the behaviour of an individual crystal of ice, and macroscopic quantities, describing the behaviour of a polycrystalline aggregate as a whole; the latter quantities will be indicated by a superposed bar. Further, the components of tensor entities expressed in the local reference frame will be denoted by the superscript g, while those expressed in the global reference frame will be left without any suffix. Thus, $\mathbf{A}^g$ indicates a microscopic tensor quantity whose components are expressed in the co-ordinate system Ox_i^g associated with a single grain, while $\bar{\mathbf{A}}$ denotes a macroscopic tensor quantity whose components are expressed in the global co-ordinate system Ox_i, etc.

Since in the problem at hand the internal structure of the material evolves, which is due to the change in time of the crystal c-axes orientations in space, the local frames Ox_i^g $(i = 1,2,3)$ associated with individual grains of ice rotate relative to the fixed global frame Ox_i $(i = 1,2,3)$ as the deformation of the polycrystalline aggregate occurs. Therefore, the matrix $\mathbf{Q}$ which describes the transformation of tensor entities between the frames Ox_i and Ox_i^g is time-dependent, that is $\mathbf{Q} = \mathbf{Q}(t)$. Hence, the relations connecting the global and local position vectors, $\mathbf{x}$ and $\mathbf{x}^g$ respectively, have the following forms:

$$\mathbf{x} = \mathbf{Q}(t)\mathbf{x}^g, \quad \mathbf{x}^g = \mathbf{Q}^T(t)\,\mathbf{x}, \quad \mathbf{x} = \mathbf{x}(\mathbf{X},t), \quad \mathbf{x}^g = \mathbf{x}^g(\mathbf{X},t), \tag{2.2}$$

with the vector $\mathbf{X}$ containing the material co-ordinates, common for both reference systems Ox_i and Ox_i^g, $\mathbf{Q}^T$ being the transpose of $\mathbf{Q}$, and t denoting time.

Differentiation with respect to time of the relations describing the properties of orthogonal matrices

$$\mathbf{Q}\mathbf{Q}^T = \mathbf{Q}^T\mathbf{Q} = \mathbf{I}, \tag{2.3}$$

where $\mathbf{I}$ is the unit tensor, yields the relations

$$\dot{\mathbf{Q}}\mathbf{Q}^T + \mathbf{Q}\dot{\mathbf{Q}}^T = \mathbf{O}, \quad \dot{\mathbf{Q}}^T\mathbf{Q} + \mathbf{Q}^T\dot{\mathbf{Q}} = \mathbf{O}, \tag{2.4}$$

in which superposed dots denote time derivatives. In view of $(2.2)_1$, the velocity fields observed in the global and local frames, $\mathbf{v}$ and $\mathbf{v}^g$ respectively, are related by

$$\mathbf{v} = \dot{\mathbf{x}} = \dot{\mathbf{Q}}\mathbf{x}^g + \mathbf{Q}\dot{\mathbf{x}}^g = \dot{\mathbf{Q}}\mathbf{x}^g + \mathbf{Q}\mathbf{v}^g. \tag{2.5}$$

By differentiating (2.5) and $(2.2)_2$ with respect to the spatial co-ordinates x_i $(i = 1, 2, 3)$, we obtain the following equation that connects the velocity gradient tensors $\mathbf{L}$ and $\mathbf{L}^g$ (whose components are $L_{ij} = \partial v_i/\partial x_j$ and $L^g_{ij} = \partial v^g_i/\partial x^g_j$, respectively), measured in the global and local co-ordinate systems:

$$\mathbf{L} = \dot{\mathbf{Q}}\mathbf{Q}^T + \mathbf{Q}\mathbf{L}^g\mathbf{Q}^T. \tag{2.6}$$

The relations (2.6) and (2.4) provide the transformation formulae for the strain-rate and spin tensors. The strain-rate tensors $\mathbf{D}$ and $\mathbf{D}^g$, the symmetric parts of $\mathbf{L}$ and $\mathbf{L}^g$, respectively, are related by

$$\mathbf{D} = \mathbf{Q}\mathbf{D}^g\mathbf{Q}^T, \tag{2.7}$$

while the spin tensors $\mathbf{W}$ and $\mathbf{W}^g$, the anti-symmetric parts of $\mathbf{L}$ and $\mathbf{L}^g$, respectively, are connected by

$$\mathbf{W} = \dot{\mathbf{Q}}\mathbf{Q}^T + \mathbf{Q}\mathbf{W}^g\mathbf{Q}^T. \tag{2.8}$$

The presence of the term $\dot{\mathbf{Q}}\mathbf{Q}^T$ in Eq. (2.8) reflects the fact that the angular velocity in the global system Ox_i is the vector sum of the angular velocity in the local system Ox^g_i and the angular velocity of Ox^g_i with respect to Ox_i. As the spin tensor $\mathbf{W}$ is a skew-symmetric tensor, it follows that the matrix equation (2.8) is equivalent to the set of three independent differential equations. Since the matrix $\mathbf{Q}(t)$, which defines the orientation of the crystal c-axis, and hence the ice fabric, is a function of two variables, the angles ϑ and φ, we need to prescribe altogether five (out of six) independent components of the spin tensors $\mathbf{W}$ and $\mathbf{W}^g$ in order to determine the rotation of an individual crystal.

Now, by equating, in turn, the components $(\ )_{12}$, $(\ )_{13}$, and $(\ )_{23}$ in (2.8), and using the definition (2.1) of the matrix $\mathbf{Q}$, we obtain the following three relations describing the evolution of the grain orientation:

$$\dot{\varphi}\cos\vartheta = W_{12}^g - W_{12}\cos\vartheta + (W_{13}\sin\varphi - W_{23}\cos\varphi)\sin\vartheta, \tag{2.9}$$

$$\dot{\vartheta} = -W_{13}^g + W_{13}\cos\varphi + W_{23}\sin\varphi, \tag{2.10}$$

$$\dot{\varphi}\sin\vartheta = -W_{23}^g - W_{12}\sin\vartheta - (W_{13}\sin\varphi - W_{23}\cos\varphi)\cos\vartheta. \tag{2.11}$$

From among five independent components of the microscopic spin tensors $\mathbf{W}$ and $\mathbf{W}^g$ which need to be prescribed, three, namely those expressed in the global frame Ox_i, will be further related to the components of the macroscopic spin tensor $\bar{\mathbf{W}}$. Accordingly, only two components of $\mathbf{W}^g$ must be determined on the microscopic level. This is done by following MEYSSONNIER and PHILIP [21], and assuming that the grain basal planes remain parallel to each other throughout the viscous deformation of the crystal, which implies that the velocity component in the direction of the c-axis (coinciding with the x_3^g axis) is a function of the x_3^g co-ordinate only, that is $v_3^g = v_3^g(x_3^g)$. Thus, $\partial v_3^g/\partial x_1^g = \partial v_3^g/\partial x_2^g = 0$, which results in the following two kinematic relations connecting the spin and strain-rate tensor components in the local reference frame Ox_i^g:

$$W_{13}^g = D_{13}^g, \quad W_{23}^g = D_{23}^g. \tag{2.12}$$

Hence, the only microscopic spin tensor component not yet prescribed is W_{12}^g. Its value can be determined from Eq. (2.9), given the current values of the angles ϑ and φ as well as the spin tensor components in the global frame Ox_i. Since W_{12}^g describes the rotation of the crystal about its axis of symmetry measured in the local reference frame Ox_i^g, and this rotation does not affect the viscous response of the crystal due to the assumed transverse isotropy of the grain, the actual value of W_{12}^g is irrelevant to our problem. For this reason, we can ignore the relation (2.9) in our considerations, and restrict our attention to Eqs. (2.10) and (2.11) which, in view of (2.12), become

$$\dot{\vartheta} = -D_{13}^g + W_{13}\cos\varphi + W_{23}\sin\varphi, \tag{2.13}$$

$$\dot{\varphi}\sin\vartheta = -D_{23}^g - W_{12}\sin\vartheta - (W_{13}\sin\varphi - W_{23}\cos\varphi)\cos\vartheta. \tag{2.14}$$

The above two kinematic equations describe uniquely the evolution of the crystal c-axis orientation as long as the microscopic strain-rates D_{13}^g and D_{23}^g measured in the lattice frame Ox_i^g are known. In the uniform strain approach adopted here, the latter variables will be expressed in terms of the macroscopic

strain-rates, while in the uniform stress model the strain-rates D^g_{13} and D^g_{23} would be related to the macroscopic (equal to microscopic) stresses through a constitutive law for the single crystal.

3. Constitutive law for a single crystal of ice

It is generally accepted in theoretical glaciology that the creep behaviour of ice obeys a Norton-Hoff-type power law, stating that, in the case of uniaxial loading, the strain-rate is proportional to some power of the applied stress magnitude (GLEN [13]). At the deviatoric stresses larger than 0.2 MPa, the power law exponent N for polycrystalline ice aggregate is equal to about 3, while for a single crystal its value is $N \sim 2$ (DUVAL *et al.* [9]). At lower stress levels, however, which are more pertinent to polar ice sheets where the deviatoric stresses are usually smaller than 0.1 MPa, both laboratory and field measurements (DOAKE and WOLFF [8], LLIBOUTRY and DUVAL [18], ALLEY [1]) give indications than the exponent N can be lower than 2, and at very low stresses possibly approaching a value close to unity. The latter flow regime corresponds to that of Harper-Dorn creep observed in many metals (LLIBOUTRY and DUVAL [18]). Such a nearly Newtonian viscous flow, with $N \sim 1$, seems to be a dominant material behaviour in the central, upper part of a large polar ice sheet, though a definite conclusion whether the assumption of $N \sim 1$ at small stress levels is the best approximation to the real ice behaviour can be made only after more empirical data is available (BARAL *et.al* [3]). In this work we restrict our attention to a linear constitutive law for ice, assuming that $N = 1$. Nonlinearity of the creep of ice can be incorporated in the constitutive model by relating the isotropic ice viscosity to the strain-rate invariant $\operatorname{tr} \mathbf{D}^2$, which is a conventional approach in glaciology.

An individual grain of ice is assumed to be a transversely isotropic material, with the crystal c-axis being the axis of the rotational symmetry. The medium is supposed to be incompressible, which is a common ice mechanics assumption, and its material behaviour is approximated by a linearly viscous flow law. Therefore, the necessary variables which the constitutive law should include are the Cauchy stress $\boldsymbol{\sigma}$ and the strain-rate $\mathbf{D}$. In order to account for the transverse symmetry of the material, we introduce a structural tensor $\mathbf{M}$ defined by

$$\mathbf{M} = \mathbf{c} \otimes \mathbf{c}, \quad M_{ij} = c_i c_j \quad (i, j = 1, 2, 3), \tag{3.1}$$

which has the property $\operatorname{tr} \mathbf{M}=1$.

Our starting point is the general theory of frame-indifferent (objective) constitutive laws (BOEHLER [5]). In accordance with this theory, the most general

linear constitutive equation for a transversely isotropic material, which relates two symmetric second-order tensors (in our case $\boldsymbol{\sigma}$ and $\mathbf{D}$), has the form

$$\boldsymbol{\sigma} = \alpha_1 \mathbf{I} + \alpha_2 \mathbf{M} + \alpha_3 \mathbf{D} + \alpha_4 (\mathbf{MD} + \mathbf{DM}), \tag{3.2}$$

where α_1 and α_2 are functions of the invariants $\operatorname{tr}\mathbf{D}$ and $\operatorname{tr}\mathbf{MD}$ and α_3 and α_4 are constants. The "anisotropic" invariant $\operatorname{tr}(\mathbf{MD}) = \mathbf{c}^T \mathbf{D}\, \mathbf{c}$ describes the components of $\mathbf{D}$ in the privileged material direction represented by the vector $\mathbf{c}$, parallel to the crystal c-axis. The coefficients α_k $(k = 1, \ldots, 4)$ are given by

$$\begin{aligned} \alpha_1 &= a_1 + a_2 \operatorname{tr}\mathbf{D} + a_3 \operatorname{tr}(\mathbf{MD}), \\ \alpha_2 &= a_4 + a_5 \operatorname{tr}\mathbf{D} + a_6 \operatorname{tr}(\mathbf{MD}), \\ \alpha_3 &= a_7, \quad \alpha_4 = a_8, \end{aligned} \tag{3.3}$$

that is there are eight material constants $(a_1, \ldots, a_8)$ in the most general linear law. However, the ice incompressibility condition imposes the restriction $\operatorname{tr}\mathbf{D} = 0$, so the parameters a_2 and a_5, providing they are of finite values, do not affect the stress response of the material and therefore can be discarded from the analysis, reducing the number of constants left for prescription to six. Further reduction of the number of constants is achieved by assuming that there exist a natural, stress-free state of the material when it does not flow, that is $\boldsymbol{\sigma} = \mathbf{O}$ when $\mathbf{D} = \mathbf{O}$. Hence,

$$\mathbf{D} = \mathbf{O} \;\Rightarrow\; \boldsymbol{\sigma} = \alpha_1 \mathbf{I} + \alpha_2 \mathbf{M} = a_1 \mathbf{I} + a_4 \mathbf{M} = \mathbf{O}, \tag{3.4}$$

as $\alpha_1 = a_1$ and $\alpha_2 = a_4$ when $\mathbf{D} = \mathbf{O}$. By multiplying both sides of (3.4) by $\mathbf{M}$ we obtain

$$\mathbf{M}\boldsymbol{\sigma} = a_1 \mathbf{M} + a_4 \mathbf{M}^2 = (a_1 + a_4)\, \mathbf{M} = \mathbf{O}, \tag{3.5}$$

due to the identity $\mathbf{M}^2 = \mathbf{M}$. Calculating now the traces of the tensors entering the relations (3.4) and (3.5) we find that

$$3a_1 + a_4 = 0 \quad \text{and} \quad a_1 + a_4 = 0, \tag{3.6}$$

resulting in $a_1 = a_4 = 0$, so there are only four non-vanishing constants left in the viscous flow law (3.2). Due to the ice incompressibility assumption, the mean pressure in the material is a workless constraint that is not given by a constitutive equation, therefore only the deviatoric stresses determine the creep response of ice. Hence, by equating the deviatoric parts of both sides of (3.2), we obtain the relation

$$\boldsymbol{\sigma}^D = \alpha_1 \mathbf{I}^D + \alpha_2 \mathbf{M}^D + \alpha_3 \mathbf{D}^D + \alpha_4 (\mathbf{MD} + \mathbf{DM})^D, \tag{3.7}$$

where:

$$\sigma^D = \mathbf{S} = \sigma - \frac{1}{3}\operatorname{tr}\sigma\mathbf{I} = \sigma + p\mathbf{I}, \quad p = -\frac{1}{3}\operatorname{tr}\sigma, \tag{3.8}$$

with $\mathbf{S}$ denoting the deviatoric Cauchy stress and p being the hydrostatic pressure, $\mathbf{I}^D = \mathbf{O}$ (as $\mathbf{I}$ is a spherical tensor), $\mathbf{M}^D = \mathbf{M} - \frac{1}{3}\mathbf{I}$, $\mathbf{D}^D = \mathbf{D}$ (as $\operatorname{tr}\mathbf{D} = 0$), and

$$(\mathbf{MD} + \mathbf{DM})^D = \mathbf{MD} + \mathbf{DM} - \frac{2}{3}\operatorname{tr}(\mathbf{MD})\mathbf{I}. \tag{3.9}$$

Accordingly, Eq. (3.7) becomes

$$\mathbf{S} = \alpha_2\mathbf{M}^D + \alpha_3\mathbf{D} + \alpha_4(\mathbf{MD} + \mathbf{DM})^D, \tag{3.10}$$

and we note that the coefficient $\alpha_1 = a_3$ does no longer appear in the constitutive relation, so it now includes only three material constants: $\alpha_2 = a_6\operatorname{tr}(\mathbf{MD})$, $\alpha_3 = a_7$, and $\alpha_4 = a_8$. Thus, the constitutive law for a single, transversely isotropic and incompressible crystal of ice can be expressed in the form:

$$\mathbf{S} = a_6\operatorname{tr}(\mathbf{MD})(\mathbf{M} - \frac{1}{3}\mathbf{I}) + a_7\mathbf{D} + a_8\Big[\mathbf{MD} + \mathbf{DM} - \frac{2}{3}\operatorname{tr}(\mathbf{MD})\mathbf{I}\Big]. \tag{3.11}$$

The three constants a_6, a_7 and a_8, defining the viscous response of the material, should (ideally) be determined from the results of simple laboratory experiments. Assume that we are able to measure three viscosities for the single crystal, namely: μ_{13} for shearing in the plane parallel to the crystal c-axis (so-called basal shearing), μ_{12} for shearing in the plane normal to the c-axis (so-called prismatic shearing), and μ_{33} for unconfined axial compression carried out along the c-axis. These three viscosities are defined in terms of the deviatoric stresses and strain-rates expressed in the local co-ordinate system Ox_i^g as follows:

$$\mu_{ij} = \frac{\mathrm{S}_{ij}^g}{2D_{ij}^g}, \tag{3.12}$$

where the factor 2 appears to conform to the classical form of the flow law for viscous isotropic fluids $\mathbf{S} = 2\mu_0\mathbf{D}$, with μ_0 denoting the isotropic fluid viscosity. Adopting the global reference frame Ox_i to coincide with the local frame Ox_i^g attached to the crystal, in which case $\mathbf{S} = \mathbf{S}^g$ and $\mathbf{D} = \mathbf{D}^g$, the tensors and their combinations entering the relation (3.11) are given by

(3.13)

$$\mathbf{M} = \begin{pmatrix} 0 & 0 & 0 \\ 0 & 0 & 0 \\ 0 & 0 & 1 \end{pmatrix}, \quad \mathbf{MD}^g = \begin{pmatrix} 0 & 0 & 0 \\ 0 & 0 & 0 \\ D_{31}^g & D_{32}^g & D_{33}^g, \end{pmatrix}, \quad \operatorname{tr}(\mathbf{MD}^g) = D_{33}^g,$$

$$\text{(3.14)}\qquad \mathbf{M}\mathbf{D}^g + \mathbf{D}^g\mathbf{M} - \frac{2}{3}\operatorname{tr}(\mathbf{M}\mathbf{D}^g)\mathbf{I} = \begin{pmatrix} -\frac{2}{3}D^g_{33} & 0 & D^g_{13} \\ 0 & -\frac{2}{3}D^g_{33} & D^g_{23} \\ D^g_{31} & D^g_{32} & \frac{4}{3}D^g_{33} \end{pmatrix}.$$

With (3.13) and (3.14), the law (3.11) provides the relations that connect the deviatoric stresses S^g_{ij} to the corresponding strain-rates D^g_{ij} by

$$\text{(3.15)}\qquad S^g_{12} = a_7 D^g_{12}, \quad S^g_{13} = (a_7 + a_8)\, D^g_{13}, \quad S^g_{33} = \frac{1}{3}\Big(2a_6 + 3a_7 + 4a_8\Big)\, D^g_{33}\,.$$

In view of (3.12), the latter equations yield the following definitions for the material constants a_6, a_7 and a_8:

$$\text{(3.16)}\qquad a_6 = 3\mu_{33} + \mu_{12} - 4\mu_{13}, \quad a_7 = 2\mu_{12}, \quad a_8 = 2(\mu_{13} - \mu_{12}).$$

Now let us introduce two dimensionless rheological parameters A and B that define the axial and prismatic shear viscosities in terms of the basal shear viscosity:

$$\text{(3.17)}\qquad A = \frac{\mu_{33}}{\mu_{13}}, \quad B = \frac{\mu_{12}}{\mu_{13}},$$

and denote the viscosity μ_{13} (the smallest viscosity among μ_{33}, μ_{12} and μ_{13}) by μ. With these definitions, the relations (3.16) become

$$\text{(3.18)}\qquad a_6 = (3A + B - 4)\,\mu, \quad a_7 = 2B\mu, \quad a_8 = 2(1 - B)\,\mu,$$

where, for physical reasons, $A \geq 1$, $B \geq 1$, and $\mu > 0$. In particular, when $A = B = 1$, then we deal with an isotropic grain, while the case $A = B \to \infty$ (infinite axial and prismatic viscosities) corresponds to the situation in which the crystal can deform only by basal slip. On substituting (3.18) into (3.11), we obtain the frame-indifferent constitutive relation for the single crystal of ice given by

$$\text{(3.19)}\qquad \mathbf{S} = 2\mu\left\{\frac{1}{2}(3A + B - 4)\operatorname{tr}(\mathbf{M}\mathbf{D})\Big(\mathbf{M} - \frac{1}{3}\mathbf{I}\Big) + B\mathbf{D} + (1 - B)\Big[\mathbf{M}\mathbf{D} + \mathbf{D}\mathbf{M} - \frac{2}{3}\operatorname{tr}(\mathbf{M}\mathbf{D})\mathbf{I}\Big]\right\}.$$

Using the Voigt notation (in which tensor components are expressed as elements of vectors), the flow law (3.19) can be re-written in the crystal co-ordinate system Ox_i^g in an alternative form as

$$(3.20)\qquad \begin{pmatrix} S_{11}^g \\ S_{22}^g \\ S_{33}^g \\ S_{12}^g \\ S_{13}^g \\ S_{23}^g \end{pmatrix} = 2\mu \begin{pmatrix} \frac{1}{2}(A+B) & \frac{1}{2}(A-B) & & & & \\ \frac{1}{2}(A-B) & \frac{1}{2}(A+B) & & & (0) & \\ & & A & & & \\ & & & B & & \\ & (0) & & & 1 & \\ & & & & & 1 \end{pmatrix} \begin{pmatrix} D_{11}^g \\ D_{22}^g \\ D_{33}^g \\ D_{12}^g \\ D_{13}^g \\ D_{23}^g \end{pmatrix},$$

with the symmetric viscosity matrix depending on the three rheological parameters of the model: basal shear viscosity μ and two dimensionless parameters A and B describing the degree of anisotropy of the single crystal. In a simplified model with $A = B$, the viscosity matrix takes a diagonal form, analogous to the form of the fluidity matrix considered by GAGLIARDINI and MEYSSONNIER [12], who used in their uniform stress model an inverse constitutive law for the crystal, in which the strain-rates are expressed in terms of the deviatoric stresses.

4. Macroscopic behaviour of a polycrystal of ice

Assuming that each grain in the polycrystal has the same volume and the number of grains at a given material point does not change with time (as a result of recrystallisation, for instance), the components of any macroscopic tensor quantity are defined as an arithmetic mean of the corresponding components associated with all constituent grains

$$(4.1)\qquad \bar{A}_{ij} = \frac{1}{N_g} \sum_{k=1}^{N_g} A_{ij}^{(k)},$$

where N_g is the number of crystals. According to ELVIN [10], the minimum number of grains required to obtain statistically satisfactory results of homogenisation should be at least 230.

The kinematic Eqs. (2.13) and (2.14) describing the evolution of the grain orientation, combined with the constitutive law for the grain given by (3.19), and supplemented by the averaging relation (4.1), do not suffice to describe completely the behaviour of the polycrystalline aggregate. For this reason, additional assumptions need to be introduced in order to provide further relations connecting the microscopic and macroscopic variables, required to close the system of equations.

In most of the models developed for ice (LLIBOUTRY [17], VAN DER VEEN and WHILLANS [32], GÖDERT and HUTTER [14], GAGLIARDINI and MEYSSONNIER [12], STAROSZCZYK [27]) it has been assumed that the stress state is uniform throughout the polycrystal , that is, at a given material point, the stress in each crystal equals that in the polycrystal. This assumption is known as the Sachs or Reuss approximation, and has been first introduced to ice mechanics by LLIBOUTRY [17], who has argued that the differences in the microstresses between adjacent ice crystals are negligibly small due to the process of continuous migration of crystal boundaries. In other branches of material science, however, for instance in metallurgy and structural geology, in common use are models, widely referred to as Taylor-Bishop-Hill (TBH) models, which are based on the assumption of the uniformity of deformation in the polycrystalline aggregate. Since both, Sachs-Reuss and Taylor, approaches do not account for the local interactions between constituent crystals, so they are both significant simplifications of the real intrinsic behaviour of the material, it seems that there is no obvious reason why one of the approaches should have much more advantage over the other. In fact, the results of numerical calculations carried out by MEYSSONNIER and PHILIP [22] by using the self-consistent model similar to that of CASTELNAU *et al.* [7], in which no assumptions on local stresses and strains are made, have demonstrated that the viscous response of isotropic polycrystalline ice aggregate given by the self-consistent approach is closer to that predicted by the Taylor model rather than the Sachs-Reuss model. In addition, which will be shown shortly, the Taylor approximation allows the theory to be correlated with the limit ice behaviour observed in simple experiments, whereas the analogous Sachs-Reuss model fails to do so (GAGLIARDINI and MEYSSONNIER [12], STAROSZCZYK [27]). It is also well known (BISHOP and HILL [4]) that the above two extreme approximations of the stress and the strain homogeneity in the polycrystal yield, respectively, lower and upper bounds for the stress at a given strain-rate. Therefore, it is of interest to develop for polycrystalline ice a model based on the deformation uniformity assumption to complement the afore-mentioned uniform stress models. Accordingly, in this work we adopt the Taylor (also known as the Voigt) assumption of the strain uniformity, which in terms of the velocity gradients takes the form:

$$\mathbf{L} = \bar{\mathbf{L}}, \tag{4.2}$$

which necessarily implies that

$$\mathbf{D} = \bar{\mathbf{D}} \quad \text{and} \quad \mathbf{W} = \bar{\mathbf{W}}. \tag{4.3}$$

A consequence of the condition (4.2) is that, in general, the local stress $\mathbf{S}$ is different in each crystal. This stress is defined by the constitutive law (3.19),

with the microscopic strain-rate $\mathbf{D}$ now replaced by the macroscopic strain-rate $\bar{\mathbf{D}}$. The components of the macroscopic stress in the polycrystal $\bar{\mathbf{S}}$ are then evaluated by applying the averaging relation (4.1), determining thus the relation between the macroscopic strain-rate and stress. In order to follow the evolution of the crystal orientation, described by Eqs. (2.13) and (2.14), we first apply the reciprocal of the relation (2.7) to find the strain-rate components expressed in the lattice frame Ox_i^g in terms of those measured in the global frame Ox_i, and then use the relations (4.3) to obtain:

$$D_{13}^g = \frac{1}{2}\sin 2\vartheta\left[\bar{D}_{11}(1+\cos^2\varphi)+\bar{D}_{22}(1+\sin^2\varphi)+\bar{D}_{12}\sin 2\varphi\right] + \cos 2\vartheta\,(\bar{D}_{13}\cos\varphi+\bar{D}_{23}\sin\varphi), \tag{4.4}$$

$$D_{23}^g = \frac{1}{2}\sin\vartheta\left[(\bar{D}_{22}-\bar{D}_{11})\sin 2\varphi+2\bar{D}_{12}\cos 2\varphi\right] - \cos\vartheta\,(\bar{D}_{13}\sin\varphi-\bar{D}_{23}\cos\varphi). \tag{4.5}$$

On substituting the above two relations into the kinematic Eqs. (2.13) and (2.14), with the spin tensor components W_{ij} replaced by $\bar{W}_{ij}$, we are able to calculate the angles ϑ and φ defining the current orientation of the crystal c-axis.

Now determine the macroscopic viscosity of the isotropic polycrystalline ice, μ_0, in terms of the single crystal rheological parameters μ, A and B. Supposing that the orientations of c-axes of all grains in the aggregate are uniformly distributed in space (an idealisation of the random fabric), and that the number of grains is sufficiently large, then each crystal (with its orientation defined by (ϑ,φ)) "occupies" the same elementary area $\sin\vartheta\,d\vartheta\,d\varphi$ on a unit hemisphere of the radius $r=1$. Hence, the number of grains on that hemisphere is $N_g = 2\pi/\sin\vartheta\,d\vartheta\,d\varphi$. With the number of grains increasing to infinity, $N_g\to\infty$, the summation in the relation (4.1) can be replaced by the surface integration, which, when applied to the deviatoric stress components, transforms the averaging formula into:

$$\bar{S}_{ij} = \frac{1}{2\pi}\int_0^{2\pi}\int_0^{\pi/2} S_{ij}(\vartheta,\varphi)\,\sin\vartheta\,d\vartheta\,d\varphi. \tag{4.6}$$

In order to establish the relation between the macroscopic and microscopic viscosities, consider a simple flow configuration, namely that of simple shear, in which the only non-zero strain-rate components are, say, $\bar{D}_{13}=\bar{D}_{31}$. For a grain

with the orientation given by (ϑ, φ), the crystal c-axis unit vector components in the global co-ordinate system are defined by $\mathbf{c} = (\sin\vartheta\cos\varphi, \sin\vartheta\sin\varphi, \cos\vartheta)^T$. The latter determines the structure tensor components $M_{ij} = c_i c_j$, which used in the constitutive law (3.19) yield the microscopic stress S_{13} as

$$S_{13} = 2\mu\bar{D}_{13}[(3A + B - 4)\sin^2\vartheta\cos^2\vartheta\cos^2\varphi + B + (1 - B)(\sin^2\vartheta\cos^2\varphi + \cos^2\vartheta)]. \tag{4.7}$$

After substituting the above equation into (4.6) and performing the prescribed integration, we find that the macroscopic stress $\bar{S}_{13}$ is given by

$$\bar{S}_{13} = \frac{2}{5}\mu\bar{D}_{13}(A + 2B + 2), \tag{4.8}$$

which, by comparing to the viscous fluid flow law $\bar{\mathbf{S}} = 2\mu_0\bar{\mathbf{D}}$, that is $\bar{S}_{13} = 2\mu_0\bar{D}_{13}$, defines the macroscopic viscosity of the isotropic ice by

$$\mu_0 = \frac{\mu}{5}(A + 2B + 2). \tag{4.9}$$

From the above relation it follows that when the single crystal is isotropic (in which case $A = B = 1$), then $\mu_0 = \mu$, implying that the microscopic and macroscopic viscous properties of ice are the same. On the other hand, when the single crystal is assumed to deform only by basal glide, which corresponds to $A \to \infty$ and $B \to \infty$, then (4.9) gives an infinite value of the viscosity μ_0, showing that in our model both the prismatic shear and axial deformations should be permitted in order to yield a bounded value of μ_0. This result differs from the prediction of the uniform stress model, which allows the basal shear to be the only active slip system in the crystal, and yields for such a limit case of the grain anisotropy the relation $\mu_0 = 2.5\mu$ (GAGLIARDINI and MEYSSONNIER [12], STAROSZCZYK [27]). In addition to (4.9), and using the results obtained in [27], we can express the ratio of the isotropic polycrystalline ice viscosities predicted by the Taylor and Sachs-Reuss theories, giving, respectively, the upper and lower bounds for μ_0, as

$$\frac{\mu_0^T}{\mu_0^S} = \frac{1}{25}(A + 2B + 2)(A^{-1} + 2B^{-1} + 2), \tag{4.10}$$

where μ_0^T and μ_0^S denote, respectively, the viscosities predicted by the Taylor and Sachs-Reuss approximations. Obviously, $\mu_0^T/\mu_0^S = 1$ for $A = B = 1$, defining isotropic grains.

As the polycrystal deforms under uniaxial compression or simple shear (which will be illustrated in the next section), the crystals gradually rotate in such a way

that, ultimately, all the c-axes are aligned in parallel. In such a limit situation, the macroscopic properties of the aggregate become those of the single crystal, with the material behaviour described by the constitutive Eqs. (3.19) and (3.20). Hence, using (3.17) and (4.9), the relation (3.20) yields the limit macroscopic viscosity for shearing in planes parallel to the crystal c-axes in the form:

$$\frac{\mu_{13}}{\mu_0} = \frac{5}{A+2B+2}. \tag{4.11}$$

Similarly, the limit macroscopic viscosities for shear in the plane normal to the crystal c-axes (prismatic shearing), for uniaxial compression along the c-axes, and for uniaxial compression in the direction normal to the c-axes, are given, respectively, by

$$\frac{\mu_{12}}{\mu_0} = \frac{5B}{A+2B+2}, \quad \frac{\mu_{33}}{\mu_0} = \frac{5A}{A+2B+2}, \quad \frac{\mu_{11}}{\mu_0} = \frac{5(A+3B)}{4(A+2B+2)}. \tag{4.12}$$

In laboratory tests carried out on samples of polycrystalline ice, usually only the viscosities for simple shear and unconfined uniaxial compression are measured. The reciprocals of the limit ratios of these viscosities to the isotropic viscosity for indefinite deformations, that is μ_0/μ_{13} and μ_0/μ_{33}, are commonly described in glaciology as enhancement factors for shear and compression, E_s and E_a, respectively (BUDD and JACKA [6]). By substituting the experimentally measured values of the enhancement factors to Eqs. (4.11) and $(4.12)_2$, we can determine the values of the two rheological parameters A and B in our model. As a result, we obtain the following relations for A and B:

$$A = \frac{E_s}{E_a}, \quad B = \frac{5E_s}{2} - \frac{E_s}{2E_a} - 1, \tag{4.13}$$

which ensure the correlation between the observed limit behaviour of polycrystalline ice and the model predictions.

5. Numerical simulations

The model formulated in the previous sections is now applied to simulate the viscous behaviour of polycrystalline ice in two simple configurations, corresponding to those occurring in typical laboratory tests, namely the unconfined uniaxial compression and simple shear. As first, we determine the microscopic rheological parameters A and B, related by Eq. (4.13) to the macroscopic enhancement factors. BUDD and JACKA [6] have measured in tests conducted on warm ice (near melting) the enhancement factors $E_a = 3$ and $E_s = 8$, whose meaning is that both axial and shear viscosities decrease with increasing deformation of ice.

However, as the data presented by PIMIENTA *et al.* [25] and THORSTEINSSON *et al.* [31] indicate, the axial viscosity of polar ice increases with deformation, hence $E_a < 1$ seems more appropriate, especially at low temperatures and low stress levels characteristic of natural ice masses. The value of E_a as small as 1/10 for a single-maximum fabric has been found experimentally by PIMIENTA *et al.* [25], although recently MANGENEY *et al.* [19] have suggested the value $E_a \sim 1/3$ for ice near the bottom of the Greenland ice cap, calculated by applying the constitutive model developed by LLIBOUTRY [17] and the field data provided by THORSTEINSSON *et al.* [31]. The shear enhancement factor for ice near the centre of the Greenland ice sheet has been evaluated to be $E_s \approx 2.5$, though it seems that further away from the centre, where shear stresses are larger (and hence fabrics are stronger), a higher value is more relevant. Accordingly, in our simulations we adopt the enhancement factors $E_a = 1/3$ and $E_s = 5$, for which the relations (4.13) give $A = 15$ and $B = 4$. It should be noted here that it is not possible to achieve the above enhancement factors by employing uniform stress models (GÖDERT and HUTTER [14], GAGLIARDINI and MEYSSONNIER [12]), with a single parameter describing the crystal anisotropy, in which case the maximum value of E_s that can be attained is 2.5.

Assume that the uniaxial compression is carried out along the x_3 direction, with equal strains in both lateral directions x_1 and x_2. Then the deformation field is described by

$$x_1 = \lambda_1 X_1, \quad x_2 = \lambda_2 X_2, \quad x_3 = \lambda_3 X_3, \quad \lambda_1 = \lambda_2 = \lambda_3^{-1/2}, \tag{5.1}$$

where λ_i $(i = 1, 2, 3)$ are the principal stretches along the x_i axes, all equal to unity at the start of flow from the isotropic state and $\lambda_3 < 1$ afterwards, and the last relation in (5.1) is due to the ice incompressibility condition $\lambda_1\lambda_2\lambda_3 = 1$. The velocities are defined by

$$v_1 = -\frac{1}{2} x_1 \dot{\lambda}_3/\lambda_3, \quad v_2 = -\frac{1}{2} x_2 \dot{\lambda}_3/\lambda_3, \quad v_3 = x_3 \dot{\lambda}_3/\lambda_3, \tag{5.2}$$

so the tensors of macroscopic velocity gradient $\bar{\mathbf{L}}$, strain-rate $\bar{\mathbf{D}}$, and spin $\bar{\mathbf{W}}$ are given by

$$\bar{\mathbf{L}} = \bar{\mathbf{D}} = \begin{pmatrix} -\frac{1}{2}\dot{\lambda}_3/\lambda_3 & 0 & 0 \\ 0 & -\frac{1}{2}\dot{\lambda}_3/\lambda_3 & 0 \\ 0 & 0 & \dot{\lambda}_3/\lambda_3, \end{pmatrix}, \quad \bar{\mathbf{W}} = \mathbf{O}. \tag{5.3}$$

In the calculations, performed for the isotropic ice viscosity $\mu_0 = 10$ MPa a, where the unit "a" stands for a year, it has been assumed that the axial strain

rate $\bar{D}_{33} = \dot{\lambda}_3/\lambda_3 = 10^{-3}$ a^{-1} is kept constant throughout the flow. All the simulations have been carried out with $N_g = 800$ discrete grains whose initial orientations have been distributed at random. In the plots, the axial deformation along the x_3-axis is expressed in terms of the axial strain ε_{33} defined by

$$\varepsilon_{33} = \lambda_3 - 1. \tag{5.4}$$

The evolution of ice fabric with the axial deformation ε_{33} is illustrated by means of the equal-area Schmid diagrams shown in Fig. 2, in which the dots represent the positions at which the individual crystal c-axes intersect the unit hemisphere, projected onto the plane of the plot. The diagrams demonstrate how the single grains rotate and gradually align in the direction of the principal axis of compression, which for large deformations gives rise to a single-maximum fabric, with nearly all c-axes clustered around the x_3-axis. Such a behaviour of polycrystalline ice aggregate, predicted by the model, agrees well with the behaviour observed in both the laboratory conditions and in the field (PIMIENTA *et al.* [25], BUDD and JACKA [6], ALLEY [1], THORSTEINSSON *et al.* [31]).

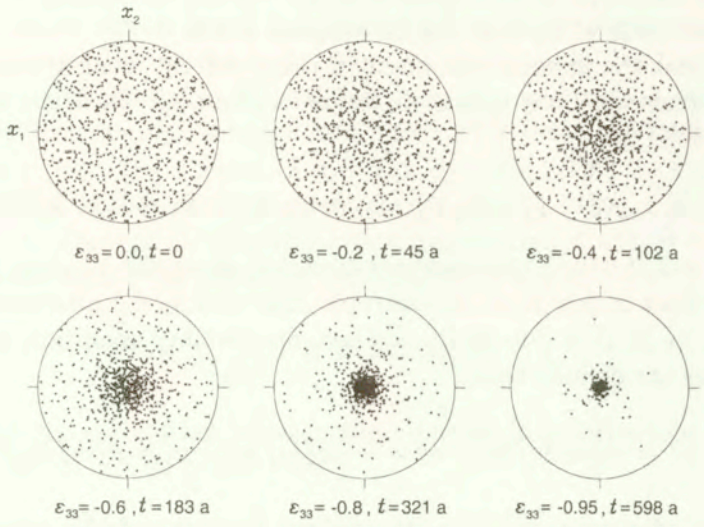

FIG. 2. Evolution of fabric in uniaxial compression along the x_3-axis as a function of the macroscopic axial strain ε_{33} and time t (in years).

Figure 3 illustrates the evolution of the macroscopic axial viscosity with increasing compressive strain as a function of the crystal rheological parameters A and B. The axial viscosity is defined in terms of the current macroscopic stress $\bar{S}_{33}$ and the prescribed strain-rate $\bar{D}_{33}$ by the relation $\mu_{33} = \bar{S}_{33}/(2\bar{D}_{33})$, and is normalised by the macroscopic viscosity μ_0, that is the ratios μ_{33}/μ_0 are plotted in the figure.

Figure 4 shows the variation of the normalised macroscopic viscosities μ_{ij}/μ_0^T (solid lines) with the strain ε_{33} for the single crystal rheological parameters $A = 15$ and $B = 4$, demonstrating the evolution of the strength of anisotropy (in this case transverse isotropy) of the aggregate with increasing macroscopic deformation. For comparison, also the results predicted by the related uniform stress model by STAROSZCZYK [27], indicated by the dashed lines, are presented

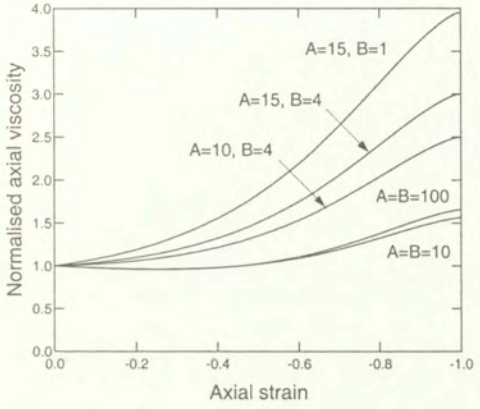

FIG. 3. Evolution of the normalised axial viscosity with the strain ε_{33} in uniaxial compression for different values of the crystal rheological parameters A and B.

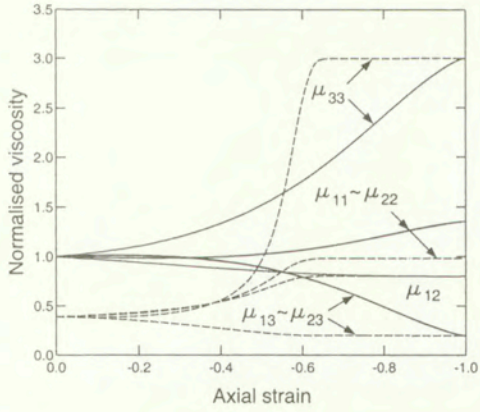

FIG. 4. Evolution of the normalised viscosities with the strain ε_{33} in uniaxial compression for the crystal rheological parameters $A = 15$ and $B = 4$. Comparison of uniform strain (——) and uniform stress (– – –) model results.

in the figure. We note that (1) the isotropic ice viscosities (occurring at $\varepsilon_{33} = 0$) predicted by the uniform strain and uniform stress models, are, for the chosen

single crystal parameters, in the ratio $\mu_0^T/\mu_0^S = 2.5667$ determined by (4.10), and (2) the same limit viscosities μ_{11}, μ_{12} and μ_{13} when $\varepsilon_{33} \to -1$, for the Taylor model given by (4.11) and (4.12), are predicted by the two theories. However, it is seen that the limit viscosities given by the two models are approached in different ways. For the uniform stress model, the most significant evolution in the fabric strength occurs for the axial strains ε_{33} changing from -0.4 to -0.6, with the limit values reached just after the latter value is exceeded, while for the uniform strain model, which predicts a "stiffer" behaviour of ice, the limit alignment of individual grains, and hence the limit viscosities, are attained much later, at ε_{33} close to -1.

Next consider a simple shear in the plane Ox_1x_3 started from an initially isotropic state. The deformation field is now described by

$$x_1 = X_1 + \kappa X_3, \quad x_2 = X_2, \quad x_3 = X_3, \tag{5.5}$$

where κ is a shear strain increasing from zero. The associated velocity field is given by

$$v_1 = \dot{\kappa} x_3, \quad v_2 = v_3 = 0, \tag{5.6}$$

yielding the macroscopic velocity gradient, strain-rate, and spin tensors of the forms:

$$\bar{\mathbf{L}} = \begin{pmatrix} 0 & 0 & \dot{\kappa} \\ 0 & 0 & 0 \\ 0 & 0 & 0 \end{pmatrix}, \quad \bar{\mathbf{D}} = \begin{pmatrix} 0 & 0 & \frac{1}{2}\dot{\kappa} \\ 0 & 0 & 0 \\ \frac{1}{2}\dot{\kappa} & 0 & 0 \end{pmatrix}, \quad \bar{\mathbf{W}} = \begin{pmatrix} 0 & 0 & \frac{1}{2}\dot{\kappa} \\ 0 & 0 & 0 \\ -\frac{1}{2}\dot{\kappa} & 0 & 0. \end{pmatrix}. \tag{5.7}$$

The process of formation and subsequent development of fabric during simple shear is illustrated in Fig. 5. We note that in this flow regime the crystals initially rotate towards the plane Ox_2x_3, and only at very large shear strains κ their c-axes cluster around the axis x_3 (which becomes the principal axis of compression as $\kappa \to \infty$). Ultimately, the same single-maximum fabric as in the uniaxial compression develops.

The evolution of the macroscopic viscosities during simple shear deformation is illustrated in Fig. 6 and 7. A characteristic feature that is seen in the figures is an initial hardening (an increase in the shear viscosity μ_{13}) of ice under shearing, with a maximum shear viscosity occurring at the strains $\kappa \sim 2$. Figure 6 shows the dependence of the normalised viscosity μ_{13}/μ_0 of the aggregate on the parameters A and B describing the anisotropy of constituent crystals. It can be observed that now, compared to uniaxial compression (see Fig. 3), the macroscopic behaviour of the polycrystal is less sensitive to particular values

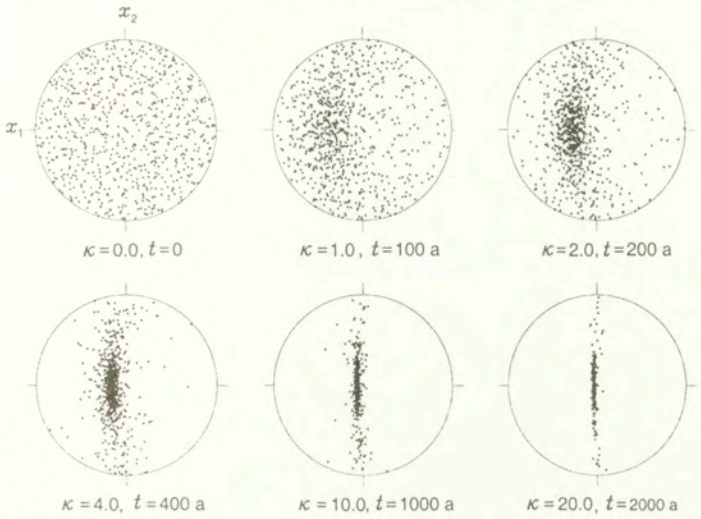

FIG. 5. Evolution of fabric in simple shear in the Ox_1x_3 plane as a function of the macroscopic shear strain κ and time t (in years).

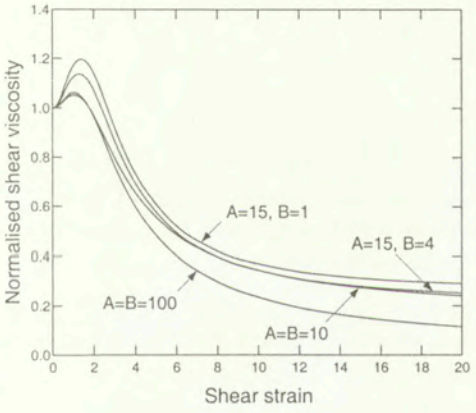

FIG. 6. Evolution of the normalised shear viscosity with the strain κ in simple shear for different values of the crystal rheological parameters A and B.

of the microscopic rheological parameters. Figure 7 demonstrates, for $A = 15$ and $B = 4$, the evolution of the instantaneous viscosities μ_{ij}/μ_0 with increasing shear strain κ, showing the development of anisotropy from the initially isotropic fabric at $\kappa = 0$. Since the fabric at the limit $\kappa \to \infty$ coincides with that created at large deformations during uniaxial compression, the full anisotropy gradually transforms into transverse isotropy, with $\mu_{13} \to \mu_{23}$ and $\mu_{11} \to \mu_{22}$. Moreover, the limit viscosities plotted in Fig. 7, as being again described by the

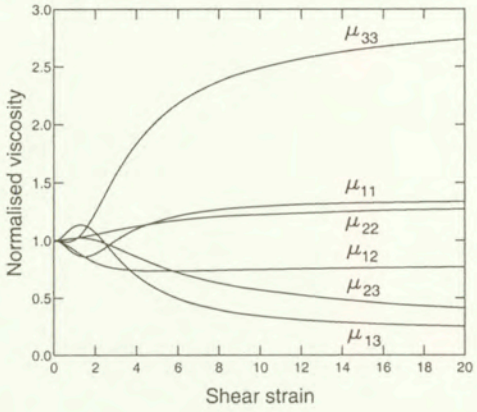

FIG. 7. Evolution of the normalised viscosities with the strain κ in simple shear for the crystal rheological parameters $A = 15$ and $B = 4$.

relations (4.11) and (4.12), are equal to the limit viscosities shown in Fig. 4: $\mu_{13}/\mu_0 = 0.2 = 1/E_s$, $\mu_{33}/\mu_0 = 3.0 = 1/E_a$, $\mu_{12}/\mu_0 = 0.8$, and $\mu_{11}/\mu_0 = 1.35$.

6. Conclusions

The process of induced anisotropy in polycrystalline ice has been modelled by assuming that an individual crystal of ice is a transversely isotropic material, and that the strain is uniform throughout the polycrystal. The creep behaviour of the single crystal has been described by two parameters defining the strength of its anisotropy. The magnitudes of these parameters have been correlated with the limit viscosities in compression and simple shear observed in experiments, something which is not possible with the analogous uniform stress models. Although the viscous response of the single crystal has been assumed to be a linear relation connecting the deviatoric stress to strain-rate, non-linearity of the material behaviour can be easily accounted for by relating the viscosity of ice to a function of the strain-rate invariant $\mathrm{tr}\,\mathbf{D}^2$, which is a well established approach in theoretical glaciology. In the proposed model only the crystal lattice rotation mechanism has been considered, and the effects of the rotation and dynamic recrystallisation on the fabric development in polycrystalline ice have not been taken into account. The reason for not including the latter mechanisms into the model is an insufficient amount of experimental data enabling the proper identification of the main factors controlling such complex microprocesses. Once these factors are identified and quantified, then the present model can be applied as a framework for incorporating more features of the creep behaviour of ice.

References

1. R. B. ALLEY, *Flow-law hypotheses for ice-sheet modelling*, J. Glaciol., **38**, 129, 245–256, 1992.
2. N. AZUMA, *A flow law for anisotropic ice and its application to ice sheets*, Earth Planet. Sci. Lett., **128**, 3-4, 601–614, 1994.
3. D. R. BARAL, K. HUTTER and R. GREVE, *Asymptotic theories of large-scale motion, temperature, and moisture distribution in land-based polythermal ice sheets: A critical review and new developments*, Appl. Mech. Rev., **54**, 3, 215–256, 2001.
4. J. F. W. BISHOP and R. HILL, *A theory of plastic distortion of a polycrystalline aggregate under combined stresses*, Phil. Mag. (7^{th} Ser.), **42**, 327, 414–427, 1951.
5. J. P. BOEHLER, *Representations for isotropic and anisotropic non-polynomial tensor functions*, [in:], Applications of Tensor Functions in Solid Mechanics, J. P. BOEHLER [Ed.], pp. 31–53, Springer, Wien 1987.
6. W. F. BUDD and T. H. JACKA, *A review of ice rheology for ice sheet modelling*, Cold Reg. Sci. Technol., **16**, 2, 107–144, 1989.
7. O. CASTELNAU, P. DUVAL, R. A. LEBENSOHN and G. R. CANOVA, *Viscoplastic modeling of texture development in polycrystalline ice with a self-consistent approach: Comparison with bound estimates*, J. Geophys. Res., **101**, B6, 13851–13868, 1996.
8. C. S. M. DOAKE and E. W. WOLFF, *Flow law for ice in polar ice sheets*, Nature, **314**, 6008, 255–257, 1985.
9. P. DUVAL, M. F. ASHBY and I. ANDERMAN, *Rate-controlling processes in the creep of polycrystalline ice*, J. Phys. Chem., **87**, 21, 4066–4074, 1983.
10. A. A. ELVIN, *Number of grains required to homogenize elastic properties of polycrystalline ice*, Mech. Mat., **22**, 1, 51–64, 1996.
11. O. GAGLIARDINI, M. ARMINJON and D. IMBAULT, *An inhomogeneous variational model applied to predict the behaviour of isotropic polycrystalline ice*, Arch. Mech., **53**, 1, 3–21, 2001.
12. O. GAGLIARDINI and J. MEYSSONNIER, *Analytical derivations for the behavior and fabric evolution of a linear orthotropic ice polycrystal*, J. Geophys. Res., **104**, B8, 17797–17809, 1999.
13. J. W. GLEN, *The creep of polycrystalline ice*, Proc.R. Soc. Lond., A **228**, 1175, 519–538, 1955.
14. G. GÖDERT AND K. HUTTER, *Induced anisotropy in large ice shields: Theory and its homogenization*, Continuum Mech. Thermodyn., **10**, 5, 293–318, 1998.
15. J. W. HUTCHINSON, *Bounds and self-consistent estimates for creep of polycrystalline materials*, Proc. R. Soc. Lond., A **348**, 1652, 101–127, 1976.
16. W. B. KAMB, *The glide direction in ice*, J. Glaciol., **3**, 30, 1097–1106, 1961.
17. L. LLIBOUTRY, *Anisotropic, transversely isotropic nonlinear viscosity of rock ice and rheological parameters inferred from homogenization*, Int. J. Plast., **9**, 5, 619–632, 1993.
18. L. LLIBOUTRY and P. DUVAL, *Various isotropic and anisotropic ices found in glaciers and polar ice caps and their corresponding rheologies*, Ann. Gheophys., **3**, 2, 207–224, 1985.

19. A. MANGENEY, F. CALIFANO and O. CASTELNAU, *Isothermal flow of an anisotropic ice sheet in the vicinity of an ice divide*, J. Geophys. Res., **101**, B12, 28189–28204, 1996.

20. A. MANGENEY, F. CALIFANO AND K. HUTTER, *A numerical study of anisotropic, low Reynolds number, free surface flow for ice sheet modeling*, J. Geophys. Res., **102**, B10, 22749–22764, 1997.

21. J. MEYSSONNIER AND A. PHILIP, *A model for tangent viscous behaviourof anisotropic polar ice*, Ann. Glaciol., **23**, 253–261, 1996.

22. J. MEYSSONNIER AND A. PHILIP, *Remarks on self-consistent modelling of polycrystalline ice*, [in:] K. HUTTER, Y. WANG and H. BEER [Eds.], Advances in Cold-Region Thermal Engineering and Sciences, pp. 225–236, Springer, Berlin 1999.

23. A. MOLINARI, G. R. CANOVA AND S. AHZY, *A self-consistent approach of the large deformation polycrystal viscoplasticity*, Acta Metall., **35**, 12, 2983–2994, 1987.

24. L. W. MORLAND AND R. STAROSZCZYK, *Viscous response of polar ice with evolving fabric*, Continuum Mech. Thermodyn., **10**, 3, 135–152, 1998.

25. P. PIMIENTA, P. DUVAL AND V. Y. LIPENKOV, *Mechanical behavior of anisotropic polar ice*, [in:] International Association of Hydrological Sciences Publication no. 170, pp. 57–66, 1987, (Symp. Physical Basis of Ice Sheet Modelling, Vancouver 1987).

26. R. STAROSZCZYK, *An orthotropic constitutive model for secondary creep of ice*, Arch. Mech., **53**, 1, 65–85, 2001.

27. R. STAROSZCZYK, *A uniform stress, discrete-grain model for induced anisotropy of ice*, [in:] Applications of Mechanics in Civil and Hydro-Engineering, K. SZMIDT [Eds.], pp. 295–314, IBW PAN Publishing House, Gdańsk 2001.

28. R. STAROSZCZYK and L. W. MORLAND, *Orthotropic viscous response of polar ice*, J. Eng. Math., **37**, 1-3, 191–209, 2000.

29. R. STAROSZCZYK and L. W. MORLAND, *Plane ice-sheet flow with evolving orthotropic fabric*, Ann. Glaciol., **30**, 93–101, 2000.

30. B. SVENDSEN and K. HUTTER, *A continuum approach for modelling induced anisotropy in glaciers and ice sheets*, Ann. Glaciol., **23**,262–269, 1996.

31. T. THORSTEINSSON, J. KIPFSTUHL and H. MILLER, *Textures and fabrics in the GRIP ice core*, J. Geophys. Res., **102**, C12, 26583–26599, 1997.

32. C. J. VAN DER VEEN AND I. M. WHILLANS, *Development of fabric in ice*, Cold Reg. Sci. Technol., **22**, 2, 171–195, 1994.

Received July 31, 2001; revised version December 3, 2001.

Arch. Mech., 54, 2, pp. 127–140, Warszawa 2002

Mean value and bounding formulae for heat conduction problems

I. ECSEDI

Department of Mechanics, University of Miskolc
3515 Miskolc-Egyetemváros
e-mail: mechecs@uni-miskolc.hu

SOME MEAN VALUE formulae and bounds on the thermal energy for the steady-state heat conduction problems are proven. The formulation is based on the analogy which exists between the linear elasticity and heat conduction. The formalism of the applied analogy follows the Wojnar's approach. Some examples illustrate the applications of the theorems derived.

1. Governing equations

CONSIDER A BODY that occupies a closed and limited region $\bar{B}$ of volume V in R^3. The set of inner points of $\bar{B}$ is denoted by B and the set of points on the boundary of $\bar{B}$ is denoted by ∂B, $\bar{B} = B \cup \partial B$. Point P of B is indicated by the vector $\mathbf{OP} = \mathbf{p} = x_1\mathbf{e}_1 + x_2\mathbf{e}_2 + x_3\mathbf{e}_3$ in a given orthogonal Cartesian coordinate system $0x_1x_2x_3$ with the unit vectors $\mathbf{e}_1, \mathbf{e}_2, \mathbf{e}_3$.

The temperature difference field in the body $\bar{B}$ is given by $\Theta = \Theta(x_1, x_2, x_3)$ [1, 2]. The heat flux vector is denoted by $\mathbf{q} = \mathbf{q}(x_1, x_2, x_3) = q_1(x_1, x_2, x_3)\,\mathbf{e}_1 + q_2(x_1, x_2, x_3)\,\mathbf{e}_2 + q_3(\mathbf{x}_1, \mathbf{x}_2, \mathbf{x}_3)\,\mathbf{e}_3$ in $\bar{B}$.

Following WOJNAR [1], we introduce the thermal intensity vector field $\mathbf{t}$ by the definition

$$\mathbf{t} = -\nabla\Theta\,. \tag{1.1}$$

In Eq. (1.1) ∇ is the gradient (del) operator.

The field equation of the steady-state heat conduction problem are the heat balance equation [6, 7, 8]

$$-\nabla \cdot \mathbf{q} + r = 0 \qquad \text{in } B\,, \tag{1.2}$$

the Fourier law of heat conduction [6, 7, 8]

$$\mathbf{q} = \mathbf{K} \cdot \mathbf{t}, \tag{1.3}$$

and the thermal intensity-temperature field relation (1.1).

In Eqs. (1.2), (1.3) the dot denotes the scalar product according to [3, 4, 5], $\mathbf{K} = \mathbf{K}(x_1, x_2, x_3)$ is the heat conductivity tensor field which is symmetric and positive definite, and the distributed heat source in B is indicated by $r = r(x_1, x_2, x_3)$.

On the boundary surface ∂B the heat source q_s is defined at every regular point of ∂B as

$$q_s = \mathbf{q}(x_1, x_2, x_3) \cdot \mathbf{n}, \qquad (x_1, x_2, x_3) \in \partial B, \tag{1.4}$$

where $\mathbf{n}$ is the outward unit normal vector to ∂B at point (x_1, x_2, x_3).

2. Mean value formulae

2.1. Mean thermal intensity vector

Throughout this paper, the mean value of a continous function $f = f(x_1, x_2, x_3)$ on $\bar{B}$ is denoted by

$$< f >= \frac{1}{V} \int_B f dV .$$

THEOREM 1. *Let Θ be a temperature field, let $\mathbf{t}$ be the corresponding thermal intensity vector field, and suppose that Θ and $\mathbf{t}$ are continuous on $\bar{B}$. Then the mean value of $\mathbf{t}$ depends only on the boundary values of Θ and is given by*

$$< \mathbf{t} >= -\frac{1}{V} \int_{\partial B} \Theta \mathbf{n} \, dA . \tag{2.1}$$

P r o o f. The validity of the relation (2.1) follows from Eq. (1.1) and the divergence theorem [3, 4, 5]. In Eq. (2.1) dA is the surface element.

2.2. Mean heat flux vector

At first, we formulate two integral relations which will be used to derive the governing relationships.

Let $\mathbf{u} = \mathbf{u}(x_1, x_2, x_3)$ and $\mathbf{v} = \mathbf{v}(x_1, x_2, x_3)$ be regular vector fields in B. From the divergence theorem we get the first integral relation

$$\int_B (\mathbf{u} \circ \nabla) \cdot \mathbf{v} \, dB = \int_{\partial B} \mathbf{u} (\mathbf{n} \cdot \mathbf{v}) \, dA - \int_B \mathbf{u} (\nabla \cdot \mathbf{v}) \, dV . \tag{2.2}$$

Here, the tensor product of two vectors is denoted by a small circle and its definition is given in [3, 4, 5].

The second integral relation is

$$\int_B \mathbf{v} \cdot \nabla U \, dV = \int_{\partial B} U \mathbf{n} \cdot \mathbf{v} \, dA - \int_B U \nabla \cdot \mathbf{v} \, dV, \tag{2.3}$$

where $U = U(x_1, x_2, x_3)$ is an arbitrary continuously differentiable scalar-valued function in $\bar{B}$. The relation (2.3) is a direct consequence of Eq. (2.2), from it we obtain by the substitution $\mathbf{u} = \mathbf{c}U$, where $\mathbf{c}$ is an arbitrary constant, vector different from zero vector.

THEOREM 2. *The mean heat flux corresponding to the Eqs. (1.2), (1.4) depends only on the associated boundary heat flux and the distributed heat source and is given by*

$$< \mathbf{q} >= \frac{1}{V} \left[\int_{\partial B} q_s \mathbf{p} \, dA - \int_B r \mathbf{p} \, dV \right]. \tag{2.4}$$

P r o o f. The proof of the mean heat flux theorem is based on the vector identity (2.2), from it we obtain by the substitutions $\mathbf{u} = \mathbf{p}, \mathbf{v} = \mathbf{q}$ and the application of the identity $\mathbf{p} \circ \nabla = \mathbf{1}$, where $\mathbf{1}$ is the unit tensor.

THEOREM 3. *For a homogeneous material we have*

$$< \mathbf{q} >= \mathbf{K} < \mathbf{t} > . \tag{2.5}$$

P r o o f. The validity of the relation (2.5) follows from the Eq. (1.3) and the definition of the mean value of $\mathbf{t}$ and $\mathbf{q}$.

Next theorem refers to a nonhomoegenous body and it can be derived from the Fourier (1.3), the divergence theorem and the mean heat flux theorem (2.4).

THEOREM 4. *For a nonhomogeneous body the solution of Eqs. (1.1), (1.2) and (1.3) satisfies the relation*

$$\int_{\partial B} \Theta \mathbf{K} \cdot \mathbf{n} \, dA = \int_B r \mathbf{p} \, dV - \int_{\partial B} q_s \mathbf{p} \, dA, \tag{2.6}$$

where q_s is given by Eq. (1.4).

3. Upper and lower bounds on the thermal energy

Two types of the boundary value problems of heat conduction are considered.

The first one is formulated by the field equations (1.1), (1.2), (1.3) with vanishing heat source in B and the following boundary conditions:

$$\Theta = \Theta_1 \quad \text{on } \partial B_1 \quad \text{and} \quad \mathbf{q} \cdot \mathbf{n} = 0 \quad \text{on } \partial B_2 , \tag{3.1}$$

where $\Theta_1 = \Theta_1(x_1, x_2, x_3)$ $(x_1, x_2, x_3) \in \partial B_1$ is a given function and $\partial B = \partial B_1 U \partial B_2$ $\partial B_1 \cap \partial B_2 = \{0\}$. It may be $\partial B_1 = \partial B$ and $\partial B_2 = \{0\}$.

The second type of the heat conduction problem is described by the field Eqs. (1.1), (1.2), (1.3) and the boundary conditions

$$\Theta = 0 \quad \text{on } \partial B_1 \quad \text{and} \quad \mathbf{q} \cdot \mathbf{n} = q_2 \quad \text{on } \partial B_2 \,. \tag{3.2}$$

It may be $\partial B_2 = \partial B$ and $\partial B_1 = \{0\}$. The prescribed heat flux $q_2 = q_2(x_1, x_2, x_3)$ $(x_1, x_2, x_3) \in \partial B_2$ and the given internal heat source $r = r(x_1, x_2, x_3)$ $(x_1, x_2, x_3) \in B$ must satisfy the global balance equation

$$\int_B r \, dV - \int_{\partial B_2} q_2 \, dA = 0, \qquad \text{if} \quad \partial B_2 = \partial B \,. \tag{3.3}$$

The definition of the thermal energy corresponding to the thermal intensity field $\mathbf{t}$ on $\bar{B}$ is as follows [1]:

$$E_K\{\mathbf{t}\} = \frac{1}{2} \int_B \mathbf{t} \cdot \mathbf{K} \cdot \mathbf{t} \, dV \,. \tag{3.4}$$

The heat flux energy corresponding to the heat flux vector $\mathbf{q}$ on $\bar{B}$ is defined as [1]:

$$E_R\{\mathbf{q}\} = \frac{1}{2} \int_B \mathbf{q} \cdot \mathbf{R} \cdot \mathbf{q} \, dV \,, \tag{3.5}$$

where $\mathbf{R} = \mathbf{R}(x_1, x_2, x_3)$ is the inverse matrix of $\mathbf{K} = \mathbf{K}(x_1, x_2, x_3)$ (the thermal resistivity tensor [1, 2, 7]). Of course, $\mathbf{R} \cdot \mathbf{K} = \mathbf{K} \cdot \mathbf{R} = \mathbf{1}$ and $\mathbf{R}$ is symmetric and positive definite second-order tensor field on $\bar{B}$. If $\mathbf{t}$ and $\mathbf{q}$ satisfy the Fourier law (1.3) then we have $E_K\{\mathbf{t}\} = E_R\{\mathbf{q}\}$.

The aim of this section is to establish the upper and lower bounds for the thermal energy computed from the solutions of the above mentioned types of heat conduction problems.

THEOREM 5. *Let U_1 be the thermal energy computed from the solution of the boundary value problem whose boundary conditions are specified in Eq. (3.1), and for it the internal heat sources vanish. In this case, we have*

$$\frac{\left(\int_{\partial B_1} \mathbf{c} \cdot \mathbf{n} \, \Theta_1 dA \right)^2}{\int_B \mathbf{c} \cdot \mathbf{R} \cdot \mathbf{c} \, dV} \leq U_1 \leq \int_B \nabla F \cdot \mathbf{K} \cdot \nabla F \, dV \,, \tag{3.6}$$

where $F = F(x_1, x_2, x_3)$ *is a sufficiently smooth scalar field defined on* $\bar{B}$ *satisfying the "temperature" boundary condition*

$$F(x_1, x_2, x_3) = \Theta_1(x_1, x_2, x_3) \quad (x_1, x_2, x_3) \in \partial B_1; \tag{3.7}$$

futhermore, $\mathbf{c} = \mathbf{c}(x_1, x_2, x_3)$ *is a sufficiently smooth vector field on* $\bar{B}$ *satisfying the conditions*

$$\nabla \cdot \mathbf{c} = 0 \text{ in } B \quad \text{and} \quad \mathbf{c} \cdot \mathbf{n} = 0 \text{ on } \partial B_2 \quad \text{and} \quad \int_B \mathbf{c}^2 dB \neq 0. \tag{3.8}$$

Equality in (3.6) is reached if

$$F = \Theta \text{ in } \bar{B} \quad \text{and} \quad \mathbf{c} = \lambda \mathbf{q} \text{ in } \bar{B}, \tag{3.9}$$

where λ *is an arbitrary constant different from zero.*

P r o o f. The proof of the upper bound relation is based on the equation

$$\int_B \mathbf{q} \cdot \nabla\Theta \, dV = \int_B \mathbf{q} \cdot \nabla F \, dV. \tag{3.10}$$

Putting in Eq. (2.3) $\mathbf{v} = \mathbf{q}$ and $U = F$, we get

$$\begin{aligned} \int_B \nabla F \cdot \mathbf{q} \, dB &= \int_{\partial B} F\mathbf{q} \cdot \mathbf{n} \, dA - \int_B F \nabla \cdot \mathbf{q} \, dV = \int_{\partial B_1} F\mathbf{q} \cdot \mathbf{n} \, dA \\ &= \int_{\partial B_1} \Theta\mathbf{q} \cdot \mathbf{n} \, dA = \int_{\partial B} \Theta\mathbf{q} \cdot \mathbf{n} \, dA \\ &= \int_B \nabla\Theta \cdot \mathbf{q} \, dV + \int_B \Theta \nabla \cdot \mathbf{q} \, dV = \int_B \nabla\Theta \cdot \mathbf{q} \, dV, \end{aligned}$$

thus the relation (3.1) is valid. The application of the Fourier law (1.3) and the definition of $\mathbf{t}$ gives

$$\int_B \nabla\Theta \cdot \mathbf{K} \cdot \nabla\Theta \, dV = \int_B \nabla\Theta \cdot \mathbf{K} \cdot \nabla F \, dV. \tag{3.11}$$

The combination of the Eq. (3.11) with the Schwarz inequality

$$\left(\int_B \nabla\Theta \cdot \mathbf{K} \cdot \nabla F \, dV \right)^2 \leq \int_B \nabla\Theta \cdot \mathbf{K} \cdot \nabla\Theta \, dV \int_B \nabla F \cdot \mathbf{K} \cdot \nabla F \, dV. \tag{3.12}$$

yields the upper bound relation formulated in (3.6).

In order to prove the lower bound relation formulated in (3.6) we substitute into Eq. (2.3) $\mathbf{v} = \mathbf{c}$ and $U = \Theta$. This substitution yields

$$\int_B \mathbf{c} \cdot \nabla\Theta \, dV = \int_{\partial B_1} \Theta_1 \mathbf{c} \cdot \mathbf{n} \, dA . \tag{3.13}$$

By application of the Schwarz inequality we can write

$$\left(\int_B \mathbf{c} \cdot \nabla\Theta \, dV \right)^2 = \left(\int_B \mathbf{c} \cdot \mathbf{R} \cdot \mathbf{q} \, dV \right)^2 \leq \int_B \mathbf{c} \cdot \mathbf{R} \cdot \mathbf{c} \, dV \int_B \mathbf{q} \cdot \mathbf{R} \cdot \mathbf{q} \, dV . \tag{3.14}$$

From Eq. (3.13) and the inequality relation (3.14) we obtain the lower bound formula of the relation (3.6).

THEOREM 6. *Let U_2 be the thermal energy computed from the solution of the boundary value problem whose boundary conditions are specified in Eq. (3.2). In this case, we have*

$$\frac{\left(\int_{\partial B_2} f q_2 \, dA - \int_B r f \, dV \right)^2}{\int_B \nabla f \cdot \mathbf{K} \cdot \nabla f \, dV} \leq U_2 \leq \int_B \mathbf{C} \cdot \mathbf{R} \cdot \mathbf{C} \, dV , \tag{3.15}$$

where $f = f(x_1, x_2, x_3)$ is a sufficiently smooth scalar field defined on $\bar{B}$ and it satisfies the conditions

$$f = 0 \quad \text{on } \partial B_1 \quad \text{and} \quad \int |\nabla f|^2 \, dV \neq 0; \tag{3.16}$$

futhermore $\mathbf{C} = \mathbf{C}(x_1, x_2, x_3)$ is a sufficiently smooth vector field defined on $\bar{B}$ satisfying the conditions

$$-\nabla \cdot \mathbf{C} + r = 0 \quad \text{in } B \quad \text{and} \quad \mathbf{C} \cdot \mathbf{n} = q_2 \quad \text{on } \partial B_2. \tag{3.17}$$

Equality in (3.15) can be reached only if

$$f = \lambda\Theta \quad \text{in } \bar{B} \quad \text{and} \quad \mathbf{C} = \mathbf{q} \quad \text{in } \bar{B} , \tag{3.18}$$

where λ is an arbitrary constant different from zero.

P r o o f. Putting in Eq. (2.3) $\mathbf{v} = \mathbf{q}$ and $U = f$, we obtain

$$\int_B \mathbf{q} \cdot \nabla f \, dV = \int_{\partial B} f \mathbf{q} \cdot \mathbf{n} \, dA - \int_B f \nabla \cdot \mathbf{q} \, dV = \int_{\partial B_2} f q_2 \, dA - \int_B r f dV. \tag{3.19}$$

We note here that

$$\int_B \mathbf{q} \cdot \nabla f dV = \int_B \nabla \Theta \cdot \mathbf{K} \cdot \nabla f dV. \tag{3.20}$$

From the Schwarz inequality we get

$$\left(\int_B \nabla \Theta \cdot \mathbf{K} \cdot \nabla f dV \right)^2 \leq \int_B \nabla \Theta \cdot \mathbf{K} \cdot \nabla \Theta \, dV \int_B \nabla f \cdot \mathbf{K} \cdot \nabla f dV. \tag{3.21}$$

The combination of Eqs. (3.19), (3.20) with inequality (3.21) gives the lower bound relation formulated in (3.15).

To prove the upper bound formulated in the relation (3.15), we start from Eq. (2.3). Putting in (2.3) $\mathbf{v} = \mathbf{C}$, $U = \Theta$, we obtain

$$\begin{aligned} \int_B \mathbf{C} \cdot \nabla \Theta \, dV &= \int_{\partial B} \Theta \mathbf{n} \cdot \mathbf{C} \, dA - \int_B \Theta \nabla \cdot \mathbf{C} \, dV = \int_{\partial B} \Theta \mathbf{n} \cdot \mathbf{q} \, dA - \int_B \Theta \nabla \cdot \mathbf{q} \, dV \\ &= \int_B \nabla \Theta \cdot \mathbf{q} \, dV + \int_B \Theta \nabla \cdot \mathbf{q} \, dV - \int_B \Theta \nabla \cdot \mathbf{q} \, dV, \end{aligned}$$

thus, we have

$$\int_B \mathbf{C} \cdot \nabla \Theta \, dV = \int_B \mathbf{q} \cdot \nabla \Theta \, dV. \tag{3.22}$$

Equation (3.22) can be written in the form

$$\int_B \mathbf{C} \cdot \mathbf{R} \cdot \mathbf{q} \, dV = \int_B \mathbf{q} \cdot \mathbf{R} \cdot \mathbf{q} \, dB. \tag{3.23}$$

The combination of Eq. (3.23) with the Schwarz inequality

$$\left(\int_B \mathbf{C} \cdot \mathbf{R} \cdot \mathbf{q} \, dV \right)^2 \leq \int_B \mathbf{C} \cdot \mathbf{R} \cdot \mathbf{C} \, dV \int_B \mathbf{q} \cdot \mathbf{R} \cdot \mathbf{q} \, dV \tag{3.24}$$

leads to the upper bound formulated in (3.15).

We know that, in the Schwarz inequality used to prove the relations (3.6) and (3.15), the sign of equality is valid when the functions appearing in them are *not* linearly independent. This fact and the structure of the boundary value problems considered determine these cases when the equality holds in (3.6) and in (3.15).

The upper bounds in (3.6) for the case $\partial B_1 = \partial B$ and in (3.15) for the case $\partial B_2 = \partial B$, were derived by the use of principles of "minimum potential thermal energy" and "minimum complementary heat flux energy" in [1].

4. Examples

4.1. Example 1. Concentrated heat sources.

The solid body under the action of two concentrated "inner" heat sources located at points P_1 and P_2 is considered. The boundary surface of the body is free from the heat flux, $q_s = 0$ on ∂B, and we have

$$r = Q\left[\delta\left(\mathbf{p} - \mathbf{p}_2\right) - \delta\left(\mathbf{p} - \mathbf{p}_1\right)\right] \qquad \mathbf{p}_i = \mathbf{0P}_i \quad (i = 1,\ 2)\ , \tag{4.1}$$

where the symbol $\delta(...)$ denotes the Dirac function.

The application of the formula (2.4) gives the result

$$\langle \mathbf{q} \rangle = -\frac{Q}{V}\left(\mathbf{p}_2 - \mathbf{p}_1\right) \tag{4.2}$$

which shows that the mean heat flux vector is parallel to the vector $\mathbf{P_1P_2} = \mathbf{p_2} - \mathbf{p_1}$.

4.2. Example 2. Hollow body subjected to surface heat flux.

The body considered is bounded by the closed surfaces A_1 and A_2. The closed surface A_1 is "inner" and the closed surface A_2 is the "outer" boundary surface of body B. It is assumed that the inner heat source r is given, and on the whole boundary of B which is $\partial B = A_1 U A_2$ the surface heat flux is known, that is

$$q_s = q_1 \quad \text{on} \quad A_1 \quad \text{and} \quad q_s = q_2 \quad \text{on} \quad A_2\,. \tag{4.3}$$

The relation between r, q_1 and q_2 is as follows (global heat balance equation):

$$\int_{A_1} q_1\, dA + \int_{A_2} q_2\, dA = \int_B r\, dV. \tag{4.4}$$

The mean heat flux vector in this problem is

$$\langle \mathbf{q} \rangle = \frac{1}{V}\left(\int_{A_1} \mathbf{p} q_1\, dA + \int_{A_2} \mathbf{p}\, q_2 - \int_V r\mathbf{p}\, dA\right). \tag{4.5}$$

Let us consider the case $r = 0$ in B and assume that q_1, q_2 are constants. For this case from Eqs. (4.4), (4.5) we obtain

$$\langle \mathbf{q} \rangle = \frac{A_2}{V} q_2 (\mathbf{p}_2 - \mathbf{p}_1) = \frac{A_2}{V} \mathbf{G_1 G_2}, \tag{4.6}$$

where

$$\mathbf{0G}_1 = \frac{1}{A_i} \int_{A_i} \mathbf{p}\, dA\,, \qquad (i = 1,2)\,. \tag{4.7}$$

4.3. Example 3. Heat conduction in cylindrical body.

This example illustrates the application of the relation (2.6). The body considered is cylindrical bounded by a cylindrical, surface which is A_3 and two planes normal to A_3 at $x_3 = 0$ and $x_3 = L$. The end cross-sections of the cylindrical bar-like body are A_1 at $x_3 = 0$ and A_2 at $x_3 = L$. The equation of A_3 is $c(x_1, x_2) = 0$ and $0 \leq x_3 \leq L$. The following problem of steady-state heat conduction is analysed:

$$\Theta(x_1, x_2, 0) = T_1(x_1, x_2) \qquad \text{on } A_1, \tag{4.8}$$

$$\Theta(x_1, x_2, L) = T_2(x_1, x_2) \qquad \text{on } A_2, \tag{4.9}$$

$$\mathbf{q} \cdot \mathbf{n} = Q(x_1, x_2, x_3) \quad \text{on } A_3. \tag{4.10}$$

In Eqs. (4.8), (4.9), (4.10) T_1, T_2 and Q are given and it is assumed that the "internal" heat source is known. The form of the thermal conductivity tensor K is as follows:

$$\begin{aligned} \mathbf{K}(x_1, x_2, x_3) &= k_{11}(x_1, x_2, x_3)\, \mathbf{e}_1 \circ \mathbf{e}_1 + k_{22}(x_1, x_2, x_3)\, \mathbf{e}_2 \circ \mathbf{e}_2 \\ &+ k_{12}(x_1, x_2, x_3)\, (\mathbf{e}_1 \circ \mathbf{e}_2 + \mathbf{e}_2 \circ \mathbf{e}_1) \\ &+ k_{33}(x_1, x_2, x_3)\, \mathbf{e}_3 \circ \mathbf{e}_3. \end{aligned} \tag{4.11}$$

We introduce the heat flux resultants at the end cross-sections A_1, A_2 by the definition

$$Q_i = \int_{A_i} \mathbf{q} \cdot \mathbf{n}_i\, dA \qquad (i = 1,2)\,. \tag{4.12}$$

We note $\mathbf{n}_1 = -\mathbf{e}_3$ and $\mathbf{n}_2 = \mathbf{e}_3$. The outer normal vector on the boundary surface segment A_3 is

$$\mathbf{n} = n_1 \mathbf{e}_1 + n_2 \mathbf{e}_2, \qquad \left(n_1^2 + n_2^2 = 1\right)\,. \tag{4.13}$$

Let Q_3 be defined as

$$Q_3 = \int\limits_{\partial A_2} \left(\int\limits_0^L Q(x_1, x_2, x_3)\, dx_3 \right) ds, \tag{4.14}$$

where ∂A_2 is the boundary curve of the cross-section A_2 and s is an arc coordinate defined on ∂A_2.

The global balance equation for the body B bounded by the surface $\partial B = A_1 U A_2 U A_3$ is

$$Q_1 + Q_2 + Q_3 - R = 0, \tag{4.15}$$

where

$$R = \int\limits_B r(x_1, x_2, x_3)\, dV. \tag{4.16}$$

In Eq. (4.15) Q_1 and Q_2 are unknown. Their values can be computed by the use of relation (2.6). From Eq. (2.6) we get

$$\int\limits_{\partial B} \Theta \mathbf{e}_3 \cdot \mathbf{K} \cdot \mathbf{n}\, dA = \int\limits_B x_3 r dV - \int\limits_{\partial B} x_3 q_s\, dA\,. \tag{4.17}$$

We define the following quantities:

$$R_1 = \int\limits_B x_3 r\, dV, \tag{4.18}$$

$$Q_4 = \int\limits_{\partial A_2} \left(\int\limits_0^L x_3 Q\, dx_3 \right) ds, \tag{4.19}$$

$$\bar{k}_1 = \frac{1}{A} \int\limits_{A_1} k_{33}(x_1, x_2, 0) dA, \tag{4.20}$$

$$\bar{k}_2 = \frac{1}{A} \int\limits_{A_2} k_{33}(x_1, x_2, L) dA, \tag{4.21}$$

$$\overline{T}_1 = \frac{1}{A\bar{k}_1} \int_{A_1} k_{33}(x_1, x_2, 0) T_1(x_1, x_2) dA, \tag{4.22}$$

$$\overline{T}_2 = \frac{1}{A\bar{k}_2} \int_{A2} k_{33}(x_1, x_2, L) T_2(x_1, x_2) dA, \tag{4.23}$$

$$A = \int_{A_1} dA = \int_{A_2} dA. \tag{4.24}$$

Introducing the quantities defined above into the Eq. (4.13) we obtain

$$Q_2 = -\frac{\bar{k}_2 \overline{T}_2 - \bar{k}_1 \overline{T}_1}{L} A - \frac{Q_4}{L} + \frac{R_1}{L}. \tag{4.25}$$

For the case $r = 0$ in B, and $\mathbf{n} \cdot \mathbf{q} = 0$ on A_3, Eq. (4.25) gives

$$Q_2 = -Q_1 = -k \frac{\overline{T}_2 - \overline{T}_1}{L} A, \qquad \text{if } \bar{k}_1 = \bar{k}_2 = k. \tag{4.26}$$

We mention that the heat conduction problem determined by the boundary conditions (4.8), (4.9) and (4.10) is a three-dimensional boundary value problem which, in general, does not have the solution in a closed form.

4.4. Example 4. Bounds for the thermal energy.

Homogeneous isotropic body is bounded by two similar ellipsoids of revolution described by the surfaces $\nu = \nu_1$ and $\nu = \nu_2$ $(0 < \nu_1 < \nu_2)$, where

$$\nu^2 = x_1^2 + x_2^2 + \left(\frac{x_3}{\alpha}\right)^2, \qquad \alpha \geq 1. \tag{4.27}$$

The "inner" boundary surface of body B is A_1 and on it $\nu = \nu_1$, the "outer" boundary surface of body B is A_2 and on it $\nu = \nu_2$. The inner heat sources vanish, $r = 0$ in B, and we have the next "temperature" boundary condition

$$\Theta_1 = T = \text{const on } A_1, \tag{4.28}$$

$$\Theta_1 = 0 \text{ on } A_2. \tag{4.29}$$

The function

$$F(x_1, x_2, x_3) = T \frac{\nu_1}{\nu_2 - \nu_1} \left(\frac{\nu_2}{\nu} - 1\right) \tag{4.30}$$

satisfies all conditions which are prescribed in (3.6) for $F = F(x_1, x_2, x_3)$. Since the hollow body considered is isotropic and homogeneous, the thermal conductivity tensor has the form $\mathbf{K} = k\mathbf{1}$ ($k = \text{const}$) and we have

$$\int_B \nabla F \cdot \mathbf{K} \cdot \nabla F dV = k \int_B |\nabla F|^2 \, dV.$$

A simple calculation gives

$$U_1 \leq T^2 \frac{4\pi k}{3\left(\frac{1}{\nu_1} - \frac{1}{\nu_2}\right)} \left(2\alpha + \frac{1}{\alpha}\right). \tag{4.31}$$

To obtain the lower bound for U_1, we use in (3.6) the divergence-free vector field $\mathbf{c} = \mathbf{c}(x_1, x_2, x_3)$

$$\mathbf{c} = \frac{\mathbf{p}}{p^3} \qquad \left(p = \sqrt{x_1^2 + x_2^2 + x_3^2}\right). \tag{4.32}$$

It is very easy to show that

$$\int_{\partial B_1} \mathbf{c} \cdot \mathbf{n} \Theta_1 dA = T \int_{A_1} \frac{\mathbf{p} \cdot \mathbf{n}}{p^3} dA = 4\pi T, \tag{4.33}$$

$$\int_B \mathbf{c} \cdot \mathbf{R} \cdot \mathbf{c} \, dV = \frac{1}{k} \int_B \frac{dV}{p^4} = 4\pi h(\alpha) \left(\frac{1}{\nu_1} - \frac{1}{\nu_2}\right) \frac{1}{k}, \tag{4.34}$$

where

$$h(\alpha) = \frac{1}{2}\left(\alpha \operatorname{arc\,tg} \alpha + \frac{\sqrt{\alpha^2 - 1}}{\alpha}\right) \text{ for } \alpha > 1 \text{ and } h(\alpha) = 1 \text{ for } \alpha = 1. \tag{4.35}$$

The combination of (3.6) with Eqs. (4.33), (4.34) leads to the lower bound

$$U_1 \geq \frac{4\pi k}{\left(\frac{1}{\nu_1} - \frac{1}{\nu_2}\right) h(\alpha)} T^2. \tag{4.36}$$

The bounds (4.31) and (4.36) for $\alpha = 1$ give the same result; in this case the boundary surfaces A_1 and A_2 are concentric spheres with their centers at the origin of the coordinate system and ν denotes the distance from the origin.

5. Conclusions

The main purpose of the present paper was to show how one can use the analogy which exists between the linear elasticity and heat conduction. The formulation of the mean value theorems of steady-state heat conduction problems follows the formulation of mean displacement, and the mean stress theorem done by GURTIN [9] in linear elasticity.

The upper and lower bounds for the heat flux are derived by the application of Schwarz inequality, avoiding the application of the minimum principles of potential thermal energy and complementary heat-flux energy which were developed by WOJNAR [1].

Examples 1 and 2 present the computation for two problems of the mean heat flux vectors.

Example 3 discusses the heat conduction in a bar-like body by the application of equation based on the concept of mean thermal intensity and the mean heat flux vector.

Example 4 gives two side bounds for the thermal energy of a hollow body bounded by two similar ellipsoids of revolution. In this example, the test functions applied can be used for the case of nonhomogeneous anisotropic bodies which have shape as the body in Example 4.

References

1. R. WOJNAR, *Upper and lower bounds on heat flux*, Journal of Thermal Stresses, 21, 381-403, 1998.
2. D. E. GARLSON, *Linear thermoelasticity*, [in:] S. FLÜGGE [Ed.], Handbuch der Physik, vol.VIa/2, Mechanics of Solids II. pp. 297-345, Springer, Berlin 1972.
3. G. T. MASE and G. E. MASE, *Continuum mechanics*, pp. 3-47, CRC Press, London 1999.
4. L. E. MALVERN, *Introduction to the mechanics of a continuous medium*, Prentice-Hall, New York 1969.
5. A. I. LURJE, *Theory of elasticity* (in Russian), Izd. Nauka, Mosco w 1970.
6. H. S. CARSLAW and J. C. JAEGER, *Conduction of heat in solids*, 2nd edition, Clarendon Press, Oxford 1986.
7. M. N. ÖZISIK, *Boundary value problems of heat conduction*, Dover Publications, Inc., New York 1989.
8. M. JACOB, *Heat Transfer*, Vol. I. John Wiley and Sons. Inc., New York 1949.

9. M. E. GURTIN, *The linear theory of elasticity*, [in:] S.FLÜGGE [Ed.], Handbuch der Physik, Vol. VIa/2 Mechanics of Solids II, pp. 1-295, Springer, Berlin 1972.

Received December 12, 2001; revised version January 23, 2002.

Arch. Mech., **54**, 2, pp. 141–153, Warszawa 2002

Basic inequalities for multipoint Padé approximants to Stieltjes functions

S. TOKARZEWSKI[1], J.J. TELEGA[1], M. PINDOR[2], J. GILEWICZ [3]

(1) *Institute of Fundamental Technological Research, Polish Academy of Sciences, Świętokrzyska 21, 00-049 Warsaw, Poland*

(2) *Institute of Theoretical Physics, Warsaw, Hoża 69, 00-681 Warsaw, Poland*

(3) *Centre de Physique Théorique, CNRS, Luminy Case 907, 13288 Marseille Cedex 09, France*

BASIC INEQUALITIES FOR DIAGONAL and subdiagonal multipoint Padé approximants to N power series expansions of Stieltjes function f_0 at points $x_1, x_2, ..., x_N$ are derived. For particular cases the inequalities obtained reduce to those obtained earlier for one-, two- and three-point Padé approximants in [1], [5] and [23], respectively. Numerical examples illustrating the relations achieved are also provided. Our results can be applied to the determination of bounds on the effective moduli of bone subjected to torsion and composites in the case of transport equations.

1. Introduction

THE PROPERTIES OF one- two- and three-point Padé approximants to Stieltjes function, say f_0, were extensively investigated in recent years. The obtained results valid in a real domain read: (i) for $x > 0$ the sequence of the diagonal and subdiagonal one-point Padé approximants to the expansion of f_0 at $x = 0$ form upper and lower bounds uniformly converging to $f_0(x)$, cf. [1], [8] and [27]; (ii) for $x > 0$ the sequence of the diagonal two-point Padé approximants to the expansions of f_0 at $x = 0$ and $x = \infty$ also form upper and lower bounds uniformly converging to $f_0(x)$, cf. [5], [22], [23] and [9]; (iii) for $x > 0$ the sequence of the diagonal three-point Padé approximants to the expansions of f_0 at $x = 0$, $x = 1$ and $x = \infty$ form upper and lower bounds uniformly converging to $f_0(x)$, cf. [9]. The Padé approximant bounds reported in (i) - (iii) are the best ones with respect to the given number of Stieltjes series coefficients.

The main aim of this paper is to extend the validity of the inequalities for one- [1], [8], [27], two-[5], [9], [22], and three-point Padé approximants [23] to the multipoint Padé ones, constructed for power expansions of f_0 at $x_1, x_2, ...,$

$x_N \leq \infty$. Nontrivial practical applications of the inequalities obtained previously to mechanical problems are presented in [21], [24], [26] and [27].

This paper is organized as follows: In Sec. 2 we introduce the basic definitions, notations and assumptions dealing with Stieltjes functions, multipoint Padé approximants and multipoint continued fractions. The basic inequalities for diagonal and subdiagonal multipoint Padé approximants to a Stieltjes function are derived in Sec. 3. In Sec. 4 illustrative examples are presented. Particular cases of the inequalities obtained are discussed in Sec. 5. In Sec. 6 the practical applications of the multipoint Padé approximants are presented. The results achieved are summarized in Sec. 7

2. Preliminaries

Let us consider a real function f analytic at N different points x_1, x_2, ..., x_N, where without loss of generality we assume

$$x_1 < x_2 < ... < x_N. \tag{2.1}$$

The power expansions of f at the above points are

$$f(x) = \sum_{k=0}^{\infty} c_k(x_j)(x - x_j)^k, \quad j = 1, 2..., N. \tag{2.2}$$

In practical situations we know only a few first coefficients of each expansion (2.1) and then we have to deal with the limited information characterized by the truncated power series

$$f(x) = \sum_{k=0}^{p_j - 1} c_k(x_j)(x - x_j)^k + O((x - x_j)^{p_j}), \quad j = 1, 2, ..., N, \tag{2.3}$$

where p_j denote the given number of coefficients of power series at each point.

Now we are in a position to recall from [2, Chap.8] the definition of multipoint Padé approximants to f.

DEFINITION 1. *The N-point Padé approximant to a function f, corresponding to the expansions (2.3), if it exists, is a rational function P_m/Q_n denoted by $[m/n]_f^{N,p}$,*

$$[m/n]_f^{N,p} = \frac{P_m(x)}{Q_n(x)} = \frac{a_0 + a_1 x^1 + a_2 x^2 + \cdots + a_m x^m}{1 + b x^1 + b_2 x^2 + \cdots + b_n x^n},$$
$$p = \sum_{j=1}^{N} p_j, \quad m + n = p - 1, \tag{2.4}$$

satisfying the following relations:

$$f(x) - [m/n]_f^{N,p}(x) = O((x - x_j)^{p_j}), \qquad j = 1, 2, ..., N. \tag{2.5}$$

In the following we deal only with diagonal and subdiagonal approximants, then

$$m = p - 1 - E\left(\frac{p-1}{2}\right), \quad n = E\left(\frac{p-1}{2}\right), \tag{2.6}$$

where $E(x)$ denotes the integer part of x.

As usual, for the ordinary one-point Padé approximants the relations (2.5), where f and $[m/n]$ must be understood as the power series expansions at the corresponding points x_j, represent a linear system defining the coefficients $(a_0, a_1, ..., a_m, b_1, b_2, ..., b_n)$.

REMARK 1. All previous definitions are also valid for analytic functions of complex variable and for points x_j in the complex domain.

In our investigations we are concerned with Stieltjes functions and the $N-$point Padé approximants to the corresponding Stieltjes series. Let f_0 be a Stieltjes function having the following representation, see [1], [9]

$$f_0(x) = f_0(0) + x \int_0^{1/\rho} \frac{d\gamma_0(u)}{1 + xu}, \tag{2.7}$$

$$\lim_{x \to 0} f_0(x) = f_0(0) \equiv g_0 > 0, \quad \lim_{x \to \infty} f_0(x) = d_0 < \infty,$$

where the spectrum γ_0 is a real, bounded non-decreasing function.

Let us introduce the following notation:

$$\underset{k=1}{\overset{r}{\mathbf{K}}} \frac{a_k}{1} := \cfrac{a_1}{1 + \cfrac{a_2}{1 + \ddots \cfrac{a_r}{1.}}} \quad \text{and} \quad g_k := f_k(x_j). \tag{2.8}$$

Functions f_k are defined in the following procedure of expansion of f_0 in one-point (afterwards: in $N-$point) continued fraction

$$f_0(x) = f_0(x_1) + (x - x_1) f_1(x) = f_0(x_1) + \frac{(x - x_1) f_1(x_1)}{1 + (x - x_1) f_2(x)} = \ldots \tag{2.9}$$

$$= f_0(x_1) + \underset{k=1}{\overset{r-1}{\mathbf{K}}} \frac{(x - x_1) f_k(x_1)}{1} + \frac{(x - x_1) f_r(x)}{1}$$

$$\equiv g_0 + \underset{k=1}{\overset{r-1}{\mathbf{K}}} \frac{(x - x_1) g_k}{1} + \frac{(x - x_1) f_r(x)}{1}.$$

All functions f_k are also Stieltjes functions.

Now we focus our attention on N-point continued fraction expansion of f_0 at the points $x_1, x_2, ..., x_N$. Let us introduce the non-decreasing step-wise function L

(2.10)
$$L(x) = \sum_{j=1}^{N} p_j H(x - x_j), \quad p = \sum_{j=1}^{N} p_j = L(x_N), \quad H(t) = \begin{cases} 0 & \text{if } t < 0, \\ 71 & \text{if } t \geq x. \end{cases}$$

The value $L(x)$ denotes the total number of given coefficients of power expansions of f_0 at all points $x_j \leq x : L(x_k) = p_1 + p_2 + ... + p_k$.

To construct the multipoint continued fraction, we begin by expanding f_0 at x_1 as shown in (2.9), we follow by expanding $f_{L(x_1)}$ at x_2, and so on:

$$(2.11) \quad f_0(x) = g_0 + \underset{k=1}{\overset{L(x_1)-1}{\mathbf{K}}} \frac{(x - x_1)g_k}{1} \quad \frac{x - x_1}{x - x_2} \underset{k=L(x_1)}{\overset{L(x_2)-1}{\mathbf{K}}} \frac{(x - x_2)g_k}{1} \ldots$$

$$+ \frac{(x - x_{N-1})}{(x - x_N)} \underset{k=L(x_{N-1})}{\overset{L(x_N)-1}{\mathbf{K}}} \frac{(x - x_N)g_k}{1} + \frac{(x - x_N)f_p(x)}{1}.$$

One can easily verify that the $N-$point Padé approximant $[m/n]_{f_0}^{N,p}$ to f_0 is equal to the following truncated continued fraction:

$$(2.12) \quad m/n]_{f_0}^{N,p}(x) = g_0 + \underset{k=1}{\overset{L(x_1)-1}{\mathbf{K}}} \frac{(x - x_1)g_k}{1} \quad \frac{x - x_1}{x - x_2} \underset{k=L(x_1)}{\overset{L(x_2)-1}{\mathbf{K}}} \frac{(x - x_2)g_k}{1} \ldots$$

$$+ \frac{(x - x_{N-1})}{(x - x_N)} \underset{k=L(x_{N-1})}{\overset{L(x_N)-1}{\mathbf{K}}} \frac{(x - x_N)g_k}{1},$$

where, because f_k are positive functions,

$$(2.13) \qquad \forall k : g_k > 0.$$

3. Basic inequality

THEOREM 1. *Let f_0 be a Stieltjes function (2. 7) and let N power series (2. 2) have nonzero radii of convergence; then the diagonal and subdiagonal N-point Padé approximants $[m/n]_{f_0}^{N,p}$ obey the following inequality:*

$$(3.1) \qquad x \in]-\rho, \infty[: \quad (-1)^{L(x)} \, [m/n]_{f_0}^{N,p}(x) \geq (-1)^{L(x)} \, f_0(x),$$

where m and n are defined by (2. 6) and the function L by (2. 10).

Sketch of the proof. Let us start from the Stieltjes function f_0 represented by the following multipoint continued fraction (one step less than in (2.11))

$$(3.2)\quad f_0(x) = g_0 + \underset{k=1}{\overset{L(x_1)-1}{\mathbf{K}}} \frac{(x-x_1)g_k}{1} + \frac{(x-x_1)}{x-x_2} \underset{k=L(x_1)}{\overset{L(x_2)-1}{\mathbf{K}}} \frac{(x-x_2)g_k}{1} \cdots$$

$$+ \frac{x-x_{N-1}}{x-x_N} \underset{k=L(x_{N-1})}{\overset{L(x_N)-2}{\mathbf{K}}} \frac{(x-x_N)g_k}{1} + \frac{(x-x_N)f_{L(x_N)-1}(x)}{1}.$$

For simplicity, choosing $x_1 = 0$ and replacing $f_{L(x_N)-1}(x)$ by $g_{L(x_N)-1} := f_{L(x_N)-1}(x_N)$, one obtains the following Padé approximant $[m/n]_{f_0}^{N,p}$ to f_0 :

$$(3.3)\quad [m/n]_{f_0}^{N,p}(x) = g_0 + \underset{k=1}{\overset{L(0)-1}{\mathbf{K}}} \frac{xg_k}{1} + \frac{x}{x-x_2} \underset{k=L(0)}{\overset{L(x_2)-1}{\mathbf{K}}} \frac{(x-x_2)g_k}{1} \cdots$$

$$+ \frac{x-x_{N-1}}{x-x_N} \underset{k=L(x_{N-1})}{\overset{L(x_N)-2}{\mathbf{K}}} \frac{(x-x_N)g_k}{1} + \frac{(x-x_N)g_{L(x_N)-1}}{1}.$$

Since all f_k are Stieltjes functions, they are decreasing positive functions on $]-\rho, \infty[$, and then the following inequalities hold:

$$(3.4)\qquad 1 + (x-x_j)g_k \geq 0, \qquad j = 1, 2, ..., N$$

and

$$(3.5)\qquad x \in [\,-\rho, \infty[: \qquad (x-x_N)f_{L(x_N)-1}(x) \leq (x-x_N)g_{L(x_N)-1}.$$

The recurrence formulae for (3.2) and (3.3) jointly with the relations (2.12) and (3.5), yield the basic inequality (3.1). □

In the next section the numerical example illustrating the universality of the inequality (3.1) will be presented.

4. Illustrative examples

Let us start our considerations from the following Stieltjes function:

$$(4.1)\qquad f_0(x) = 1 + \ln(0.5(x+1))$$

having at $x = 0$, 1, 10^3 and 10^6 the truncated power expansions

$$(4.2)\quad \begin{aligned} f_0(x) &= 0.307 + O(x), \\ f_0(x) &= 1 + 0.500(x-1) - 0.125(x-1)^2 + O((x-1)^3), \\ f_0(x) &= 7.21 + 10^{-3}(x-10^3) + O((x-10^3)^2), \\ f_0(x) &= 14.1 + 10^{-6}(x-10^6) + O((x-10^6)^2). \end{aligned}$$

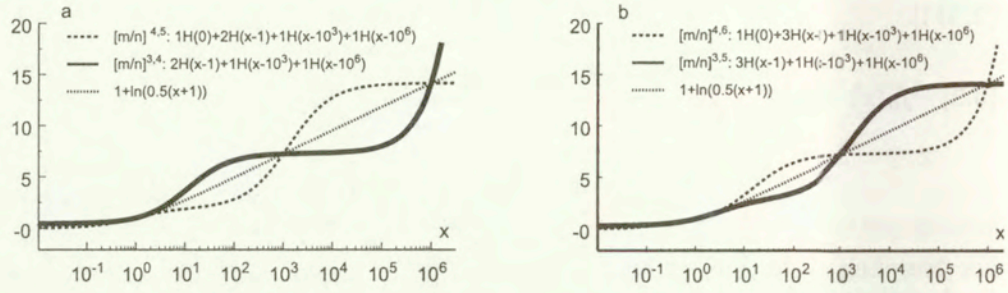

FIG. 1. Three- and four-points Padé approximants to the Stieltjes function $f_0(x) = 1 + \ln(0.5(x+1))$, see Theorem 1.

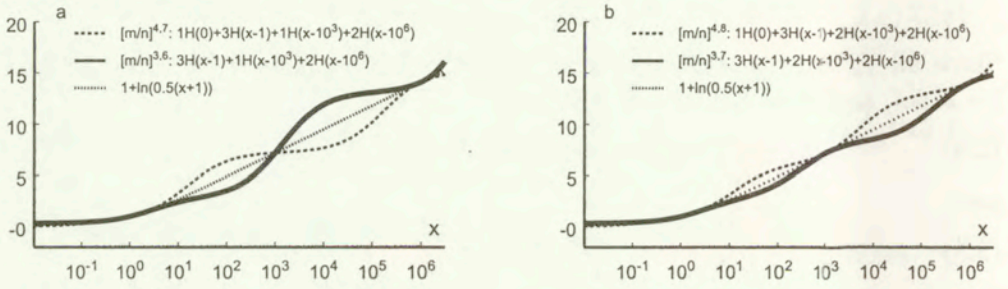

FIG. 2. Three- and four-points Padé approximants to the Stieltjes function $f_0(x) = 1 + \ln(0.5(x+1))$, see Theorem 1.

Evaluated from the input data (4.2), the four-point Padé approximant $[m/n]^{4,4}_{f_0}$, $L(x) = 1H(x) + 1H(x-1) + 1H(x-10^3) + 1H(x-10^6)$, to $1 + \ln, (0.5(x+1))$ takes the form

$$[m/n]^{4,4}_{f_0} = 0.307 + \frac{0.693x}{1} + \frac{0\ .099(x-1)}{1} + \frac{0\ .983 \times 10^{-6}(x-10^3)}{1}. \tag{4.3}$$

The discrete values of $L(x)$, $(-1)^{L(x)} f_0(x)$ and $(-1)^{L(x)}[m/n]^{4,4}_{f_0}(x)$ taken at $x = -0.5,\ 0.5,\ 500,\ 5 \times 10^5,\ 10^8$ are gathered in Table 1. The functions $(-1)^{L(x)} f_0(x)$ and $(-1)^{L(x)}[m/n]^{4,4}_{f_0}$ (see Table 1) satisfy the inequality (3.1). Also the values of $[m/n]^{N,p}_{f_0}$ to $1 + \ln(0.5(x+1))$ presented in Figs. 1 and 2 obey the basic inequality (3.1).

Table 1. The input data $(-1)^{L(x)} f_0(x)$ and $(-1)[m/n]_{f_0}^{4,4}$ for numerical verification of the basic inequality (3.1), where $f_0(x) = 1 + ln(0.5(x+1))$ and $L(x) = 1H(x) + 1H(x-1) + 1H(x-10^3) + 1H(x-10^6)$.

x	-0.5	0.5	500	5×10^4	10^8
$L(x)$	0	1	2	3	4
$(-1)^{L(x)} f_0(x)$	-0.386	-0.712	6.52	-11.1	18.7
$(-1)^{L(x)}[m/n]_{f_0}^{4,4}(x)$	-0.100	-0.672	7.15	-7.61	692

5. Particular cases of the basic inequality

In this section we will discuss the particular cases of the basic inequality (3.1). We start from one-point Padé approximants $[m/n]_{f_0}^{1,p_0}$ to Stieltjes function f_0. For such a case, Theorem 1 reduces to (we recall our choice $x_1 = 0$)

COROLLARY 1. Diagonal and subdiagonal one-point Padé approximants $[m/n]_{f_0}^{1,p_1}$ to power series of Stieltjes

$$f_0(x) = \sum_{k=0}^{\infty} c_k(0) x^k \tag{5.1}$$

with $L(x) = p_1 H(x)$ obey the following inequality:

$$(-1)^{p_1 H(x)} \, [m/n]_{f_0}^{1,p_1}(x) \geq (-1)^{p_1 H(x)} \, f_0(x) \quad \text{in} \quad -\rho < x < \infty. \tag{5.2}$$

For diagonal and subdiagonal one-point Padé approximants the Corollary 1 coincides with Theorem 15.2 proved by BAKER in his book [1].

For two-point Padé approximants $[m/n]_{f_0}^{2,p}$ to the Stieltjes function f_0, the basic Theorem 1 is formulated as follows.

COROLLARY 2. Diagonal and subdiagonal two-point Padé approximants $[m/n]_{f_0}^{2,p}$ to the series of Stieltjes

$$f_0(x) = \sum_{k=0}^{\infty} c_k(0) x^k, \quad f_0(x) = \sum_{k=0}^{\infty} c_k(x_2)(x - x_2)^k \tag{5.3}$$

with $L(x) = p_1 H(x) + p_2 H(x - x_2)$ obey the following inequality:

$$(-1)^{p_1 H(x) + p_2 H(x-x_2)} \, [m/n]_{f_0}^{2,p}(x) \geq (-1)^{p_1 H(x) + p_2 H(x-x_2)} \, f_0(x) \tag{5.4}$$

$$\text{in} \quad -\rho \leq x \leq \infty.$$

Further, if $x_2 \to \infty$ then from Corollary 2 we infer

COROLLARY 3. Let us denote by $[m/n]^{2,p}_{f_0,x_2}$ the two-point Padé approximants at the points $x_1 = 0$ and x_2 to the series of Stieltjes

$$f_0(x) = \sum_{k=0}^{\infty} c_k(0)x^k, \quad f_0(x) = \sum_{k=0}^{\infty} c_k(x_2)(x - x_2)^k \tag{5.5}$$

with $L(x) = p_1 H(x) + p_2 H(x - x_2)$. For $x_2 \to \infty$ these diagonal and subdiagonal two-point approximants have finite limits denoted as follows

$$\lim_{x_2 \to \infty} [m/n]^{2,p}_{f_0,x_2}(x) = [m/n]^{2,p}_{f_0,\infty}(x). \tag{5.6}$$

Moreover, in $-\rho \leq x \leq \infty$ the following inequalities are satisfied:

$$(-1)^{p_1 H(x)} \, [m/n]^{2,p}_{f_0,\infty}(x) \geq (-1)^{p_1 H(x)} \, f_0(x). \tag{5.7}$$

Corollary 3 coincides with Corollaries 4.6 and 4.7 proved by A. BULTHEEL *et al.* in [5] and also with Theorems 5.1 and 5.2 reported by TOKARZEWSKI and TELEGA in [26].

Let us discuss the three-point Padé approximants $[m/n]^{3,p}_{f_0,x_3}$ to f_0 for the case $x_3 \to \infty$. Then Theorem 1 yields:

COROLLARY 4. For $x_3 \to \infty$, the diagonal and subdiagonal three-point Padé approximants $[m/n]^{3,p}_{f_0,x_3}$ to the series of Stieltjes

$$\begin{aligned} f_0(x) &= \sum_{k=0}^{\infty} c_k(0)x^k, \\ f_0(x) &= \sum_{k=0}^{\infty} c_k(x_2)(x - x_2)^k, \\ f_0(x) &= \sum_{k=0}^{\infty} c_k(x_3)(x - x_3)^k, \end{aligned} \tag{5.8}$$

with $L(x) = p_1 H(x) + p_2 H(x - x_2) + p_3 H(x - x_3)$, obey in $-\rho \leq x \leq \infty$ the following inequality:

$$(-1)^{p_1 H(x) + p_2 H(x - x_2)} [m/n]^{3,p}_{f_0,\infty}(x) \geq (-1)^{p_1 H(x) + p_2 H(x - x_2)} f_0(x), \tag{5.9}$$

where

$$\lim_{x_3 \to \infty} [m/n]^{3,p}_{f_0,x_3}(x) = [m/n]^{3,p}_{f_0,\infty}(x). \tag{5.10}$$

Corollaries 4 and 3 coincide with Theorem 10.1 derived by TOKARZEWSKI in [23].

6. Padé approximants application

PERRINS *et al.* [19] investigated numerically and experimentally the effective conductivity ε_{ef} of hexagonal array of cylinders embedded in an infinite matrix (see Fig. 3) as a function of φ and $h = \varepsilon_2/\varepsilon_1$, where φ, ε_1 and ε_2 denote the volume fraction of cylinders and the conductivities of the matrix and inclusions, respectively. It is well known that ε_{ef} has a Stieltjes integral representation, cf. [4] and [10]

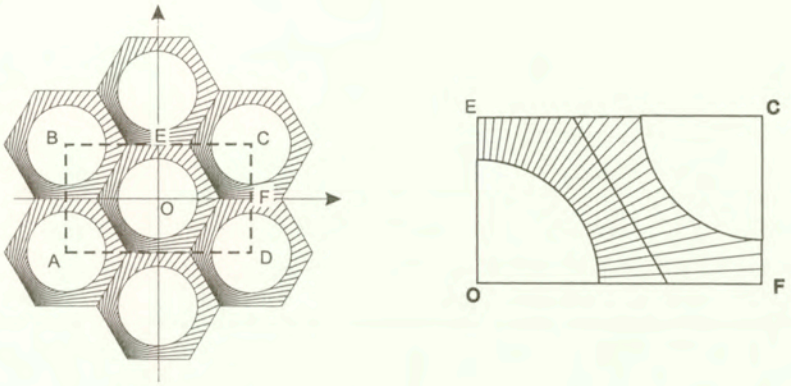

FIG. 3. Hexagonal array of cylinders embedded in an infinite matrix; ABCD-the unit cell, OECF-the sub-unit cell.

$$\frac{\varepsilon_{ef}(h)}{\varepsilon_1} = \frac{\varepsilon_{ef}(0)}{\varepsilon_1} + h\int_0^\infty \frac{d\gamma(u)}{1+hu}. \tag{6.1}$$

From (6.1) it follows that Padé approximants to power expansions of $\varepsilon_{ef}/\varepsilon_1$ satisfy the basic inequality (3.1).

Now we are in a position to recall the experiment performed by PERRINS *et al.* [19], see Fig. 4. The measurements of $\varepsilon_{ef}(h)/\varepsilon_1$ elaborated by these authors allowed to construct the following power expansions of $\varepsilon_{ef}(h)/\varepsilon_1$:

(i) For $\varphi = 0.65$:

$$\begin{aligned} &\frac{\varepsilon_{ef}(h)}{\varepsilon_1} = 0.203 + O(h), \\ &\frac{\varepsilon_{ef}(h)}{\varepsilon_1} = 1 + 0.65(h-1) - 0.114(h-1)^2 + O(h-1)^3, \\ &\frac{\varepsilon_{ef}(h)}{\varepsilon_1} = 4.93 + O(1/h). \end{aligned} \tag{6.2}$$

(ii) For $\varphi = 0.76$:

$$\begin{aligned} \frac{\varepsilon_{ef}(h)}{\varepsilon_1} &= 0.132 + O(h), \\ \frac{\varepsilon_{ef}(h)}{\varepsilon_1} &= 1 + 0.76(h-1) - 0.091(h-1)^2 + O(h-1)^3, \\ \frac{\varepsilon_{ef}(h)}{\varepsilon_1} &= 7.58 + O(1/h). \end{aligned} \tag{6.3}$$

(iii) For $\varphi = 0.80$:

$$\begin{aligned} \frac{\varepsilon_{ef}(h)}{\varepsilon_1} &= 0.203 + O(h), \\ \frac{\varepsilon_{ef}(h)}{\varepsilon_1} &= 1 + 0.80(h-1) - 0.080(h-1)^2 + O(h-1)^3, \\ \frac{\varepsilon_{ef}(h)}{\varepsilon_1} &= 10.34 + O(1/h). \end{aligned} \tag{6.4}$$

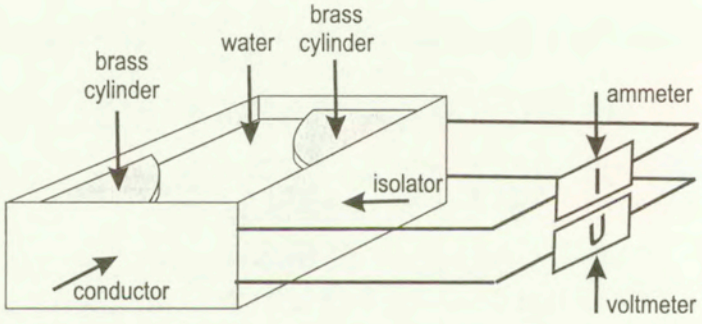

FIG. 4. Scheme of experiment performed by Perrins *et al.* [19] for the sub-unit cell of hexagonal array of cylinders, cf. Fig. 3.

The coefficients of (6.2), (6.3) and (6.4) are obtained by experimental measurements of the electrical potentials and the electrical currents appearing in the two-phase system shown in Fig. 4.

The multipoint Padé approximants $[2/2]^{3,4}$ (solid line) and $[1/1]^{1,2}$ (dashed lines) have been evaluated to "experimental" power expansions of $\varepsilon_{ef}/\varepsilon_1$ represented by series (6.2)-(6.4), see Fig. 5. According to Theorem 1 those series form the upper and lower bounds on the effective conductivity $\varepsilon_{ef}/\varepsilon_1$ of hexagonal array of cylinders, respectively. The theoretical conductivity $\varepsilon_{ef}/\varepsilon_1$ evaluated in [19] is also shown in Fig. 5 for comparison.

7. Final remark

A new basic inequality (3.1) for diagonal and subdiagonal multipoint Padé approximants $[m/n]_{f_0}^{N,p}$ to a Stieltjes function $f_0(x)$, $-\rho \leq x \leq \infty$, has been derived. This inequality generalizes the previous ones formulated for one-, two-, and three- point Padé approximants $[m/n]_{f_0}^{N,p}$ to f_0.

The transport coefficients such as thermal conductivity, magnetic permeability, dielectric constant, diffusion coefficient, have Stieltjes integral representation. On account of that, inequality (3.1) yields upper and lower bounds on the transport moduli of macroscopically isotropic two-phase media, cf. [24] and [27]. They are the most general bounds reported until now in both the mathematical and mechanical literature and can also be used to the study of bone torsion, cf. [25].

Multipoint Padé approximants approach presented in this paper is particular useful for the prediction of the effective moduli of inhomogeneous two-phase media from both the theoretical and experimental data, cf. Fig. 5.

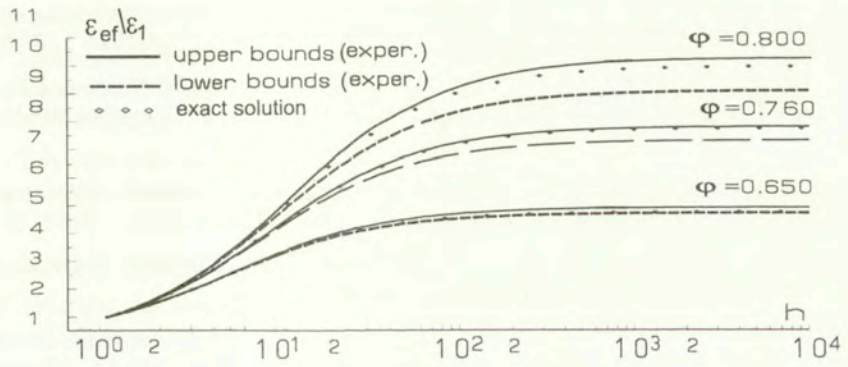

FIG. 5. The multipoint Padé approximants $[2/2]^{3,4}$(solid line), $[1/1]^{1,2}$(dashed lines) to the "experimental" power expansions of $\varepsilon_{ef}/\varepsilon_1$ given by (6.2)-(6.4) and the theoretical power expansion of $\varepsilon_{ef}/\varepsilon_1$ (scattered line) reported in [19].

Acknowledgement

The authors would like to thank CNRS and Polish Academy of Sciences for the financial support of this work within the framework of the French-Polish Project 9330. The first two authors were also supported by the State Committee for Scientific Research (KBN, Poland) through the Grants No 8 T07A 052 21 and No 8 T11F 017 18.

References

1. G. A. BAKER JR., *Essentials of Padé approximants*, Acad. Press, London 1975.
2. G. A. BAKER JR. and P.GRAVES-MORRIS, *Padé approximants*, Cambridge University Press, second edition, 1996.
3. D. J. BERGMAN, *The dielectric constant of a composite material- A problem in classical physics*, Phys. Report., **C43**, 377-407, 1978.
4. D. J. BERGMAN, *Bounds for the complex dielectric constant of a two-component composite material*, Phys. Rev. B, **23**, 3058-3065, 1981.
5. A. BULTHEEL, P. GONZÁLES-VERA and R.ORIVE, *Quadrature on the half-line and two-point Padé approximants to Stieltjes functions. Part I. Algebraic aspects*, J. of Comp. Appl. Math, **65**, 57-72, 1995.
6. J. GILEWICZ, *Approximants de Padé*, Lecture Notes in Mathematics vol. **667**, Springer Verlag, 1978.
7. J. GILEWICZ and A. P. MAGNUS, *Inverse Stieltjes iterates and errors of Padé approximants in the whole complex plane*, J. Comput. Appl. Math. **49**, 79-84, 1993.
8. J. GILEWICZ and A. P. MAGNUS, *Optimal inequalities of Padé approximants errors in the Stieltjes case: closing result*, Integral Transforms and Special Functions **1**, 9-18, 1993.
9. J. GILEWICZ, M. PINDOR, J. J. TELEGA and S. TOKARZEWSKI, *Continued fractions, two-point Padé approximants and errors in the Stieltjes case*, J. Comp. Appl. Math. (to appear).
10. K.GOLDEN and G. PAPANICOLAOU, *Bounds for effective parameters of heterogeneous media by analytic continuation*, Com. Math. Phys., **90**, 473-491, 1983.
11. P.GONZALEZ-VERA and O.NJÅSTAD, *Convergence of two-point Padé approximants to series of Stieltjes*, J. of Comp. Appl. Math., **32**, 97-105, 1990.
12. W. B. GRAGG, *Truncation error bounds for T-fractions*, [in:] Approximation Theory III, E. W. CHENEY [Ed.] 455-460, Academic Press, New York 1980.
13. Z. HASHIN and S. SHTRIKMAN, *A variational approach to the theory of the effective magnetic permeability of multiphase materials* J. Appl. Phys. Sol., **33**, 3125-3131, 1962.
14. W. B. JONES, O.NJÅSTAD and W. J. THRON, *Two-point Padé expansions for a family of analytic functions*, J. Comp. Appl. Math., **9**, 105-123, 1983.
15. W. B. JONES and W. J. THRON, *Continued fraction analytic theory and its applications*, Encyclopedia of Mathematics and its Applications, Vol. **11**, Addison-Wesley Publ. Co., London 1980.
16. L. LORENTZEN and H. WAADELAND, *Continued Fraction with Applications*, [in:] Studies Computational Mathematics 3, C. BREZINSKI and L. WUYTACK [Eds.] Elsevier Science Publishers 1992.
17. G. W. MILTON, *Bounds on the complex permittivity of a two-component composite material*, J. Appl. Phys., **52**, 5286-5293, 1981.
18. G. W. MILTON, *Bounds on the transport and optical properties of a two- component composite material*, J. Appl. Phys., **52**, 5294-5304, 1981.

19. W. T. PERRINS, D. R. MCKENZIE and R. C. MCPHEDRAN, *Transport properties of regular array of cylinders*, Proc. R. Soc. Lond. A **369**, 207-225, 1979.

20. R. C. MCPHEDRAN and G. W. MILTON, *Bounds and exact theories for the transport properties of inhomogeneous media*, Appl. Phys. A, **26**, 207-220, 1981.

21. J. J. TELEGA, S. TOKARZEWSKI and A. GAŁKA, *Modelling torsional properties of human bones by multipoint Padé approximants*, [in:] Numerical Analysis and its Application, L. VULKOV, J. WAŚNIEWSKI and P. YALAMOV [Eds.], 741-748, Springer-Verlag, Berlin 2001.

22. S. TOKARZEWSKI, *Two-point Padé approximants for the expansion of Stieltjes functions in a real domain*, J. Comp. Appl. Math, **67**, 59-72, 1996.

23. S. TOKARZEWSKI, *N-point Padé approximants to real valued Stieltjes series with nonzero radii of convergence*, J. Comp. Appl. Math, **75**, 259-280, 1996.

24. S. TOKARZEWSKI, A. GAŁKA and I. ANDRIANOV, *Bounds on the effective transport coefficients of two-phase media from discrete theoretical and experimental data*, Comp. Assis. Mech. and Eng. Sc., **4**, 229- 241, 1997.

25. S. TOKARZEWSKI, J. J. TELEGA and A. GAŁKA, *Torsional rigidities of cancellous bone filled with marrow: The application of multipoint Padé approximants*, Engineering Transactions **49**, 135-153, 2001.

26. S. TOKARZEWSKI and J. J. TELEGA, *Inequalities for two-point Padè approximants to the expansions of Stieltjes functions in a real domain*, Acta Applicandae Mathematicae, **48**, 285-297, 1997.

27. S. TOKARZEWSKI and J. J. TELEGA, *Bounds on effective moduli by analytical continuation of the Stieltjes function expanded at zero and infinity*, Z. angew. Math. Phys. **48**, 1-20, 1997.

28. H. S. WALL, *Analytic theory of continued fractions*, Van Nostrand, New York 1948.

29. O. WIENER, *Abhandlungen der mathematisch-physischen Klasse der Könighlichen Sachsischen Gesellschaft der Wissenschaften*, Abh. Sächs. Akad. Wiss. Leipzig Math.- Naturwiss. Kl., **32**, 509, 1912.

Received December 3, 2001; revised version January 31, 2002.

Arch. Mech., **54**, 2, pp. 155–174, Warszawa 2002

Experimental study of a PA66 solid polymer in the case of cyclic shear loading

G. BLES[1], S.P. GADAJ[2], W.K. NOWACKI[2], A. TOURABI[1]

(1) *Laboratoire Sols Solides Structures, Domaine Universitaire, B.P. n° 53, 38041 Grenoble cedex 9, France*

(2) *Center of Mechanics and Information Technology, Institute of Fundamental Technological Research, Polish Academy of Sciences, Świętokrzyska 21, 00-049 Warsaw, Poland*

EXPERIMENTAL MECHANICAL RESULTS concerning cyclic shear tests without lateral force and simple shear tests with measurement of temperature, performed on sheet samples of PA66 polyamide, are presented. These tests are performed using special shear devices, attached to a classical tensile testing machine. The aim of our work was the examination of thermomechanical characteristics of solid polyamide during shear loading. This study allowed us to analyse the changes of the stress and strain characteristics, shear modulus, ratcheting, relaxation effects and thermomechanical effects.

1. Introduction

SINCE THE BEGINNING of the twentieth century, it is an established fact that the mechanical behaviour of solid materials under rotational loading shows second-order effects [1,2]. Thus, during torsion of a wire, a bar or a tube, we measure the variation in the axial strain if the axial load is kept equal to zero [3], and a variation in the axial load if the axial strain is kept equal to zero [4]. When the rotational loading is cyclic, these effects accumulate and show a phenomenon of ratchet [5]. The experimental study of this phenomenon gives essential information to make theoretical choices about the second-order tensorial coupling effects of the ratchet type. These effects are very sensitive to the definition of Preferred Reference Frames spins [6,7]. The present work is a preliminary study in order to find the generic parts of the thermomechanical behaviour of the PA66 polyamide during the rotational loading of shear.

Two types of shear devices were used. The first one allows the shear tests without lateral force in order to characterise the mechanical behaviour during cyclic shear tests, relaxation and creep tests. The first and the second-order effects were observed. The second device performs a simple shear test with

a measurement of temperature. An infrared thermovision camera was used. The thermomechanical effects were observed.

This paper presents at first the experimental facilities used; we explain the principle of the shear devices with which a classical tensile machine can make the shear test. The material and the shear samples are presented. A local strain measure was done in a homogeneous area of the sample. Secondly, we present the results of these tests. During symmetric cyclic shear tests with several amplitudes, the shear stress and strain were observed. Then, the evolution of the second-order effects or ratchet during these cyclic shear tests is presented. Tests with relaxations and creeps show specific evolution of the first and second-order effects. During the simple shear tests, thermomechanical coupling was examined.

2. Experimental facilities and methods

2.1. Shear device without lateral force

The cyclic shear is obtained using a device allowing to change the tension-compression mode of loading into cyclic shear mode of loading [9]. This shear device is essentially composed of a very rigid frame consisting of a rectangular box, inside which vertical and a horizontal carriages move (Fig.1). The device is attached to a classical tensile testing machine by means of a fixed and a moving grip. The horizontal carriage is capable of performing vertical and horizontal translations, in the plane of shear. The sample is connected to the apparatus, between the frame and the horizontal carriage, by two clamping devices.

The vertical translation of the moving grip imposes the shear motion on the sample; the horizontal translation is free of load and allows a shear with no lateral force, like the simple torsion test tube without axial force [10]. These two translations are obtained using two pairs of linear guides located symmetrically with respect to the horizontal and vertical carriages. To obtain a shear test as correct as possible, we control the mechanical clearance for each pair of linear guides by using two adjustable looseness devices. The aim of this adjustment is an ideal situation of motion without friction and slack. This adjustable looseness device avoids an excessive friction, which hampers the shear test and its measurement. This device avoids mechanical clearances too, which are not convenient for the shear test while the machine load is changing from tension to compression. The shear device is fitted on the testing machine with a counterweight. Thus, in addition to the mobility of the horizontal carriage, it is possible to clamp the sample without any stress. Moreover, the dimensions of the shear device were overestimated toward the effective loading, in order to get a high stiffness for an allowed shear force of 25 KN [9].

The principle of this present device differs from other shear devices [11,12] because it can perform a shear in which the lateral load is equal to zero. During the shear, the horizontal carriage movement free of load makes the lateral strain ratchet possible. The measure of this displacement during cyclic shear gives interesting information. Using this device, the characterisation of material's behaviour is more precise owing to the measure of both the main and the second-order effects.

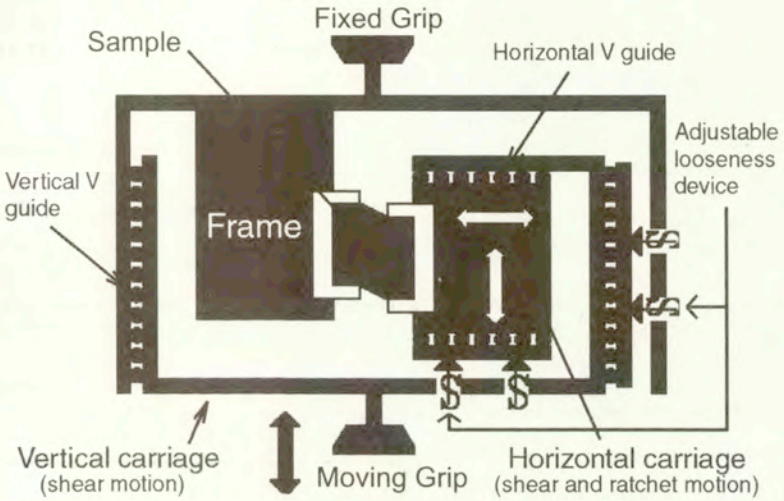

FIG. 1. Principle of the shear device without lateral force.

2.2. Simple shear device with measurement of temperature

The simple shear was made in a specially designed grip, transforming the compression into a simple plain shear. Construction of this arrangement practically eliminates sliding of the specimen in the grip and ensures that the process of shear takes place on two parallel shear bands of the specimen [13]. This grip was fitted in the testing machine.

During the deformation, the load, displacement and the distribution of infrared radiation emitted by shear paths are continuously registered. The infrared radiation is measured using the thermovision camera [13].

The distribution of intensity of the infrared radiation, recorded during investigation in a digital form, allows us to reconstruct thermal pictures (thermograms) of the specimens. In Fig. 2, an example of a thermogram of the shear zones of the deformed specimen is shown.

After measurement on each of the sheared paths of the thermogram, the central line along the shear direction is drawn (Fig. 2). The temperature changes are found as average values of the temperature along these lines.

The mean-square error of temperature evaluation, obtained in this way, is 0,2 / 0,3 K.

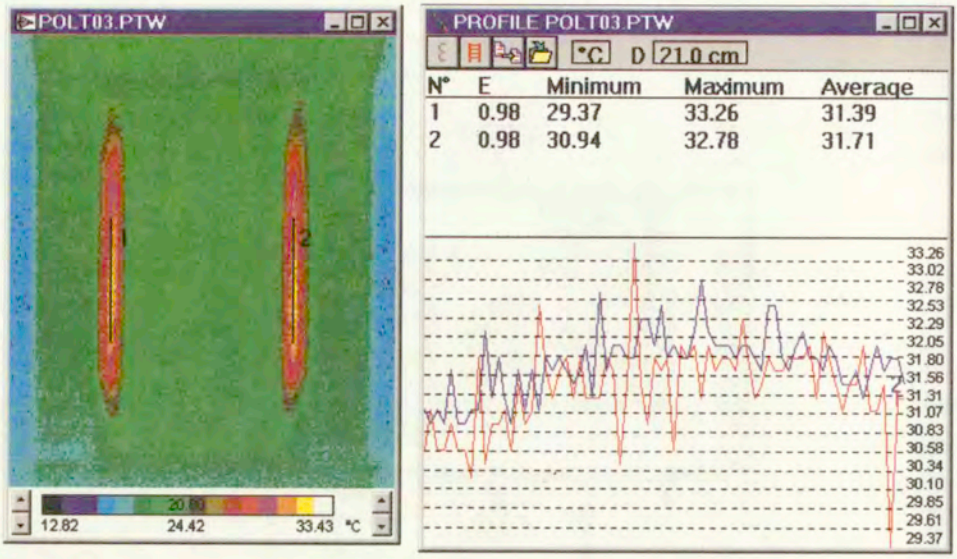

FIG. 2. Example of a thermogram obtained during simple shear tests.

2.3. Edge effects

The shear test has several advantages from the fundamental point of view and the experimental point of view. Nevertheless, it has a disadvantage because of its principle; the shear stress field is heterogeneous along the shear band. Actually, the shear stress is constant inside the $\alpha\beta\chi\delta$ zone in the middle of the sample (Fig. 3a), but it vanishes at the two free ends of the sample at points A, B, C and D. The equilibrium of this $\alpha\beta\chi\delta$ element, in the sheared zone, requires that shear stresses on perpendicular faces should be equal in magnitude and have directions such that the resulting moment acting on the element is balanced. This property is the result of Cauchy's principle of reciprocity of shear stress. On the edges AB and CD, the stress at these sides is equal to zero. So, the shear stress field is not homogeneous in the αABβ and χCDδ zones, near the ends of the sample. In order to reduce the effect of the edge heterogeneity, we choose usually the shear band height greater than ten times its width: $H/B > 10$ [13, 14].

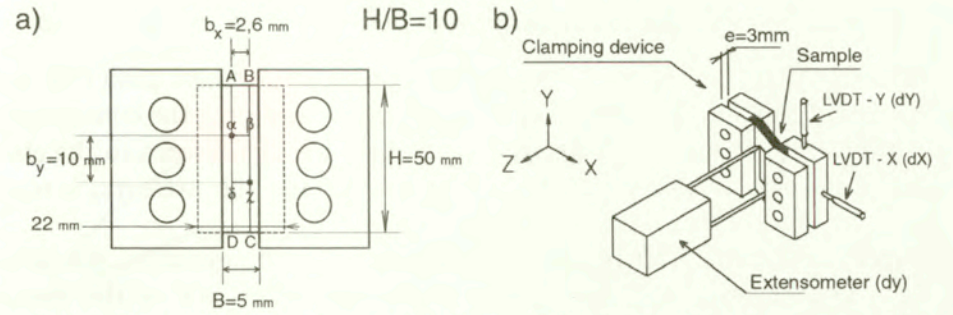

FIG. 3. (a) dimensions of the shear sample clamped, (b) global and local measures of the two shear strains.

2.4. Studied material and shear samples

The material is the polyamide PA66, that is a semicrystalline thermoplastic polymer. Differential Scanning Calorimetry (DSC) method gives the glass transition temperature T_g, the melting temperature T_m and the percentage of crystallinity C. Supposing a normal distribution, we determine the mean value $<x>$ of T_g, T_m and C as well as the standard deviation σ_x of the n individual values distribution, and $\sigma_{<x>}$ of the mean value distribution (Table 1).

Table 1. Glass transition, melting temperatures and percentage of crystallinity of sample's material (PA66).

Measure	$< x >$	$+/- 2\ \sigma_{<x>}$
T_g	51.8 °C	+/- 1.9 °C
T_m	263.6 °C	+/- 1.7 °C
C	34.7 %	+/- 3.5 %

The investigations were performed on PA66 sheet samples. Thickness e of these samples is 3 mm. The overall dimensions of the samples used with the shear device without lateral force are 50 mm x 22 mm x 3 mm (Fig. 3). The dimensions of the samples used with the simple shear device are 30 mm x 42,3 mm x 3 mm. The dimensions of the shear band in the two cases are :

- shear device without lateral force; $H = 50$ mm, $B = 5$ mm, $e = 3$ mm,
- simple shear device; $H = 30$ mm, $B = 3$ mm, $e = 3$ mm.

Then two conditions for the shear tests are satisfied [1]:

- the ratio of B to e (B/e=1,66 and B/e=1) is small enough to avoid buckling of the sheared zone,
- the ratio of H to B (H/B=10) is great enough to minimise the error due to non-homogeneity of the shear stress and strain at the two free ends.

2.5. Principles of stress and strain measurements

Assuming that there is no change in the cross section of shear path [3], and assuming that the ratio H/B equal to 10 is sufficient concerning the homogeneity of stress field, we can obtain the stress σ_{xy} as the ratio of the force to the cross section. In the case of a shear device without lateral force, the stress σ_{xx} is equal to zero.

During the simple shear tests with measurement of temperature, the strain ε_{xy} was obtained classically from the relative displacement dY of the clamps and the width B of the shear band:

$$\varepsilon_{xy} = dY/2B. \tag{2.1}$$

During the shear tests without lateral force, values ε^g_{xy} and ε^g_{xx} of the strains ε_{xy} and ε_{xx} were obtained from the relative displacement of the clamps, dX and dY (Fig. 3b). These measures are called global, as opposed to the local strain measure performed by means of an extensometer (Fig. 3b) in an area in the middle of the shear sample. ε^g_{xy} and ε^g_{xx} were not calculated classically using the width of the shear band, but with a corrected value of this width, called B_g:

$$\varepsilon^g_{xy} = dY/2B_g, \quad \varepsilon^g_{xx} = dX/B_g. \tag{2.2}$$

This value B_g was obtained by comparison (Fig. 4c) of the measure Y and a measure ε_{xy} realised locally by the extensometer (Fig. 3b) ; $B_g = 6{,}49$ mm. This value is greater than the width of the shear band $B = 5$ mm; in fact, a small slide of the sample inside the clamps occured as it was observed on the clamp impression on the sample, which is bell-shaped over a distance of 1 mm from the clamp edge; $B + 1$ mm $+ 1$ mm $= 7$ mm $\sim B_g$.

A special extensometer allowed us to measure the shear strain ε_{xy} in a local area in the middle of the sample; the $\alpha\beta\chi\delta$ rectangle in the Fig. 3a. Assuming the strain homogeneity in this reference rectangle, this value ε_{xy} was obtained from the relative displacement dy (Fig. 3b), given by the extensometer, and the initial width b_x (Fig. 3a) of the $\alpha\beta\chi\delta$ area:

$$\varepsilon_{xy} = dy/2b_x. \tag{2.3}$$

The necessity of local strain measurement is fully justified in the case of metallic materials (Fig. 4b) [9]. We can compare the measure Y of relative displacement of the clamps and the local strain measure ε_{xy} in the Fig. 4d; a large hysteresis loop appears in the Y-ε_{xy} graph. In the case of PA66 polyamide, the thickness of the loop is smaller. It indicates that clamping of the polyamide sample is more efficient and the sliding zone under the clamps is smaller than that in the case of metallic samples.

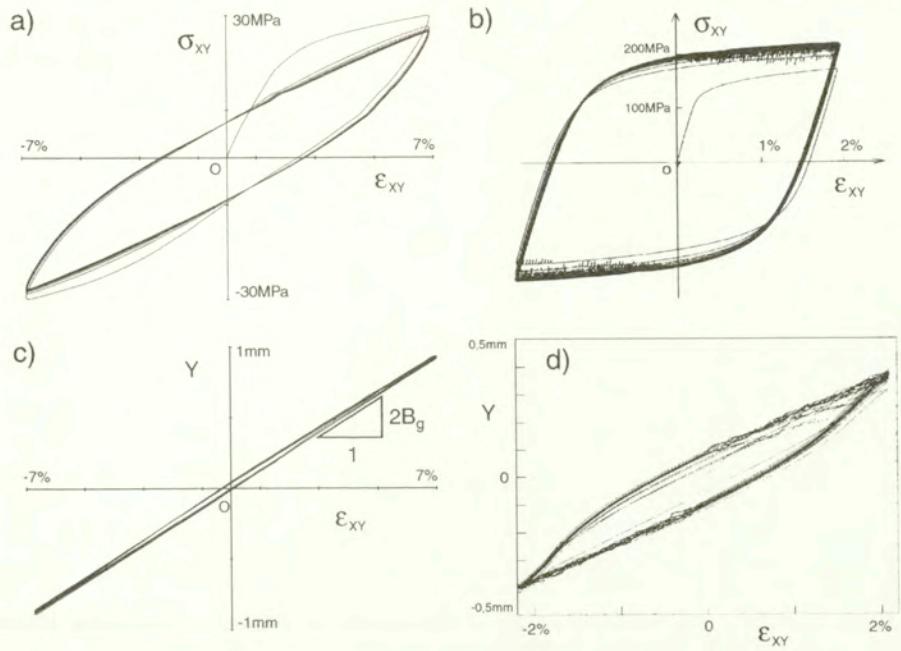

FIG. 4. (a,c) cyclic shear of a polyamide PA66 sample, (b,d) cyclic shear of a metallic sample [9].

3. Results and discussion

This section presents first (Secs. 3.1, 3.2, 3.3, and 3.4) the experimental results obtained with the shear device without lateral force. Secondly Sec. 3.5, the thermomechanical results obtained by the simple shear device with measure of temperature are presented.

3.1. Cyclic shear at constant intensity of strain rate

Two kinds of cyclic shear test at constant intensity of strain rate ($\dot{\varepsilon}_{xy} = 1,1.10^{-3}s^{-1}$) were performed; one with decreasing and one with increasing amplitudes of cycles (Fig. 5a and 5b, respectively). Elastic (or highly-elastic) hysteresis-type behaviour with transient hardening effect during the first loading and weak softening during the cyclic path is observed.

The evolution diagram of the shear stress at the reversal points (Fig. 5c) shows that the saturation values seem to be independent of the history of the cycle amplitudes; increasing and decreasing amplitudes of the cycle do not change the stress saturation value of the cyclic softening.

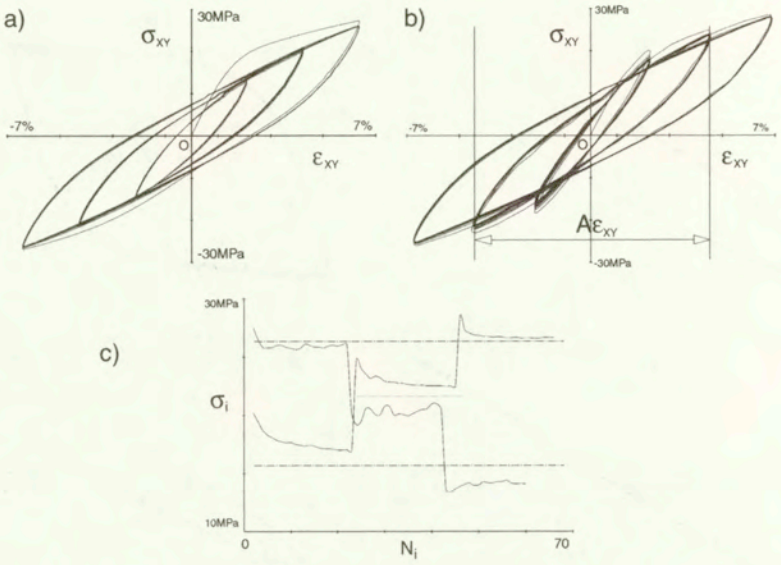

FIG. 5. (a) cyclic shear at decreasing amplitudes and (b) at increasing amplitudes, (c) shear stress at the reversal points during the tests of the Figs. 5a and 5b.

The shear modulus μ was determined by separating the stress-strain curve in loading branches, starting at the origin or at the inversion state (Fig. 6a). The experimental data were transformed in the loading branch space by the co-ordinates (Fig. 6b):

$$\Delta\sigma_{xy} = \sigma_{xy} - {}_R\sigma_{xy}, \quad \Delta\varepsilon_{xy} = \varepsilon_{xy} - {}_R\varepsilon_{xy} \tag{3.1}$$

where: ${}_R\sigma_{xy}$ and ${}_R\varepsilon_{xy}$ were the reference "R_i" co-ordinates of each "i" loading branch. The slope M_μ

$$M_\mu = \frac{1}{2}\left(\frac{d(\Delta\sigma_{xy})}{d(\Delta\varepsilon_{xy})}\right) = \frac{1}{2}\frac{d\sigma_{xy}}{d\varepsilon_{xy}} \tag{3.2}$$

was determined by a spline technique; Fig. 6c.

The shear moduli μ and $\hat{\mu}$ are the slopes at the beginning and at the end of each branch (Fig. 7a):

$$\mu = \lim_{\Delta\varepsilon\to 0} M_\mu, \quad \hat{\mu} = \lim_{\Delta\varepsilon\to\infty} M_\mu \tag{3.3}$$

The distinction between the initial modulus μ and the residual modulus $\hat{\mu}$ evolution during cyclic test is shown in Figs. 7b and 7c. These figures show plainly a transient stage followed by a saturation; according to the modulus μ, the transient stage occurs until the fifth reversal point or during the first two cycles,

whereas the transient stage of the modulus $\hat{\mu}$ is finished at the third reversal point or after the first cycle.

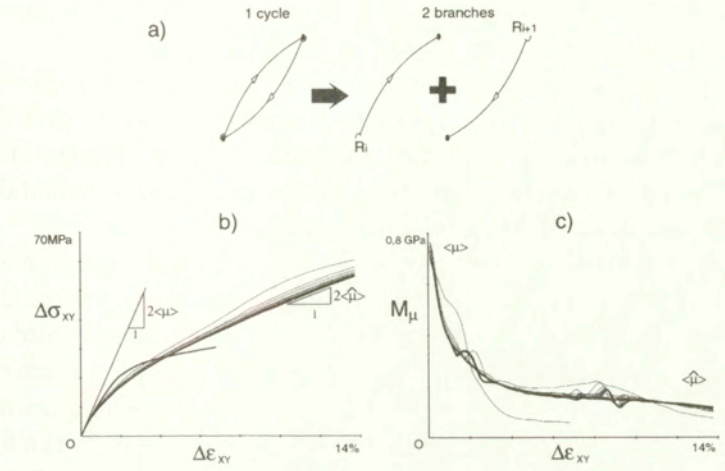

FIG. 6. (a) definition of a branch in a cycle and its reference state "R_i", (b) branches during the cyclic shear test given by the Fig. 4a, (c) shear modulus in the branches at the Fig. 6b.

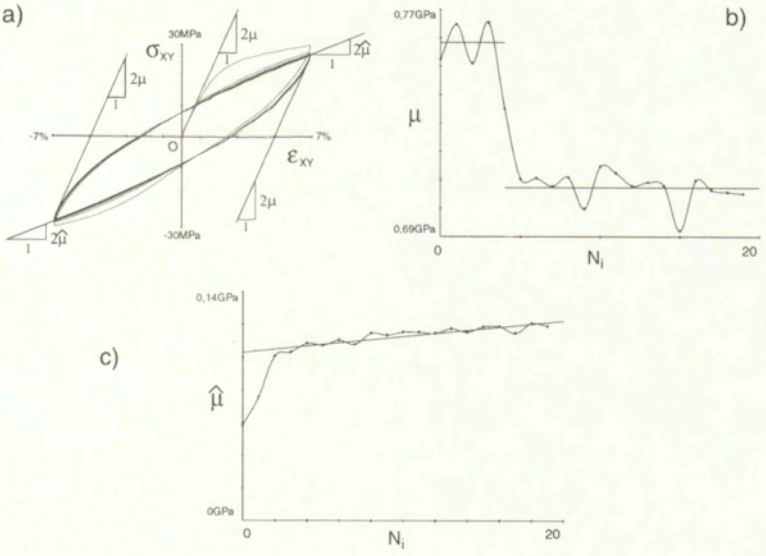

FIG. 7. (a) definition of the shear moduli μ and $\hat{\mu}$, (b) variations of the initial shear modulus μ, (c) variations of the residual shear modulus $\hat{\mu}$.

3.2. Second-order effects

A simple shear with no lateral force leads also to a lateral deformation, which is a lengthening. This is the second-order effect of the shear, comparable to the axial deformation of a torsion test with no axial force [2].

The evolution of lateral deformation versus shear strain for the cyclic tests with decreasing and increasing amplitudes is shown in Figs. 8a and 8b, respectively. This lateral deformation is very small in comparison with the shear strain, but it is not possible to neglect it since this deformation accumulates during cyclic loading and leads to a ratchet phenomenon.

The lateral ratchet evolution can be displayed by the evolution of the lateral strain at the reversal point of each loading branch $\varepsilon_{xx}^{g\,i}$ versus the loading branch number N_i. This is shown in the Fig. 8c for the tests with decreasing and increasing amplitudes of shear cycles. The evolution of the ratcheting effect depends on the order (increasing or decreasing) of the cycle amplitude. But, at the end of these two tests, at about the sixtieth reversal point in the Fig. 8c, the reached ratchet value is the same for these two orders of cycle amplitude. Then, we can say that the ratchet, reached after a series of cyclic tests with different amplitudes, is independent of the order of tests of this series.

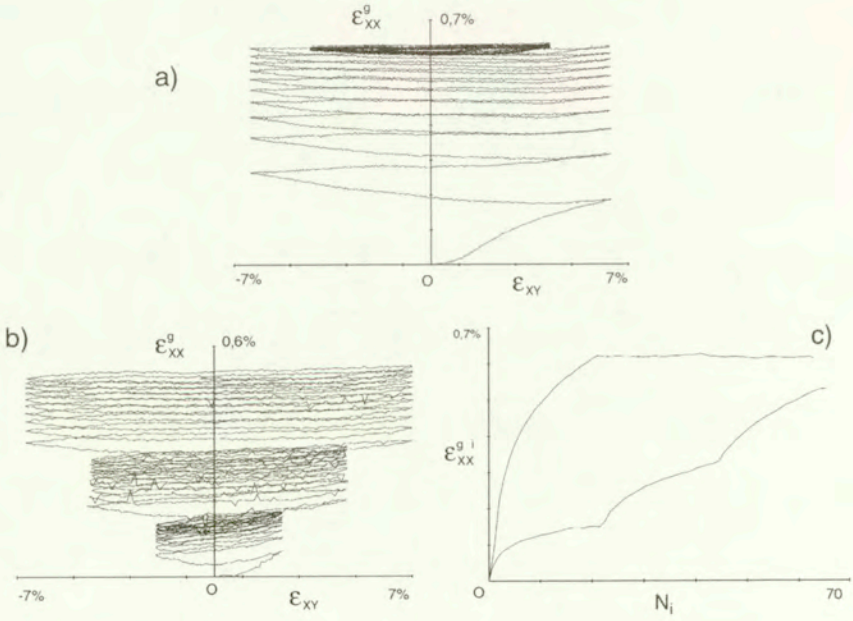

FIG. 8. (a) second-order effect during the shear test with decreasing amplitudes (Fig. 5a), (b) second-order effect during the shear test with increasing amplitudes (Fig. 5b), (c) lateral strain at the reversal point during the shear tests with decreasing and increasing amplitudes.

The ratchet intensity may be characterised by the ratio K of the amount of the ratchet per cycle:

$$K = \Delta\varepsilon^g_{xx}/A\varepsilon_{xy}, \tag{3.4}$$

where $\Delta\varepsilon^g_{xx}$ is the ratchet amplitude per cycle and $A\varepsilon_{xy}$ – the shear strain amplitude of the cycles. For a given shear strain amplitude $A\varepsilon_{xy}$, the ratio K systematically diminishes with the number of cycles, from an initial value $K_{(1)}$ defined in the beginning of cyclic sequence, to a final value $K_{(2)}$ defined at the end of the cyclic sequence. Figure 9a illustrates the variations of the rate of the ratchet $\Delta\varepsilon^g_{xx(1)}$ and $\Delta\varepsilon^g_{xx(2)}$, at the beginning and the end of two cyclic sequences $A\varepsilon^{\mathrm{I}}_{xy}$ and $A\varepsilon^{\mathrm{II}}_{xy}$ $(A\varepsilon^{\mathrm{I}}_{xy} < A\varepsilon^{\mathrm{II}}_{xy})$, which correspond respectively with the definition of the ratios $K_{(1)}$ and $K_{(2)}$, for each of the two amplitudes. In the Fig. 9b are shown changes of the values $K_{(1)}$ and $K_{(2)}$ as a function of $A\varepsilon_{xy}$ obtained for three samples tested with three different shear strain amplitudes, and in the Fig. 9c those obtained for only one sample tested with three increasing amplitudes of cycles. In the first case, the initial value $K_{(1)}$ increases monotonously versus the shear amplitude and the value $K_{(2)}$ is almost in a steady state. In the second one, when the shear strain amplitude increases, using the same sample, we observe a strong decrease in $K_{(1)}$. This result shows the influence of the succession of the cyclic sequences at increasing shear strain amplitudes over the variations of the ratio K, which characterises the amount of the ratchet per cycle.

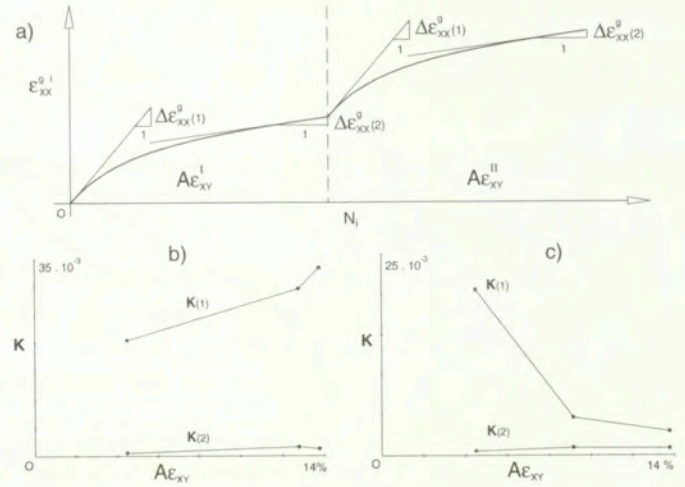

FIG. 9. (a) illustration of the rate of variation of the lateral strain at the beginning and the end of two cyclic sequences $(A\varepsilon^{\mathrm{I}}_{xy} < A\varepsilon^{\mathrm{II}}_{xy})$, (b) rate K of variation of the lateral strain during cyclic shear tests at three amplitudes on three samples, (c) rate K of variation of the lateral strain during one cyclic shear test at three increasing amplitudes on the same sample.

3.3. Relaxation effects

To study the relaxation effects, a strain-controlled test with a constant intensity of strain rate was performed. This test contains two parts:

- In the first one (Fig. 10a), the sample was submitted to a symmetric cyclic loading through ten cycles. During this preliminary cyclic shear, the quasi-stabilised state was reached, what is indicated by stress at the reversal point of cycles (Fig. 10c).
- In the second one (Fig. 10b), only one cycle was performed endowed with relaxation sequences in several points, with the unique duration of 300 seconds. In the $\sigma - \varepsilon$ diagram, the relaxation sequences are pointed by AB, CD, EF, GH and IJ.

A comparison of the $\sigma - \varepsilon$ diagrams of these parts are shown in the Fig. 10d. In first step of the test, we can observe a transient hardening effect during the first cycle loading, and stabilisation in the successive step. During the cycle with the relaxation sequences, the $\sigma - \varepsilon$ hysteresis loop becomes distanced from this stabilised cycle. We observe a hardening phenomenon during this cycle, after the relaxation sequences, very close to the first loading.

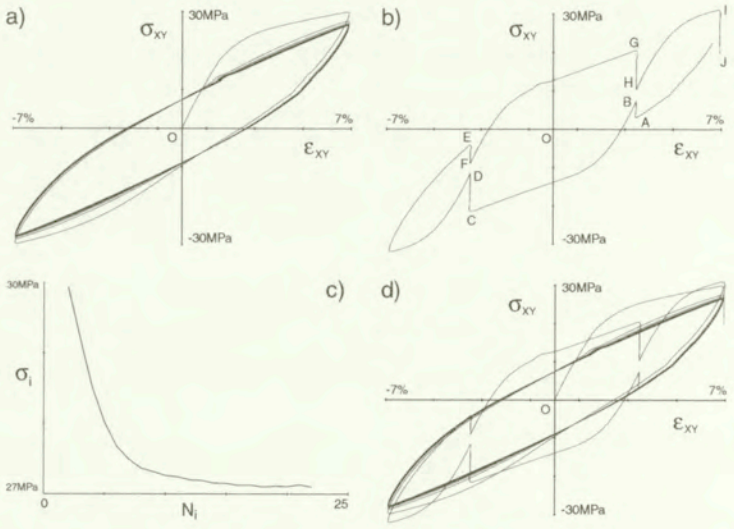

FIG. 10. (a) cyclic symmetric shear test, (b) one cycle with relaxations during 300 seconds, (c) variations of the shear stress at the reversal point during the cyclic shear test (Fig10a), (d) comparison of the cyclic shear test to the cycle with relaxations.

The relaxation effects could be shown from the second-order point of view (Fig. 11). During the first part of the test (ten symmetric cycles), the ratchet evolution is classic (Fig. 11a and 11b). The ratchet intensity increases quickly at

the beginning of the test and seems to tend to a stabilisation value at the end. During the relaxation sequences of the last cycle, a sharp drop in ratchet intensity occurs (Fig. 11c and 11d); and regardless of the position of the relaxation sequence in the cycle.

It should be noted that the drop of the ratchet intensity during relaxation seems to be related to the viscous phenomenon: two ratchet relaxations in the same branch seem, indeed, to have the same saturation threshold (AB and CD or EF and GH in the Fig. 11d).

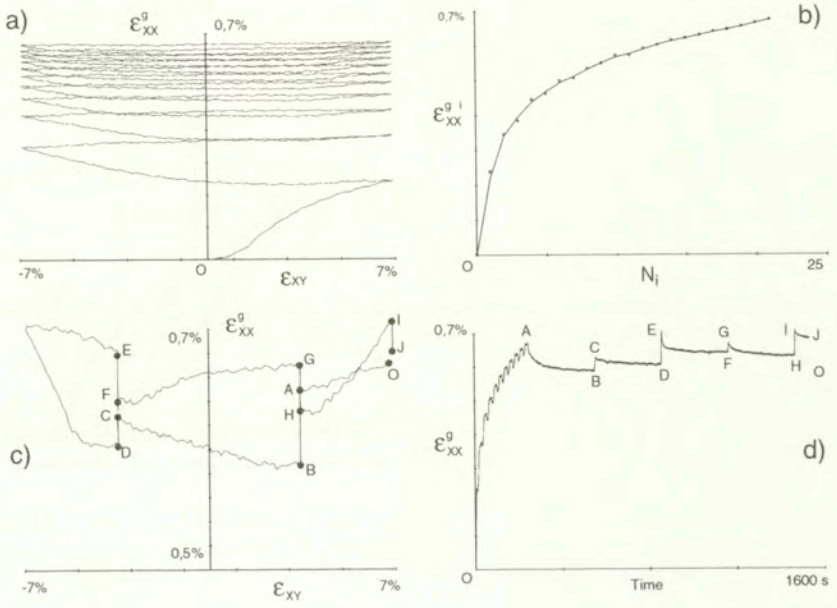

FIG. 11. Second-order effect (a,b) during the cyclic symmetric shear test of the Fig. 10a, and (c,d) during the cycle with relaxations (Fig. 10b).

The stress, during the relaxation sequences, increases or decreases according to the position of the relaxation in the $\sigma - \varepsilon$ hysteresis loop (Fig. 12a). It has a sign opposite to the stress rate in the $\sigma - \varepsilon$ cycle before relaxation.

During relaxation, the variation in stress could be analysed as the evolution of the stress value as a function of time (Fig. 12b). The existence of three main stages is observed: at first, the stress increases and decreases quickly during a few seconds (stage I), in the next (stage II), the evolution of the stress is cut down and we can observe a saturation state in stage III.

To compare the stress and ratchet evolution during relaxation sequence, for example EF, we use a norm by values of stress and lateral strain in the saturation state: $\frac{\varepsilon^g_{xx}}{\varepsilon^{g\,\infty}_{xx}}$ and $\frac{\sigma}{\sigma^\infty}$ (Fig. 12c). Their comparison shows already the connection

between the decrease of ratchet intensity and the stress evolution during the relaxation due to the viscous phenomena.

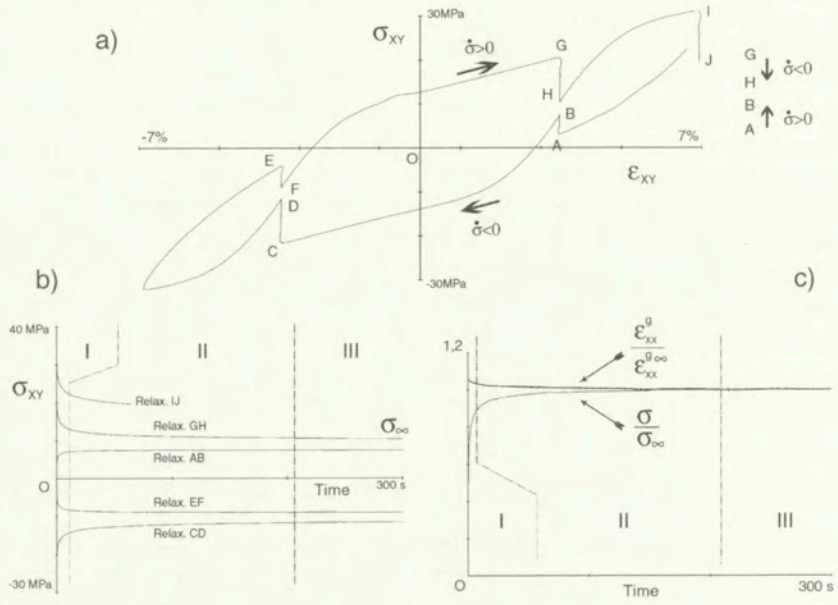

FIG. 12. Variations of the shear stress (a,b) during the relaxations, and (c) comparison of the stress variations to the lateral strain variations during the EF relaxation.

3.4. Creep effects

To observe the creep effects during cyclic shear, a stress-controlled test with a constant intensity of stress rate was performed. This test has two parts (Fig. 13):

- At first the sample was submitted to an asymmetric cyclic loading (OA in Fig. 13a), next two cyclic creep sequences AB and CD are applied, then a second series of cycles EF, and finally two other creep sequences, FG and HI,
- during the second part, a symmetric cyclic loading JK (Fig. 13b) was performed.

The comparison of modes of loading is shown in the Fig. 13c.

The diagrams, shown in Figs. 13a, 13b and 13c, highlight the first order cyclic ratcheting effect during asymmetric cyclic loading for a stress control process. The total shear strain evolution during the test is shown in the Fig. 13d. We can see that the creep sequences (AB, CD, FG and HI) have shapes of creep curves and their unique duration is equal to 900 seconds. The duration of creep sequences is not long enough to reach the saturation stage but we can observe

the existence of two stages: at first (stage I) the shear strain variation is quite fast, and next it is cut down at the end of the creep sequence (stage II).

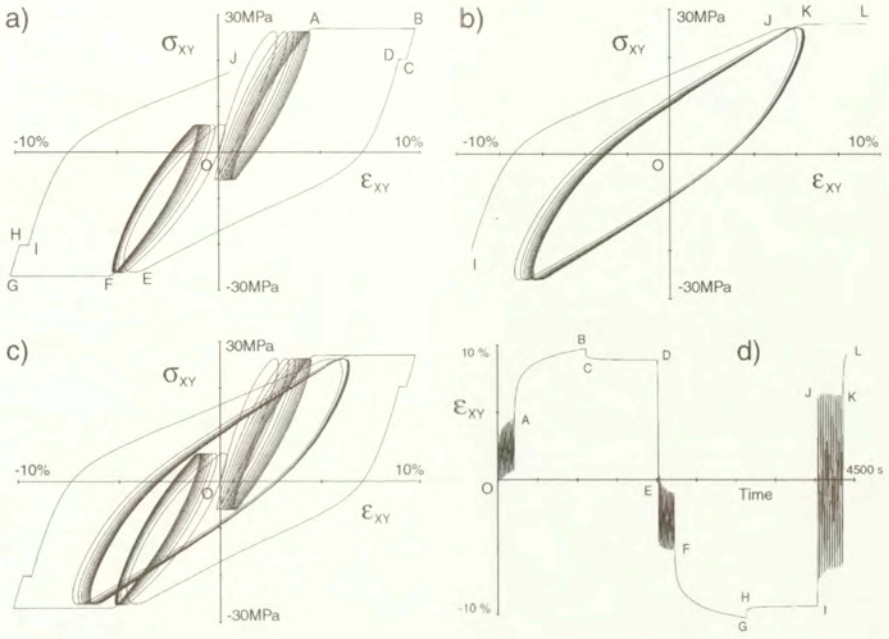

FIG. 13. (a,b,c) cyclic shear at constant intensity of stress rate with creeps, and (d) variations of the shear strain during this test.

These creep effects could be displayed by the variations of the second-order effects (Figs. 14, 15 and 16). Analysing the first part of the cyclic shear test (Fig. 14), we can see that the lateral strain ε^g_{xx} raises during the first sequences of asymmetric cyclic loading (OA in Fig. 14a) and stops during the second one (EF in Fig. 14b). Like in the case of relaxation, we observe a sharp drop in the ratchet intensity during creep sequences AB and CD, but during sequences FG and HI the ratchet intensity drop is negligible. During the second part of the test, when symmetric cyclic loading takes place (JK in Fig. 15a), we notice the return of the ratchet phenomenon. The same is shown in the Fig. 15b as a function of time.

At last, in the Figs. 16a and 16b is shown the evolution of ratchet during the whole cyclic shear at a constant intensity of the stress rate as a function of shear strain and time, respectively.

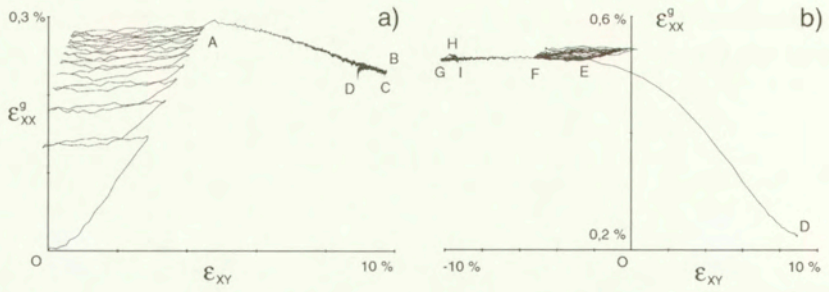

FIG. 14. (a) second-order effect during the OABCD part of the test at the Fig. 13, and (b) during the DEFGHI part of this test.

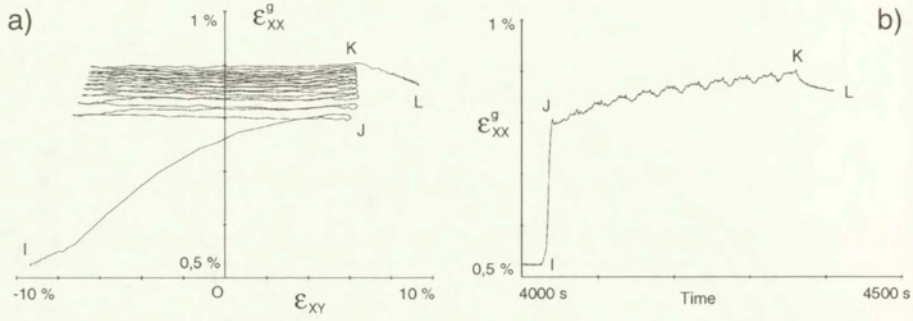

FIG. 15. (a, b) second-order effect during the IJKL part of the test at the Fig. 13.

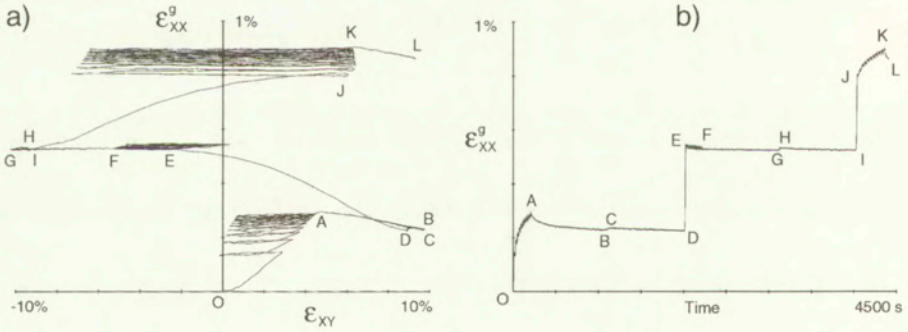

FIG. 16. (a, b) second-order effect during the whole test at the Fig. 13.

3.5. Thermomechanical effects

Comparing mechanical and thermal characteristics obtained during simple shear, we can find the temperature–stress relations $\Delta T(\sigma_{xy})$. Example of this relation is shown in Figs. 17 and 18.

Analysing the obtained results, three stages of deformation – elastic, highly-

elastic and plastic – are noticeable in polyamide PA66 from the thermomechanical coupling point of view:

- In the elastic range of deformation, in agreement with the Kelvin law [15], there are no temperature changes during shearing – the thermoelastic effect is negligibly small.
- During highly-elastic range of deformation, we observe a decrease of temperature; this stage is not observed in metals.
- In the plastic range of deformation, temperature of shear bands always increases.

A thermoelastic effect was not observed during unloading. Temperature decreased as a result of exchange of the heat with metallic grips.

As it was mentioned previously, lateral deformation during cyclic deformation is very small in comparison with the shear strain, then the temperature changes during this process would be similar as during simple shear.

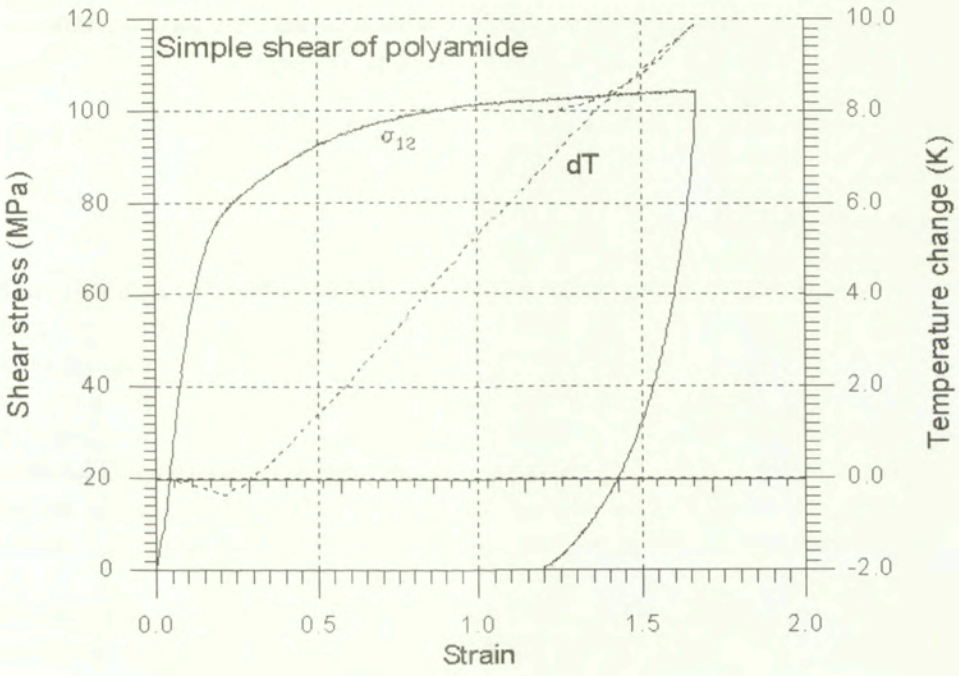

FIG. 17. Stress-strain and temperature-strain relation obtained during simple shear of polyamide.

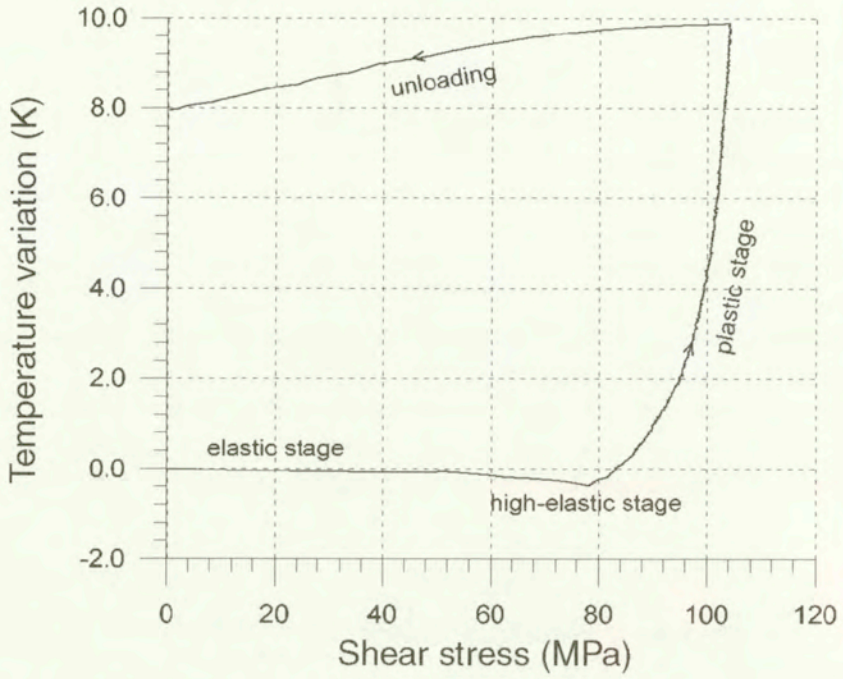

FIG. 18. Thermomechanical effect during simple shear of polyamide.

4. Concluding remarks

Among other conclusions following these shear tests on the PA66 solid polymer, the following phenomena are observed. Firstly, during symmetric cyclic shear tests at constant intensity of strain rate, a transient hardening effect occurs at the first loading, followed by a weak softening with the cyclic path. The limit cycle, reached by softening, is a function of the cycle strain amplitude, independently of the order of the cyclic tests with different amplitudes. The effects of this cyclic softening vanish during a relaxation or a creep sequence. Second-order effects increase the lateral strain ε^g_{xx} during shear without σ_{xx} stress; a ratchet phenomenon occurs during cyclic shear.

In the course of the relaxation sequences, three main stages describe the evolution of the σ_{xy} stress versus the time; the first one is very short and shows quick variations of σ_{xy}, during the second stage the stress evolution is cut down, and the third one is a saturation stage. The ratchet phenomenon on ε^g_{xx} goes back in the opposite direction, during relaxations. According to the comparison of the lateral strain and the shear stress evolution versus the time, the first-order and the second-order effects are very close, during a relaxation sequence.

Finally, investigation of simple shear indicates that the temperature decreases

during the highly-elastic range of deformation. Such phenomenon was not observed in metallic sheets.

With these two series of experiments, we can observe evolution of the shear stress, shear strain and lateral strain when the lateral stress is equal to zero, and the thermomechanical effects in the case of simple shear. Cyclic, relaxation and creep loading were performed. These experimental results give interesting information about the thermomechanical behaviour of the PA66 polyamide in the case of rotational loading of shear.

Acknowledgements

This paper has been partially supported by the Polish Committee for Scientific Research (KBN) under Grant No 8 TO7A0462 : "Thermomechanics of viscoelastoplastic materials subjected to deformation". The first author – G.B., acknowledges the invitation to the Institute of Fundamental Technological Research of PAS, in August-December 2001, in the frame of the Center of Excellence AMAS (Advanced Material and Structures).

References

1. J. H. POYTING, *On pressure perpendicular to the shear planes in finite pure shears, and on the lengthening of loaded wires when twisted*, Proc. Roy. Soc. London, Serie A, **82**, 546-559, 1909.
2. J. H. POYTING, *On the changes in the dimensions of a steel wire when twisted, and on the pressure of distortional waves in steel*, Proc. Roy. Soc. London, Serie A, **86**, 534-561, 1912.
3. A. FOUX, *An experimental investigation of Poynting effect*, Proc. Int. Sym. Second Order Effects Haifa, 228-251, 1962.
4. R. S. RIVLIN, D. W. SAUNDERS, *Large elastic deformations of isotropic materials. VII Experiments on the deformation of rubber*, Phil. Trans. Roy. Soc. London, A 865, **243**, 251-288, 1951.
5. H. W. SWIFT, *Length changes in metals under torsional overstrain*, Engineering, 253-257, April 4, 1947.
6. A. TOURABI, P. GUELIN, D. FAVIER, *Towards the modelling of deformable ferromagnets and ferroelectrics*, Arch. Mech., **47**, 3, 437-483, 1995.
7. P. GUELIN, W. K. NOWACKI, D. QUEREYRON, A. TOURABI, *Ratcheting and constitutive patterns of rate-form defined in Preferred Reference Frames*, Arch. Mech., **51**, 3-4, 357-390, 1999.
8. G. BLES, S. P. GADAJ, P. GUELIN, W. K. NOWACKI, A. TOURABI, *Thermomechanics of viscoplastic large strains of solid polymers*, Arch. Mech, **52**, 3, 397-427, 2000.
9. B. WACK, A. TOURABI, *Cycling shear of metallic sheets: application to aluminium-lithium alloy*, J. Mater. Sci., **28**, 4735-4743, 1993.

10. B. WACK, *The torsion of a tube (or a rod): General cylindrical kinematics and some axial deformation and ratchet measurements*, Acta Mech., **80**, 39, 1989.

11. C. G'SELL, S. BONI, S. SHRIVASTAVA, *Application of the plane simple shear test for determination of the plastic behaviour of solid polymers at large strains*, J. Mater. Sci. Eng. **18**, 903-918, 1983.

12. E. F. RAUCH, J. H. SCHMITT, *Dislocation substructures in mild steel deformed in simple shear*, Mater. Sci. Eng., **A113**, 441-448, 1989.

13. S. P. GADAJ, W. K. NOWACKI, E. A. PIECZYSKA, *Changes of temperatures during the simple shear test of stainless steel*, Arch. Mech., **48**, 4, 779-788, 1996.

14. NGUYEN H. V. W. K. NOWACKI, *Simple shear of metal sheets at high rates of strain*, Arch. Mech., **49**, 2, 369-384, 1997.

15. W. THOMSON,(Lord Kelvin), Quart. J. Pure and Appl. Math, 1, 57, 1857; Math. and Phys. Papers, Cambridge, **1**, 291, 1882.

Received December 19, 2001; revised version February 28, 2002.

Centre International des Sciences Mecaniques — *International Centre for Mechanical Sciences*

International Centre for Mechanical Sciences (CISM)
Programme 2002

Advanced Dynamics and Control of Structures and Machines *H. Irskik (Linz), K. Schlacher (Linz)*	**April 15-19**
Light Gauge Metal Structures: Recent Advances *J. Rondal (Liege), Dubina D. (Timisoara)*	**June 3-7**
Deformation in the Earth's Continental Crust: Theory, Experiment and Modeling *Y. Leroy (Palaiseau), F.K. Lehner (Salzburg)*	**June 17-21**
Cardiovascular Fluid Mechanics *G. Pedrizzetti (Trieste), K. Perktold (Graz)*	**July 1-5**
Multiscale Modeling in Continuum Mechanics and Structured Deformations *G. Del Piero (Ferrara), D.R. Owen (Pittsburgh)*	**July 15-19**
Modern Trend in Composite Laminates Mechanics *H. Altenbach (Halle), W. Becker (Siegen)*	**July 22-26**
Phase Change with Convection: Modelling and Validation *T.A. Kowalewski (Warsaw), D. Gobin (Orsay)*	**Sept. 2-6**
Modeling and Control of Two-Phase Flow Phenomena *V. Bertola (Turin)*	**Sept. 9-13**
Computational Micromechanics of Materials *P. Wriggers (Hannover), C. Schwab (Zurich), T.I. Zohdi (Hannover)*	**Sept. 23-27**
Mechanics and Thermomechanics of Rubberlike Solids *G. Saccomandi (Lecce), R.W. Ogden (Glasgow)*	**Sept.30-Oct.4**
Moving Discontinuities in Crystalline Solids *F.D. Fischer (Leoben), M. Berveiller (Metz)*	**October 7-11**
Liquid Films Theory, Experiments and Industrial Applications *N. Aksel (Bayreuth)*	**October 14-18**

Palazzo del Torso, Piazza Garibaldi, 18, 33100 Udine (Italy) • *e-mail: cism@cism.it* • *http://www.cism.it*
Tel. : +390432248511(6 lines)/Fax + 390432248550• Printing Office Tel. and Fax +39 0432572206 • Partita IVA 00401650304

The 7th Conference "Shell Structures, Theory and Applications"
Gdańsk-Jurata, Poland, 9-11 October 2002

organized by

Polish Academy of Sciences, Committee for Civil Engineering, Section of Structural Mechanics
Technical University of Gdańsk, Faculty of Civil Engineering, Structural Mechanics Department
Polish Society of Theoretical and Applied Mechanics, Gdańsk Branch

Call For Papers

Conferences "Shell Structures, Theory and Applications" (SSTA in short) have been organized in Poland since 1974. The aim of these meetings is always the same: to bring together scientists, designers, engineers and other specialists of shell structures in order to discuss important results and new ideas in this broad field of activity. The goal is to pursue more accurate theoretical models, to develop more powerful and versatile numerical methods for computerized analysis, and to disseminate expertise in design and maintenance of various shell structures and elements commonly used in science, technology and everyday life.

While earlier SSTA Conferences were primarily Polish national meetings, the last 6th SSTA98 in Jurata became a truly international event. It was attended by 170 participants from 14 countries. This confirmed our feeling that there is a need for a specialized international meeting in the field of shell structures, and the SSTA Conference may be an adequate forum for it. It is expected that the next 7th SSTA 2002 will bring together even more specialists of shell structures from international scientific and engineering community.

CONFERENCE TOPICS

- The theory and analysis of shells, including:
  - linear and nonlinear theory;
  - constitutive laws;
  - shells and plates with internal microstructure;
  - hybrid and branched structures;
  - beam - shell interaction;
  - stability, dynamics, optimization, reliability, sensitivity, limit load analysis etc.
- Numerical analysis of shell structures and elements, including:
  - computer methods: FEM, BEM and others;
  - analysis of nonstandard problems;
  - development of software packages.
- Design and maintenance of shell structures, including:
  - industrial applications in civil, power, mining and mechanical engineering, as well as in automotive, shipbuilding, aerospace and chemical processing industries;
  - shell design codes and procedures (e.g. Eurocode);
  - case studies of various shell structures and failure problems.

SCIENTIFIC COMMITTEE

Wojciech Pietraszkiewicz - chairman

Jan Awrejcewicz, Jacek Chróścielewski, Michal Kleiber,

Paweł Kłosowski, Piotr Konderla, Marian Królak,

Tomasz Lewiński, Czesław Szymczak,

Krzysztof Wiśniewski, Rościsław Tribiłło,

Zenon Waszczyszyn, Czesław Woźniak, Jerzy Ziółko

THE MAIN DEADLINES

- Submission of registration form: December 31, 2001
- Second announcement: March 31, 2002
- Submission of 2 pages abstract: April 30, 2002
- Notification to accepted authors: June 30, 2002

GENERAL INFORMATION

- The Conference program will include general lectures and contributed papers presented as lectures. The Conference lecture can be delivered in English or in Polish.
- All the contribution abstracts (2 pages) will be rigorously reviewed prior to acceptance. The accepted abstracts will be included in the Conference book of abstracts. Full length manuscripts of the selected papers will be further considered for publication in a special volume of a recognized technical journal.
- An exhibition related to the Conference themes provided by contractors, system manufacturers and consultants will be organized during the event.
- The Conference venue will be the comfortable hotel "Neptun" located in the attractive leisure region of the Hel Peninsula (www.hotelneptun.gda.pl).
- The registration fee, which will cover the full board accommodation and the book of abstracts, will be approximately 300 US dollars and 250 US dollars for accompanying person.
- The second announcement with more details about the Conference fees, general lectures and the abstract format will be sent to persons who return the preliminary registration form.
- Registration by Internet Homepage (http://www.pg.gda.pl/ssta2002) will be welcomed.
- For more details please visit our Internet Homepage or contact the conference secretariat.

ADDRESS FOR CORRESPONDENCE

SSTA2002 Organizing Committee
Department of Structural Mechanics
Faculty of Civil Engineering
Technical University of Gdańsk
ul. G. Narutowicza 11/12
80-952 Gdańsk, POLAND

http://www.pg.gda.pl/ssta2002
E-mail: ssta2002@pg.gda.pl
Phone.:+48-58-347-21-47, Fax:+48-58-347-16-70

Thermal Stresses 2003

CALL FOR PAPERS

Fifth International Congress on Thermal Stresses and Related Topics
http://www.esm.vt.edu/ts2003/

Blacksburg, Virginia, USA
June 8 - 11, 2003
hosted by the Department of Engineering Science and Mechanics
Virginia Polytechnic Institute and State University

Abstracts: Participants who wish to contribute a paper are requested to submit an abstract (about 500 words with 4 or 5 key words) including figures, tables and references, by mail, telefax, or E-mail to: ts2003@vt.edu. When the abstract is submitted by mail, two copies are required. The abstracts should be mailed to:

Mrs. Lisa Smith, TS2003, Virginia Tech, 219 ESM Department, Blacksburg, VA 24061, E-mail: ts2003@vt.edu
The abstract should include the title, full name of the author(s), affiliation, mailing address, telephone and telefax numbers, and E-mail address. See the web page of the Congress for the abstract format.

Deadlines:
Final date for receipt of abstracts: September 30, 2002 Authors informed concerning acceptance: November 15, 2002 Final date for receipt of camera-ready manuscript: January 31, 2003

Inquires regarding the program should be directed to:
Professor Liviu Librescu, General Chair of the Congress, Engineering Science and Mechanics, VIRGINIA POLYTECHNIC INSTITUTE AND STATE UNIVERSITY, Blacksburg, VA. 24061-0219, USA
Phone: (540) 231-5916, Telefax: (540) 231-4574, E-mail: librescu@vt.edu

IUTAM

International Congress
of Theoretical and Applied Mechanics
August 15 - 21, 2004 ♦ Warsaw, Poland

President: Witold Gutkowski, *PAN, Warszawa*
Co-Chairman: Michał Kleiber, *IPPT PAN, Warszawa*
Co-Chairman: Włodzimierz Kurnik, *Politechnika Warszawska*
Secretary-General: Tomasz Kowalewski, *IPPT PAN, Warszawa*

Preliminary Announcement

Scientific Program

The scientific program will start and end with opening and closing lectures, presented by prominent scientists. Titles of lectures and names of lecturers will be announced in October 2002, in the First Announcement and Call for Papers for the Congress.

The program will consist, moreover, of sectional lectures, mini-symposia and contributed papers presented in lecture and seminar presentation sessions. Invitations to present the contributed papers will be made on the recommendation of the International Paper Committee, based on their reviews of submitted abstracts and extended summaries.

Mini-Symposia

- Smart materials and structures.
- Tissue, cellular and molecular biomechanics.
- Mechanics of thin films and nanostructures.
- Microfluidics.
- Microgravity flow phenomena.
- Atmosphere and ocean dynamics.

Pre-Nominated Sessions

In Fluid Mechanics

Biological fluid dynamics • Boundary layers • Combustion and flames • Complex and smart fluids • Compressible flow • Computational fluid dynamics (jointly with IACM) • Convective phenomena • Drops and bubbles • Environmental fluid mechanics • Experimental methods in fluid mechanics • Flow control • Flow in porous media • Flow instability and transition • Flow in thin films • Fluid mechanics of materials processing • Granular flows • Low-Reynolds-number flow • Magnetohydrodynamics • Multiphase flows • Solidification and crystalgrowth • Stirring and mixing • Suspension mechanics • Topological fluid mechanics • Turbulence • Vortex dynamics • Waves

In Solid Mechanics

Computational solid mechanics (jointly with IACM) • Contact and friction problems (jointly with IAVSD)g • Control of multibody systems • Control of structures • Damage mechanics • Dynamic plasticity of structures • Elasticity • Experimental methods in solid mechanics • Fatigue • Fracture and crack mechanics (jointly with ICF) • Functionally graded materials • Impact and wave propagation • Material instabilities • Mechanics of composites • Mechanics of phase transformations (jointly with IACM) • Mechanics of porous materials • Multibody dynamics • Plasticity and viscoplasticity • Plates and shells (jointly with IACM) • Rock mechanics and geomechanics • Solid mechanics in manufacturing • Stability of structures • Stochastic micromechanics • Structural optimization (jointly with ISSMO) • Structural vibrations • Viscoelasticity and creep

Topics involving both fluid mechanics and solid mechanics

Acoustics • Chaos in fluid and solid mechanics • Continuum mechanics • Fluid-structure interaction • Mechanics of foams and cellular materials • Multiscale phenomena in mechanics

Details on preparation of manuscripts will be provided in the First Announcement and Call for Papers in October 2002.

It is planned to provide all future information mostly by e-mail. If you are interested in receiving future information, ***please pre-register on the Congress World Wide Web site*****:**

http://ictam04.ippt.gov.pl

On this site, you can already find many interesting information concerning the Congress

Correspondence related to the Congress should be sent to:

Prof. Tomasz Kowalewski, ICTAM04 Secretary-General

Institute of Fundamental Technological Research

Świętokrzyska 21, 00-049 Warszawa, Poland

e-mail: ictam04@ippt.gov.pl

INSTITUTE OF FUNDAMENTAL TECHNOLOGICAL RESEARCH
publishes the following periodicals:

ARCHIVES OF MECHANICS — bimonthly (in English)
ARCHIVES OF ACOUSTICS — quarterly (in English)
ARCHIVES OF CIVIL ENGINEERING — quarterly (in English)
ENGINEERING TRANSACTIONS — quarterly (in English)
COMPUTER ASSISTED MECHANICS AND ENGINEERING SCIENCES — quarterly (in English)
JOURNAL OF TECHNICAL PHYSICS — quarterly (in English)

Subscription orders for all journals edited by IFTR may be sent directly to:
Editorial Office
Institute of Fundamental Technological Research
Świętokrzyska 21, p. 508
00-049 Warszawa, POLAND

DIRECTIONS FOR THE AUTHORS

The journal *ARCHIVES OF MECHANICS* (ARCHIWUM MECHANIKI STOSOWANEJ) deals with the printing of original papers which should not appear in other periodicals.

As a rule, the volume of a paper should not exceed 40 000 typographic signs, that is about 20 type-written pages, format: 210×297 mm, leaded. The papers should be submitted in two copies. They must be set in accordance with the norms established by the Editorial Office. Special importance is attached to the following directions:

1. The title of the paper should be as short as possible.
2. The text should be preceded by a brief introduction; it is also desirable that a list of notations used in the paper should be given.
3. The formula number consists of two figures: the first represents the section number and the other the formula number in that section. Thus the division into subsections does not influence the numbering of formulae. Only such formulae should be numbered to which the author refers throughout the paper, and also the resulting formulae. The formula number should be written on the left-hand side of the formula; round brackets are necessary to avoid any misunderstanding. For instance, if the author refers to the third formula of the set (2.1), a subscript should be added to denote the formula, viz. $(2.1)_3$.
4. All the notations should be written very distinctly. Special care must be taken to write small and capital letters as precisely as possible. Semi-bold type should be underlined in black pencil. Explanations should be given on the margin of the manuscript in case of special type face.
5. It has been established to denote vectors by semi-bold type. Trigonometric functions are denoted by sin, cos, tg and ctg, inverse functions – by arc sin, arc cos, arc tg and arc ctg; hyperbolic functions are denoted by sh, ch, th and cth, inverse functions – by Arsh, Arch, Arth and Arcth.
6. Figures in square brackets denote reference titles. Items appearing in the reference list should include the initials of the first name of the author and his surname, also the full title of the paper (in the language of the original paper); moreover;
   a) In the case of books, the publisher's name, the place and year of publication should be given, e.g., 5. S. ZIEMBA, *Vibration analysis*, PWN, Warszawa 1970;
   b) In the case of a periodical, the full title of the periodical, consecutive volume number, current issue number, pp. from ... to ..., year of publication should be mentioned; the annual volume number must be marked in black pencil so as to distinguish it from the current issue number, e.g., 6. M. SOKOŁOWSKI, *A thermoelastic problem for a strip with discontinuous boundary conditions*, Arch. Mech., **13**, 3, 337–354, 1961.
7. The authors should enclose a summary of the paper. The volume of the summary is to be about 100 words.
8. The authors are kindly requested to enclose the figures prepared on diskettes (format WMF, EMF, GIF, PCX, BitMaP, EPS or PostScript).

Upon receipt of the paper, the Editorial Office forwards it to the reviewer. His opinion is the basis for the Editorial Committee to determine whether the paper can be accepted for publication or not.

The printing of the paper completed, the author receives 25 copies of reprints free of charge. The authors wishing to get more copies should advise the Editorial Office accordingly, not later than the date of obtaining the galley proofs.

The papers submitted for publication in the journal should be written in English. No royalty is paid to the authors. Please send us, in addition to the typescript, the same text prepared on a diskette (floppy disk) 3 1/2" as an ASCII file, preferably in the TEXor LATEXformat in Dos or Unix format.

EDITORIAL COMMITTEE
ARCHIVES OF MECHANICS
(ARCHIWUM MECHANIKI STOSOWANEJ)

Archives of Mechanics

Contents of issue 2 vol. 54

103 R. STAROSZCZYK, *A uniform strain, discrete-grain model for evolving anisotropy of polycrystalline ice*

127 I. ECSEDI, *Mean value and bounding formulae for heat conduction problems*

141 S. TOKARZEWSKI, J. J. TELEGA, M. PINDOR, J. GILEWICZ, *Basic inequalities for multipoint Padé approximants to Stieltjes functions*

155 G. BLES, S. P. GADAJ, W. K. NOWACKI, A. TOURABI, *Experimental study of a PA66 solid polymer in the case of cyclic shear loading*

Arch. Mech., **54**, nr 2, str. 101–182, Warszawa 2002